RCA REVIEW

a technical journal

RADIO AND ELECTRONICS
RESEARCH • ENGINEERING

VOLUME X SEPTEMBER 1949 NO. 3

RCA REVIEW

GEORGE M. K. BAKER
Manager

CHAS. C. FOSTER, JR.
Business Manager

SUBSCRIPTIONS:

United States, Canada, and Postal Union: One Year $2.00, Two Years $3.50, Three Years $4.50
Other Countries: One Year $2.40, Two Years $4.30, Three Years $5.70

SINGLE COPIES:

United States: $.75 each. Other Countries: $.85 each

Published quarterly in March, June, September, and December by Radio Corporation of America, RCA Laboratories Division, 30 Rockefeller Plaza, New York 20, N. Y.

Editorial and General Offices: RCA Review, Radio Corporation of America, RCA Laboratories Division, Princeton, New Jersey

Entered as second class matter April 3, 1946, at the Post Office at New York, New York, under the act of March 3, 1879

RADIO CORPORATION OF AMERICA

DAVID SARNOFF, *Chairman of the Board*

FRANK M. FOLSOM, *President*

LEWIS MACCONNACH, *Secretary* ARTHUR B. TUTTLE, *Treasurer*

PRINTED IN U.S.A.

RCA REVIEW

a technical journal

RADIO AND ELECTRONICS
RESEARCH • ENGINEERING

Published quarterly by
RADIO CORPORATION OF AMERICA
RCA LABORATORIES DIVISION
in cooperation with

RCA VICTOR DIVISION
RADIOMARINE CORPORATION OF AMERICA
RCA INTERNATIONAL DIVISION
RCA COMMUNICATIONS, INC.
NATIONAL BROADCASTING COMPANY, INC.
RCA INSTITUTES, INC.

VOLUME X SEPTEMBER 1949 NUMBER 3

CONTENTS

RCA Review is regularly abstracted and indexed by *Industrial Arts Index, Science Abstracts* (I.E.E.-Brit.), *Engineering Index, Electronic Engineering Master Index, Abstracts and References (Wireless Engineer*-Brit. and *Proc. I.R.E.)* and *Digest-Index Bulletin.*

RCA REVIEW

PENCIL-TYPE UHF TRIODES*

By

G. M. Rose, D. W. Power and W. A. Harris

Tube Department, RCA Victor Division,
Harrison, N. J.

Summary—A new construction of triode for ultra-high-frequency use is described which not only satisfies the basic requirements of minimum transit time, lead inductance, and internal capacitance, but also incorporates other desirable design features such as small size, good thermal stability, low heater wattage, and convenience of use in circuits. In addition, the construction lends itself to high-volume production methods. A double-ended type of structure is used in which the rod-type anode and cathode connections extend outward from each side of a control-grid disk. The internal elements are cylindrical in shape and are arranged coaxially. Electrical characteristics, and operation and performance data are given for four different tubes of this construction. Typical applications for the tubes are described.

Introduction

PENCIL-TYPE ultra-high-frequency triodes are tubes designed for use as amplifiers or low-power oscillators at frequencies from 300 megacycles to more than 3000 megacycles. This paper describes four different tubes, one of which is commercially available under type number 5794; the other three are still in a developmental status. The type of structure which has been developed for these tubes is well adapted for operation at ultra-high frequencies and, in addition, has a number of advantages over alternative designs with respect to manufacturing processes. These advantages are described in the discussion of the method of assembly which follows.

The performance of negative-grid triodes at ultra-high frequencies depends on the accurate maintainance of very small interelectrode spacings. Also, it is essential that the interelectrode capacitances and the inductances associated with the leads be as small as possible for the tube characteristics chosen. Many of the miniature tube types in current use in television and other high-frequency applications use grid-to-cathode spacings of only a few thousandths of an inch — examples are types 6J6, 6AG5, and 6AK5. The additional improvements in operation at still higher frequencies obtained by reducing lead inductances and lead losses are exemplified by the Acorn types

* Decimal Classification: R 339.2.

and more emphatically by the disk-seal "Lighthouse" types. The disk-seal type of electrode connection permits the utilization of closed-cavity resonators which minimize power loss through radiation, besides giving much lower inductance values and higher resonant frequencies than are obtainable with wire leads.

Construction Features

The pencil-type tubes use the disk-seal principle. One of the tubes is illustrated in Figure 1. The upper metal cylinder is the anode, the lower cylinder is the cathode support, and the central disk supports the grid. These metal parts are joined together by the two glass cylinders. Heater connections are made to two wires projecting through a glass button sealed in the cathode end of the tube. The over-all length of the tube is about two inches. The anode and cathode cylinders are each one-quarter inch in diameter and the diameter of the grid disk is 13/16 inch. Connections to the heater can be made with a small socket using contacts such as those designed for sub-miniature tubes; in some instances wires may be soldered to the heater leads. The pencil tubes are readily adaptable to coaxial circuits, when maximum performance at the highest frequencies is sought. At lower frequencies, lumped-circuit systems have been made in which the tubes are inserted transversely into fuse clips used as holders.

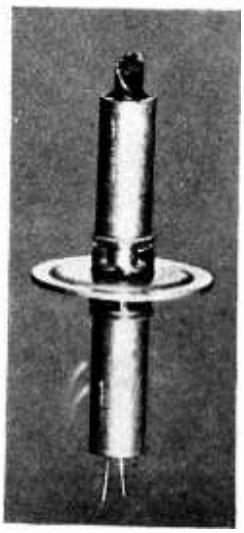

Fig. 1—Pencil-type triode.

A particular feature of the pencil-tube design is the use of coaxial cylindrical elements. A cross-sectional view of a pencil tube is given in Figure 2. Cylindrical elements were chosen for several reasons. First, cylinders are inherently strong and stable. Second, the cylindrical cathode completely surrounds the heater thus making the most efficient use of the heater power. Third, as the electrodes warm up during operation, the longitudinal expansion of the cathode has little effect on the spacing; the radial expansions of the electrodes are all in the same direction thus tending to maintain the relative spacings. A fourth reason, very important when the problems of production in large volume are considered, is that the jigs required for assembly are simple metal pins which can be turned on a lathe with a high degree of accuracy.

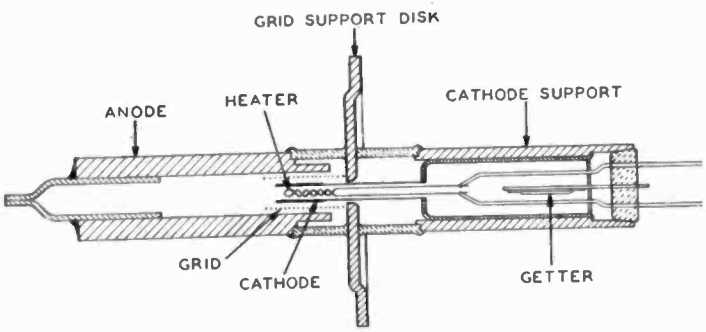

Fig. 2—Cross section of pencil-type triode.

The anode is a steel cylinder, heavily silver plated to prevent oxidation and to minimize high-frequency resistance. The effective diameter of the anode as a tube element is determined by the size of its central hole. The disk which supports the grid is a punched steel part, also heavily plated. The grid itself is a seamless cylindrical mesh which surrounds the cathode; it is supported from one end by the grid support disk. The construction of the grid is shown in Figure 3. A number of longitudinal members of fine wire are wrapped with a spiral of even finer wire, and each of the crossover points is silver-soldered to provide structural strength. A typical grid for one of the tubes consists of 18 longitudinal wires of 0.002-inch diameter wrapped with 0.0008-inch wire with a pitch of 88 turns per inch. The wrapping wire is silver plated. The grids are wound as long strips on a mandrel of suitable diameter. While on the mandrel the strips are heated in a hydrogen atmosphere and the silver from the wrapping wire flows into the crossover joints to solder the wires together. Finished grids of the required length may then be cut from the strips. This grid structure has the advantage of circular symmetry, thereby allowing the use of a cylindrical anode and the utilization of the whole of the cathode surface.

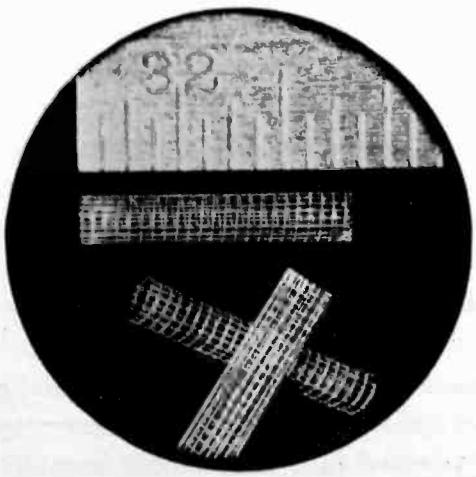

Fig. 3—Grids. Smallest division of scale shown is 1/32 inch.

The cathode is a short length of nickel tubing mounted on a thin-walled Kovar cylinder which provides both mechanical support and thermal isolation. The Kovar cylinder is supported by a larger cylinder

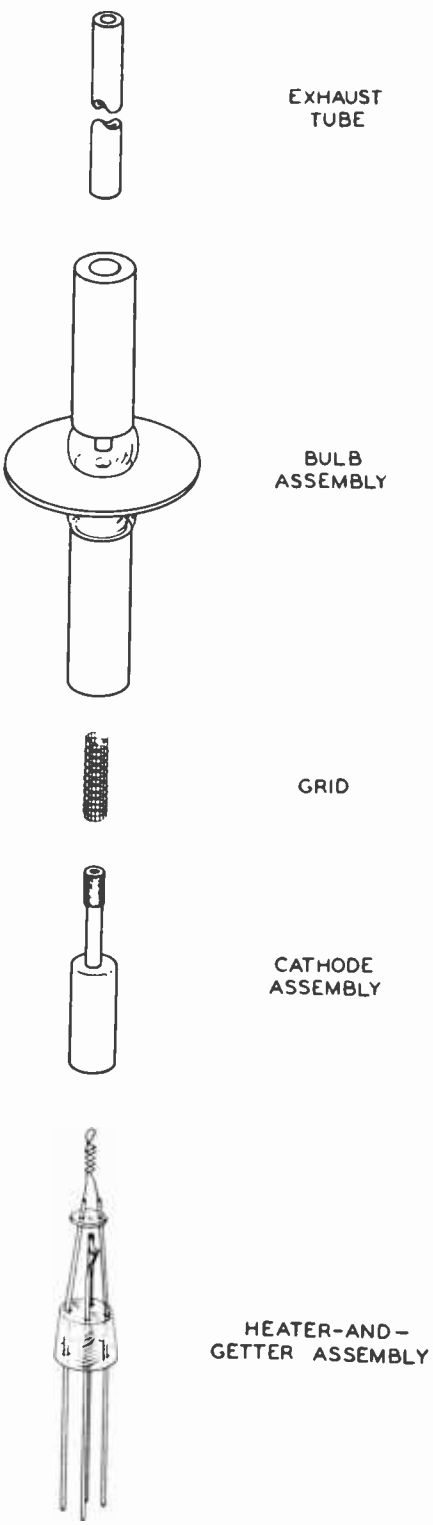

Fig. 4—Exploded view of pencil-type triode.

which makes a close sliding fit with the inside of the cathode-support cylinder. The length-to-diameter ratio of the cathode and the length of the Kovar support were chosen to give the lowest heat loss consistent with the requirements of sufficient cathode area, rigid support, low inductance, and low resistance. The heater and getter constitute a subassembly formed on a glass button which is eventually sealed in the end of the cathode-support sleeve.

Assembly and Exhaust

The assembly procedure is as follows: First, the bulb assembly consisting of the anode cylinder, the grid disk, the cathode support cylinder, and the glass insulators is prepared. Refer to Figure 4. These parts are joined together by metal-to-glass seals while being held in accurate axial alignment on a turned metal pin. High-frequency heating is used to make the seals. The grid and cathode are not in place at this time so these parts are not exposed to the sealing heat. The grid is next welded to the grid disk by a set of electrodes designed to give alignment as well as to make the weld. The cathode subassembly is pressed into the cathode support sleeve. Then the heater-getter subassembly is inserted into the cathode support sleeve and the glass stem is sealed into the end of the cathode support sleeve. The copper exhaust tube is then brazed into

the end of the anode cylinder. The ends of the anode and cathode cylinders nearest the grid disk are held in water-cooled chucks during these last operations.

All the subassemblies and the final assembly of the tube are made on simple, accurate jigs which can readily be adapted to the mechanization necessary to obtain large-scale manufacture at reasonable cost. The only hand operations required occur in the preparation of the cathode and stem subassemblies.

During exhaust the gas from the space inside the cathode support sleeve flows through the end of the cathode. The getter is inside the cathode support sleeve, so there is no tendency for the getter to deposit on the plate-grid or grid-cathode seals. Also, because the active cathode surface is completely inside the anode, evaporation of cathode material onto the seals is prevented both during exhaust and during life.

Tube Designs

The pencil-tube structure can be used for tubes with a wide range of characteristics. Parameters at the designer's disposal are the diameters of the anode hole, grid mandrel, and cathode; the size and number of the longitudinal grid wires; and the size and number of grid wrapping turns. Any of these may be varied over a considerable range without requiring changes in the outside dimensions of the tube. Some latitude in the choice of the cathode length is also available. The designs which have received the most attention to date are:

1. Developmental No. A-2352 is a medium-mu triode intended primarily for low-power oscillator service. As an oscillator, this type will give a minimum power of 50 milliwatts at 3000 megacycles. Because a plate dissipation up to 6.3 watts is allowable for this triode when provision is made for conducting heat away from the anode, several watts of power output can be obtained at lower frequencies.

2. Developmental No. A-2351 is a high-mu triode. The high amplification factor is desirable for grounded-grid radio-frequency amplifiers and for frequency multipliers. This type can be used under "class A" conditions in receiving circuits, as a radio-frequency amplifier or as a mixer.

3. RCA-5794 illustrated in Figure 5 is a fixed-tuned complete oscillator triode designed for radiosonde systems operating at a frequency of 1680 megacycles. It has two resonators which are integral parts of the tube. A coaxial radio-frequency output termi-

nal is loop-coupled to the resonator between grid and plate. The internal structure is similar to that of Developmental No. A-2352 except for the use of a heater with ratings corresponding to the requirements of radiosonde batteries. The over-all length is a little under three inches; the weight is one ounce. The circuit components, which on assembly become permanent parts of the tube, are fabricated from thin sheet metal on the same type of equipment used for making tube parts.

When normal operating voltages are supplied to the RCA-5794, the radio-frequency output is in excess of 400 milliwatts. Radiosonde applications require that a tube give substantial output for a few hours with battery voltages down to about 75 per cent of their initial values; the output of the RCA-5794 is above 200 milliwatts under these conditions.

Fig. 5—Fixed-tuned oscillator triode RCA-5794.

4. Developmental No. A-2317 is a pencil-type triode designed for pulse service. This tube has a larger-diameter cathode and larger clearances between cathode and grid and between grid and anode. The diameters of the glass insulators are also greater, but the diameters of the anode, the grid disk, and the cathode support cylinder are the same as those of the other pencil types.

Electrical Characteristics

Characteristics and ratings for the four tubes are given in Tables I and II.

Measurements of short-circuit input conductance in a grounded-cathode circuit have been made on Developmental Nos. A-2351, A-2352, and A-2317. The grounded-cathode circuit was used for these measurements because a considerable amount of comparable data is available for other tube types under this operating condition. A test frequency of 100 megacycles was used for most of the measurements for the same reason.

Table I—Tentative Ratings and Typical Operating Conditions for Developmental Nos. A-2351, A-2352, and A-2317

	Dev. No. A-2351	Dev. No. A-2352	Dev. No. A-2317
Heater Voltage	6.3	6.3	6.0 volts
Heater Current	0.135	0.135	0.33 amperes
Direct Interelectrode Capacitances:			
Grid to Plate	1.4	1.3	1.75 $\mu\mu$f.
Grid to Cathode	2.5	2.3	2.5 $\mu\mu$f.
Plate to Cathode	0.035	0.09	0.07 max. $\mu\mu$f.
Maximum Ratings; Absolute Values:			
D.C. Plate Voltage	250	250	300 max. volts
Plate Dissipation* (Osc.)	6.3	6.3	6.3 max. watts
Plate Dissipation (Ampl.)	5	5	5 max. watts
Grid Current**	5	5	15 max. ma.
Negative Grid Voltage	100	100	100 max. volts
Temperature at Any Seal	175	175	180 max. °C
Typical Operation as Class A Amplifier:			
Plate Voltage	250	120	200 volts
Cathode Resistor	50	39	100 ohms
Amplification Factor	58	21	27
Plate Resistance	8300	3200	4500 ohms
Transconductance	7000	6400	6000 μmhos
Plate Current	20	24.5	25 ma.

* When plate dissipation exceeds 2.5 watts a heat-conducting clip must be connected to the anode.

** As oscillator or class C amplifier.

The curves of Figure 6 show the relation between short-circuit input conductance and transconductance for Developmental No. A-2351 at four different bias voltages. The plate voltage is varied to obtain the indicated transconductance. The observed ratios of short-circuit input conductance to transconductance are less than half those observed on other tube types with similar electrode spacings. A noteworthy feature of the curves of Figure 6 is the indicated dependence of the input conductance on grid-to-plate transit time. For a transconductance of 4500 micromhos the conductance observed with a bias of -3 volts is a little over half that with a bias of -1 volt; the difference is due primarily to the higher plate voltage used in obtaining the same transconductance at the higher grid bias and the consequent shorter grid-to-plate transit time. Also, the shorter grid-to-plate transit time at higher plate voltages accounts for the maxima observed as the transconductance is increased. The increase in capacitance from a cold to a hot cutoff condition is 0.2 micromicrofarads. The total increase from cold to operating condition for a transconductance of 4500 micromhos is 1.1 micromicrofarads at a bias of -1 volt and 0.8 micromicrofarads at a bias of -3 volts.

Table II—Technical Data for RCA-5794, Fixed-Tuned Oscillator Triode for Radiosonde Service at 1680 Megacycles

Electrical:	
Heater, for Unipotential Cathode:	
Voltage Range* (AC or DC)	4.8 to 6.3 volts
Current with 6.0 volts on heater	0.160 ampere
Frequency (Approx.)	1680 Mc.
Frequency Adjustment Range	± 12** Mc.
Maximum Ratings, Absolute Values:	
DC Plate Voltage	120 max. volts
DC Plate Current	30 max. ma.
Plate Dissipation	3.6 max. watts
Peak Heater—Cathode Voltage	0 max. volts
Ambient Temperature Range	— 55 to + 75 °C
Operating Frequency Drift:	
Heater-Voltage Range	6.0 to 4.8 volts
Plate-Voltage Range	108 to 85 volts
Ambient Temperature Range	+ 22 to — 40 °C
Maximum Frequency Drift	$\begin{cases} +4 \\ -1 \end{cases}$ Mc.

* This range of heater voltage is for radiosonde applications in which the heater is supplied from batteries and in which the equipment design requirements of minimum size, light weight, and high efficiency are the primary considerations even though the average life expectancy of the 5794 in such service is only a few hours.

** As supplied, tubes are adjusted to 1680 ± 4 megacycles.

Figure 7 shows the variation of input conductance with transconductance for Developmental Nos. A-2351, A-2352, and A-2317, and a special laboratory tube identified as Tube "A" using A-2352 parts mounted on a 9-pin miniature stem. A grid bias of — 2 volts was used for all the curves of Figure 7. The effect of the wider spacings used in Developmental No. A-2317 is apparent in these curves. Because this tube is normally used with peak pulse voltages many times greater than the direct-current voltages used in obtaining this curve, the transit-time effects are correspondingly reduced. The almost linear rise of input conductance with transconductance observed for Tube "A" is characteristic of conventionally-based tubes. The excess of conductance for Tube "A" over that of Developmental No. A-2352 is principally caused by the higher cathode-lead inductance. Tube "A", however, shows an excellent ratio of input conductance to transconductance. Because the grid-to-cathode and grid-to-anode spacings for this tube are no smaller than those used for other types showing higher input conductance it is probable that the cylindrical symmetry maintained with the pencil-tube parts is an important factor in accounting for the good results obtained.

Figure 8 shows that the relation between input conductance and frequency observed for Developmental No. A-2351 follows a square-law curve, as expected from theoretical considerations, over the frequency range of 50 to 140 megacycles.

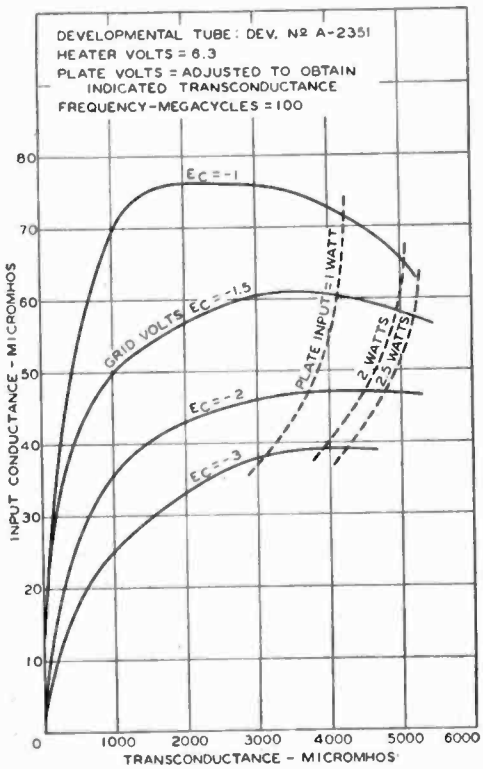

Fig. 6—Change of short-circuit input conductance with transconductance at 100 megacycles for Developmental No. A-2351 (grounded-cathode circuit).

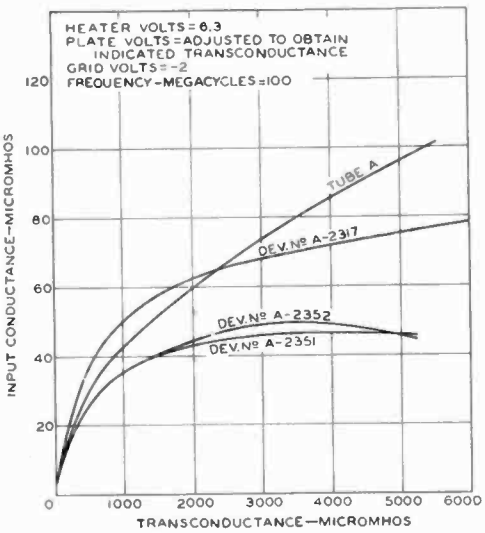

Fig. 7—Change of short-circuit input conductance with transconductance at 100 megacycles for Developmental Nos. A-2317, A-2351, and A-2352 and for a special laboratory tube, Tube A, using A-2352 parts mounted on 9-pin miniature stem (grounded-cathode circuit).

These measurements can be used directly in estimating the performance obtainable from a pencil-type tube as a neutralized triode amplifier or as a mixer in a grounded-cathode circuit. They are of more immediate interest, however, in demonstrating some of the basic advantages inherent in the pencil-tube construction. Incidentally, the results obtained suggest that the pencil-tube structure will be of considerable utility as the basis for tubes constructed solely to investigate the relations between electrode dimensions and performance.

Data at 1200 Megacycles

Data for evaluating the performance of pencil-type tubes at high frequencies are presented at 1200 megacycles, with the tubes operated in a grounded-grid circuit. In these data measurements, the cathode

and plate of the tube under test are connected to the inner conductors of two concentric-line cavities and the grid disk is clamped between a pair of plates forming the boundary between the cavities. One of the plates is slotted radially to cushion the grid disk. Sheets of mica insulate the parts actually contacting the grid from the grounded cylinders, permitting application of direct-current bias while providing negligible reactance to the 1200-megacycle radio-frequency currents. A conical blocking capacitor in the central conductor of the plate cavity provides direct-current insulation for the plate. The heater leads are brought out through the inside of the inner conductor of the cathode cavity. Signal is introduced into the cathode cavity through a slotted line by direct connection to the cathode line. Tuneable probes containing crystal diodes are used for measurements along the slotted line and for the measurement of relative power output. For the latter purpose, an opening in the plate cavity close to the tube is provided.

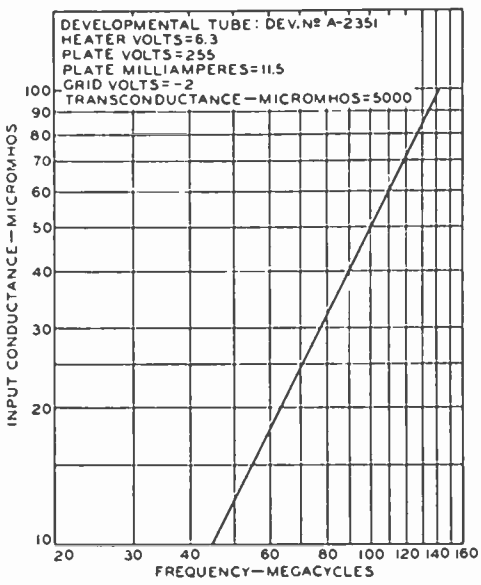

Fig. 8—Change of short-circuit input conductance with frequency for Developmental No. A-2351 (grounded-cathode circuit).

For short-circuit input conductance measurements at 1200 megacycles, the plate circuit is first tuned to resonance and then is detuned far enough from resonance so that the output voltage may be considered negligible in comparison with the value observed at resonance. Measurements of standing-wave ratio in the slotted line are then used to determine the resistance and reactance effective at the point where the measuring line connects to the cathode line. Comparisons of such measurements on a cold tube with the known capacitance of the tube, at several frequencies, are used to determine the amount of series inductance and shunt capacitance between the point of measurement and the internal structure of the tube.

The curves of Figure 9 show the variation of short-circuit input conductance and short-circuit input capacitance with transconductance for three pencil-tube types at 1200 megacycles. In a grounded-grid circuit it is expected that the electrons in the tube under test will have a negligible influence on the cathode circuit after they pass

through the grid. Consequently, the conductance as measured at the cathode should be the conductance of an ideal diode, with an anode at the effective grid plane collecting all the current. The observed decrease in input capacitance with increasing transconductance is in accord with diode theory. The observed input conductance, however, is higher in value than the low-frequency transconductance, whereas theoretical considerations would indicate a lower value, decreasing with increasing frequency. Also, no explanation can be offered at present for the differences between the curve for Developmental No. A-2317 and the curves for Developmental Nos. A-2351 and A-2352. The curves of

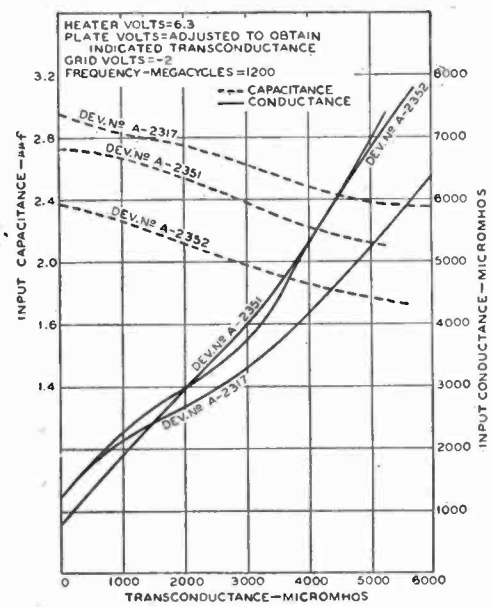

Fig. 9—Change of short-circuit input conductance and input capacitance with transconductance at 1200 megacycles for Developmental Nos. A-2317, A-2351, and A-2352 (grounded-grid circuit).

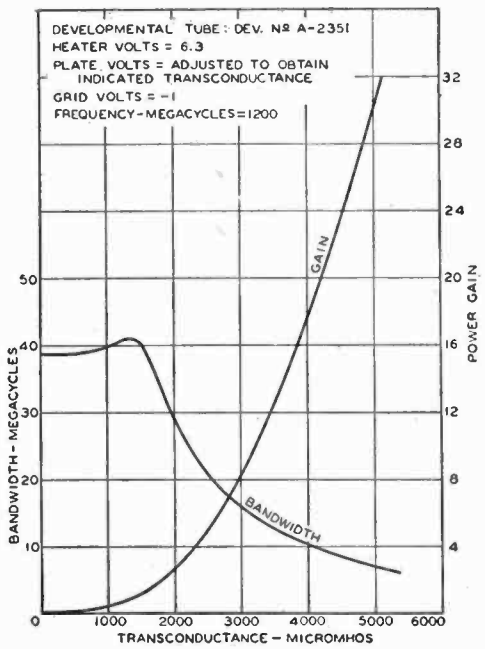

Fig. 10—Change of power gain and bandwith with transconductance at 1200 megacycles for Developmental No. A-2351 (grounded-grid circuit).

Figure 10, however, show that the observed conductance is close enough to the transconductance to allow application of low-frequency grounded-grid operation formulas for obtaining a first-approximation estimate of pencil-tube performance at 1200 megacycles.

Power Gain Measurements

Power gain measurements are made in the following manner: The tube is removed from the test circuit and a crystal probe is inserted

in a convenient place in the input cavity. Matching stubs between the signal generator and the measuring line are adjusted to obtain maximum current from the crystal; the coupling of the crystal to the line and the tuning adjustments for the crystal and the input cavity are also adjusted until it becomes evident that no higher current reading can be obtained. It is then assumed that the total available power from the signal generator is being absorbed by the crystal probe.

The tube to be tested is then reinserted in the cavity and the same probe is coupled to the plate line. The degree of coupling used determines the effective plate load impedance. The output capacitance of the tube and the characteristic impedance of the plate cavity are known; consequently, it is possible to determine the total output impedance by measuring the change in length of the plate-circuit line required to reduce the crystal output current reading to half its maximum value. Some energy reaches the output cavity through the cathode-to-plate capacitance of a cold tube. Because the output impedance of the cold tube and the resonant impedance of the cavity are large in comparison with the load impedances found useful for gain measurements, the load impedance can be found to a reasonable approximation by the method described above, using a cold tube in the circuit. The effective bandwidth of the plate circuit, either with a cold tube or with any stable set of adjustments with an operating tube, can be determined by the same methods. Because the input circuit is relatively broad, the plate circuit bandwith is approximately the bandwidth of the whole amplifier.

Gain measurements are made by adjusting the generator matching stubs and the plate and cathode tuning to give maximum crystal current, then setting the calibrated attenuator on the signal generator to make the crystal current the same as that previously recorded as the maximum obtainable in the input cavity. The required attenuation is then equal to the power gain.

When the coupling between the crystal probe and the output circuit is insufficient, the circuit oscillates when the attempt is made to maximize the gain. As the circuit approaches oscillation the gain becomes very high and the bandwidth approaches zero. The curves of Figure 10 show the power gain and bandwidth for a Developmental No. A-2351 tube plotted against transconductance, at a fixed grid bias voltage. The coupling was tight enough to avoid oscillation up to the highest value of plate voltage used, but a considerable amount of regeneration is indicated by the decrease of the bandwidth to less than one-quarter of the cold-tube value. The significance of these

curves is in the demonstration that a power gain of 20 or 30 can be obtained with Developmental No. A-2351 at a frequency of 1200 megacycles, with a bandwidth sufficient for handling many types of signals. The load used does not necessarily give the optimum gain-bandwidth characteristic, and the accuracy claimed for the bandwidth determination is not very great.

PERFORMANCE

The production tests made on the radiosonde tube, RCA-5794, serve to illustrate the performance obtainable from pencil tubes as low-power oscillators at high frequencies. As mentioned, the RCA-5794 is a fixed-tuned oscillator triode designed to operate at a frequency of 1680 megacycles. The adjustment operations to be described are properly considered as part of the fabrication operations for the tube. Figure 11 shows the arrangement of test equipment. The tube is

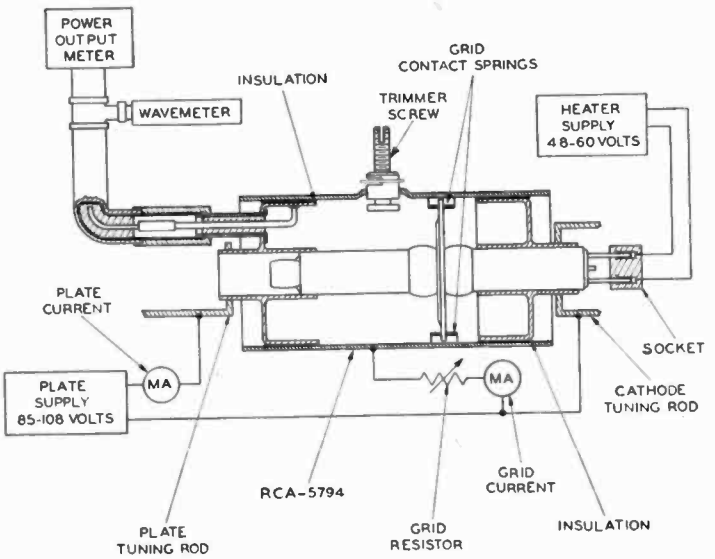

Fig. 11 — Arrangement for testing and adjusting fixed-tuned oscillator triode RCA-5794.

placed in a jig which has chucks engaging the cathode and plate tuning plungers. The first test is for power output at the operating frequency of 1680 megacycles with heater and plate voltages at 4.8 volts and 85 volts, respectively; these values correspond to the radiosonde battery voltages expected at the end of a long flight. The frequency is adjusted by movement of the plate and cathode tuning rods, with the trimming screw at the center of its range. The power output must equal or exceed 200 milliwatts with the grid resistor adjusted to give a plate current of 20 milliamperes. Then, with the heater and plate voltages increased to 6.0 volts and 108 volts, respectively, the

plate current with the same grid resistor value must not exceed 30 milliamperes. A higher value would cause excessive drain on the radiosonde batteries during the first stages of a flight. The power output with these voltages is in the order of 500 milliwatts. The trimming screw is then checked to determine that the required tuning range, ± 12 megacycles, can be covered. If the tube passes all tests, the locking clip is crimped to hold the tuning plungers in place and the tube is ready for use. A suitable percentage of the completed tubes are subjected to tests for frequency drift, resistance to vibration, and other items required for quality control.

The cavity dimensions used for RCA-5794 serve to indicate the tuning characteristics of Developmental Nos. A-2351 and A-2352 as well. The RCA-5794 dimensions give the cavity sizes for tuning to 1680 megacycles. With most tubes after the tuning adjustment the

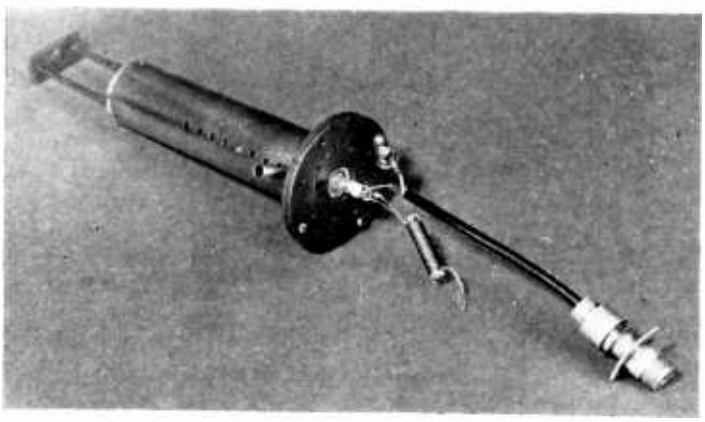

Fig. 12 — Cavity used for power amplifier tests.

surface of the cathode tuning plunger is about ½ inch from the grid disk and the surface of the plate tuning plunger is about ¾ inch from the grid disk. Operation at much higher frequencies requires that the cavities used be tuned for a ¾-wave or 5/4-wave mode. Power outputs somewhat over 50 milliwatts have been measured from Developmental No. A-2352 at 3000 megacycles.

Developmental No. A-2351, with an amplification factor of 56, is intended for use as a frequency doubler or tripler. Tests have been made on this tube, using the concentric-cylinder plate circuit shown in Figure 12 and a lamp load, with output frequencies in the range 400 to 1000 megacycles. The circuit is of the grounded-grid type. A line of adjustable length may be used to feed power to the cathode, or the line may be fitted with tuning stubs. Alternatively, when the input frequency is not too high, adjustable inductances or capacitors

may be connected to the cathode. The tests made so far give the following results:

1. Apparent plate circuit efficiencies observed when Developmental No. A-2351 is used as a tripler or a doubler are 20 to 30 per cent and 30 to 50 per cent, respectively. The corresponding power outputs are 1 to 1.5 watts and 2 to 3 watts.
2. Power gains of approximately unity in tripler service and of 1.5 to 2 in doubler service are observed.
3. Efficiency, power output, and power gain do not change radically over an output frequency range of 400 to 1000 megacycles.

Suggested operating conditions for doubler and tripler circuits are:

Plate Voltage		250 volts
Plate Current		15-20 milliamperes
Grid Current:	Doubling	3- 4 milliamperes
	Tripling	4- 5 milliamperes
Grid Resistor		20000 ohms

The high-mu triode, Developmental No. A-2351, used as a straight-through grounded-grid amplifier operates with an apparent plate-circuit efficiency of 60 to 75 per cent in the range from 400 to 1000 megacycles. The power output is 3 to 4 watts, and the power gain is approximately 5. For this type of service the grid resistor may be lower in value and the plate current higher than for doubler or tripler applications. The circuit used may be similar, except that neutralization of the feedback capacitance is desirable in some cases.

Developmental No. A-2317 may be used as a class C amplifier when more power output is needed than can be obtained from Developmental No. A-2351. Because the amplification factor of Developmental No. A-2317 is lower (approximately 26), a higher bias is required. This tube, however, has a maximum grid current rating of 15 milliamperes and a maximum plate current rating of 35 milliamperes; these values are higher than the corresponding ratings for Developmental No. A-2351. Developmental No. A-2317 can deliver power of 6 to 8 watts at approximately 1000 megacycles with efficiency and power gain of the same order as obtained from Developmental No. A-2351.

Developmental No. A-2317 is intended particularly for pulse service at frequencies up to 3000 megacycles. Figure 13 shows an oscillator cavity of the re-entrant type used for testing Developmental No. A-2317 at 3000 megacycles. The cavity illustrated was designed for a "Lighthouse" type tube, but Developmental No. A-2317 can be inserted

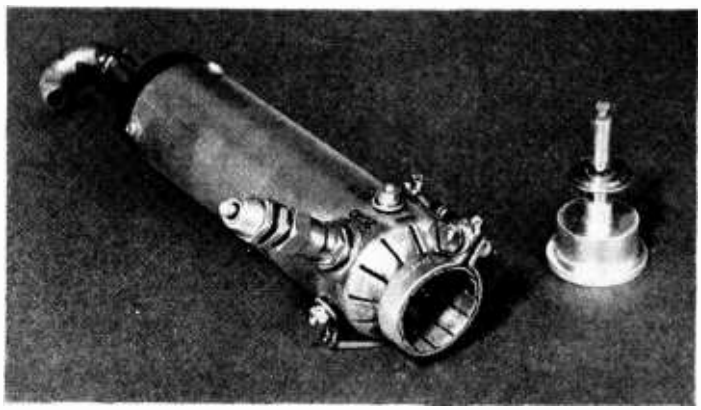

Fig. 13—Pulse test cavity and adaptor for Developmental No. A-2317.

with the addition of a simple circuit part which slides onto the cathode end of the tube. The standard test conditions are:

Heater voltage	6.0 volts
Peak plate voltage	1500 volts
Pulse duration	1 microsecond
Pulse repetition rate	1000 pulses per second
Grid resistor	100 ohms
Average plate current	2.75 milliamperes
Minimum peak power output	650 watts

The average peak power output based on measurements of a number of tubes is approximately one kilowatt; the indicated efficiency for this power output is about 24 per cent.

Applications

Figure 14 shows an experimental receiver operating in the 420- to 450-megacycle amateur band which illustrates one of the possible pencil-tube applications. This receiver used three Developmental No. A-2351 tubes; the first (left) is a grounded-grid radio-frequency amplifier, the second is a grounded-grid mixer, and the third is the

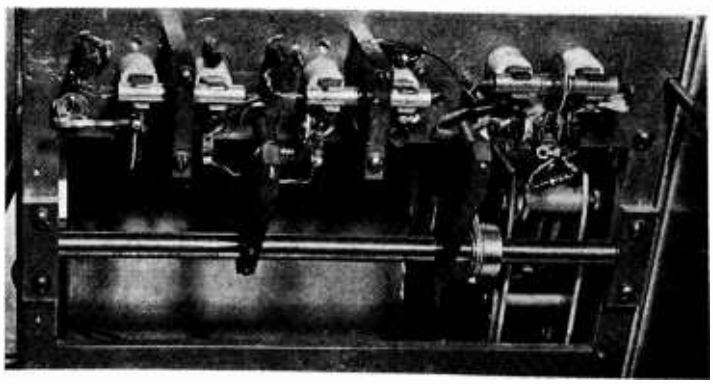

Fig. 14—Tuner, 415 to 455 megacycles.

local oscillator. The circuits are hairpin or single-turn loops. They are aligned by the adjustment of concentric capacitors and tuned with brass cones connected to the manual tuning drive. The tuning range obtained is 415 to 455 megacycles. The intermediate frequency used is 35 megacycles, and the local oscillator is tuned above the signal frequency.

The radio-frequency and mixer tubes are held in place by fuse clips making contact with the anode and cathode, and a cushioning spring which surrounds the grid disk and makes contact with the grid clamping blocks. For the oscillator tube, contact to the grid is made with a spring clip. The local oscillator is coupled to the cathode of the mixer by means of a wire approximately a quarter-wavelength long, capacitively coupled to the oscillator anode and the mixer cathode. The voltage injected into the mixer stage is sufficient to increase the cathode bias from 9 volts to 12 volts.

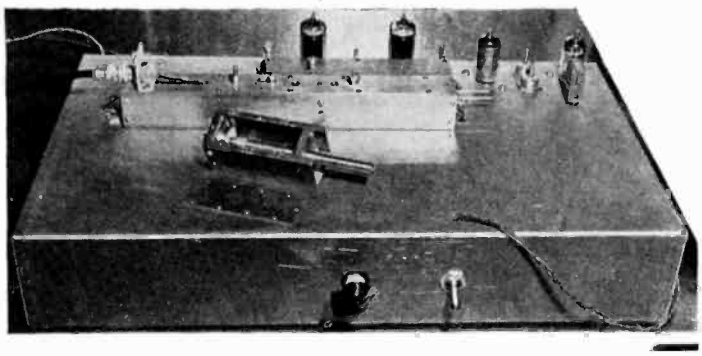

Fig. 15 — Crystal-controlled transmitter, 432 megacycles.

The coupling circuit between the antenna terminal and the cathode of the radio-frequency amplifier tube is tuned near the center of the desired frequency band. The bandwidth of this circuit is wide enough so that no additional tuning is required. The noise factor for this receiver has not been measured, but tests made so far indicate that voice-modulated signals with carrier strengths below one microvolt can be understood.

An experimental low-power crystal-controlled transmitter is shown in Figure 15. The crystal frequency is 5333 kilocycles and the output frequency is 432 megacycles. The oscillator tube is an RCA-6C4. The oscillator is followed by an RCA-6AG5 tripler stage giving an output frequency of 16.0 megacycles, an RCA-5763 tripler giving 48 megacycles, and a second RCA-5763 tripler giving 144 megacycles. The next tube is a pencil triode, Developmental No. A-2351; this tube is also used as a tripler and gives approximately 1.5 watts output at 432 megacycles. The final tube is a Developmental No. A-2317 pencil tube,

operated as an amplifier. The output from this tube is approximately 6 watts. With a grounded-grid amplifier it is desirable to modulate the driving voltage simultaneously with the plate voltage; in this circuit simultaneous modulation is accomplished by modulating the plate voltages of both of the pencil tubes. The direct-current power input to the final amplifier is 10 watts (300 volts, 33 milliamperes); the apparent plate-circuit efficiency, therefore, is 60 per cent.

In Figure 15, the 432-megacycle tripler is mounted in one end of the shorter of the two rectangular boxes, and the final amplifier is mounted near the center of the longer box. These boxes* constitute the plate-tuning cavity for the tripler and the cathode and plate-tuning cavities for the final amplifier. An adjustable loop couples the plate of the tripler to the cathode of the final amplifier. The 144-megacycle driving power for the tripler is obtained from a coil mounted inside the chassis. The small rectangular box on top of the chassis is not a part of this equipment but is included in the photograph to show the method of mounting the tubes.

Conclusion

Experience with the pencil-type ultra-high-frequency triodes indicates that they will be applicable to a wide range of equipment, including transmitters and receivers for mobile communications and point-to-point directional systems; tuners for ultra-high-frequency television receivers; amateur receivers and low-power transmitters; wide-band fixed-frequency amplifiers; remote signalling devices such as the radiosondes.

It is expected that the advantages of small size, low power consumption, and high efficiency obtained by the combination of disk-seal and cylindrical-element construction will give the pencil-type tubes an important place in future ultra-high-frequency equipment.

---

* Mechanical construction of rectangular cavities based on suggestions made by Bell Telephone Laboratories.

DIRECTIONAL MICROPHONE*

By

Harry F. Olson and John Preston

Research Department, RCA Laboratories Division,
Princeton, N. J.

Summary — *The directional microphone is a second order gradient system exhibiting a uniform and narrow directivity pattern and a smooth response frequency characteristic over the frequency range of 50 to 15000 cycles. The directional efficiency, that is, the energy response to random sounds is one-tenth. This order of directivity makes it possible to use a pickup distance up to 12 feet with speech in conventional studios. The use of several of these microphones, fixed in position and each microphone covering a section of the total action, together with a monitoring console makes it possible to cover rapidly changing and larger areas of action with smaller variations in the output level than is possible with the conventional microphone and boom arrangement.*

Introduction

DIRECTIONAL microphones are universally employed to discriminate against all types of undesired sounds in the acoustical pickup system of a sound reproducing system. It has been established that a directional sound collecting system, with a directivity pattern which does not vary materially with the frequency, is the most desirable. Directional sound collecting systems may be divided into two classes, namely, wave and gradient types. Wave type sound collecting systems include line microphones, reflectors, and lenses. The dimensions of a wave type microphone must be of the order of a wavelength or more to obtain any semblance of directivity. A few years ago a line type microphone[1,2] with a high order of directivity was developed and commercialized. The application of this microphone to sound pickup problems has shown that a highly directional microphone is useful in many sound pickup problems. However, the large size (10 feet in length) made it somewhat impractical for many pickup problems. In the case of gradient systems, size is not a requirement. Since gradient systems depend upon differences, there are two major problems, namely, similarity of frequency response of the units,

---

* Decimal Classification: R 385.54.

[1]H. F. Olson, "Line Microphones", *Jour. Inst. Rad. Eng.*, Vol. 27, No. 7, p. 438, July, 1939.

[2]H. F. Olson, ELEMENTS OF ACOUSTICAL ENGINEERING, 2nd Ed., D. Van Nostrand Company, New York, 1947.

and sensitivity. Similarity of frequency response of the units is required in order to obtain a high order of discrimination. High sensitivity is required because the pickup distance becomes greater as the directivity is increased. On the other hand, high sensitivity is difficult to obtain because the system is of the differential type. These two problems have been solved in the development of a second order gradient microphone with a high order of directivity and sensitivity. It is the purpose of this paper to describe a wide frequency range

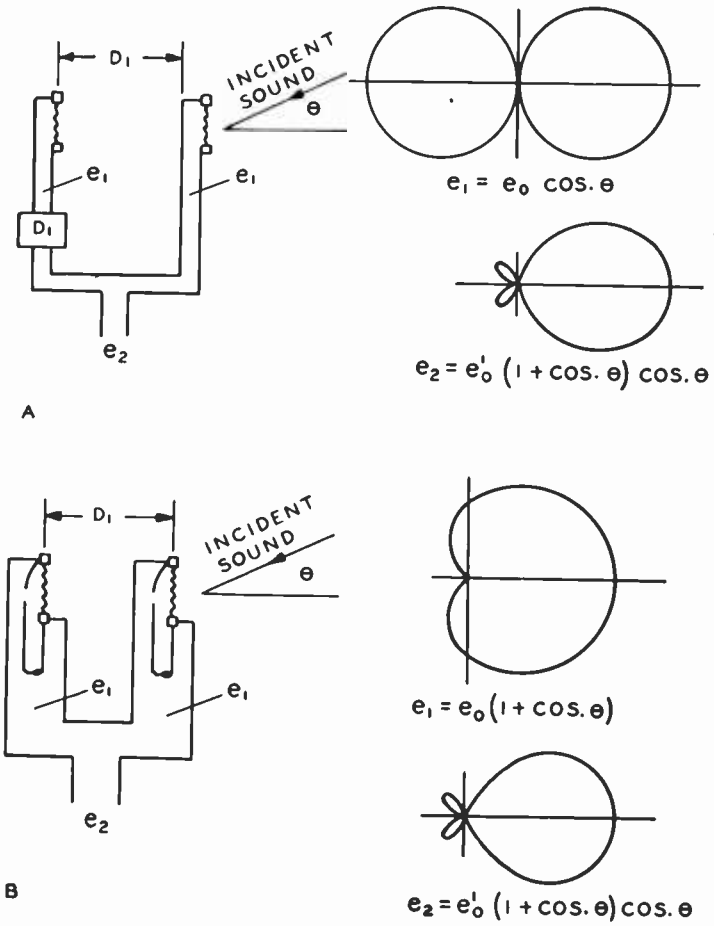

Fig. 1 — Directional microphones. A. Two velocity microphones are combined with a delay network to give a narrow unidirectional pattern. B. Two unidirectional microphones with cardioid characteristics are combined to give a narrow unidirectional pattern.

second order gradient microphone with a high order of directivity and sensitivity.

THEORY

A second order gradient microphone with a unidirectional directivity pattern may be obtained from a combination of two first order gradient microphones and a suitable delay network, or from the combination of two unidirectional microphones each consisting of a first order gradient microphone and a zero order gradient microphone as depicted in Figure 1. The theory of these systems has been given

elsewhere[2,3] and will not be repeated here. Both of these systems have been developed and tested. One system does not appear to possess any particular advantages over the other. However, for the particular principles used in the system which will be described in this paper, the system depicted in Figure 1B was the more suitable. The considerations in this paper will be confined to this arrangement.

The upper limit of the useful frequency range of a second order gradient microphone of the type shown in Figure 1B is determined by the distance between the units. This upper frequency limit is given by

$$f_c = \frac{c}{D} \tag{1}$$

where f_c = upper frequency limit in cycles per second,

c = velocity of sound, in centimeters per second, and

D = distance between the units, in centimeters.

The voltage output of a gradient microphone of the type shown in Figure 1B in the low frequency range, that is, in the range for which $D \ll \lambda$, is given by

$$e = 2e_o \frac{D}{\lambda} \pi \tag{2}$$

where e = voltage output of the combination, in volts,

e_o = voltage output of an individual unit, in volts,

D = distance between the units, in centimeters, and

λ = wavelength, in centimeters.

If the upper limit is 10,000 cycles the distance between the units will be relatively small as given by Equation (1). Under these conditions, Equation (2) shows that the voltage output in the low frequency range will be low. There are two alternatives, namely, to use two systems of the type shown in Figure 1B, one covering the low frequency range, with a relatively large distance between the units, and one covering the high frequency range, with a relatively small distance between the units, or to use a gradient system of the type shown in Figure 1B for the low frequency range, and a wave type system for

[3]H. F. Olson, "Gradient Microphones", *Jour. Acous. Soc. Amer.*, Vol. 17, No. 3, p. 192, March, 1946.

directivity in the high frequency range. A microphone employing the latter combination system will be described in the next section.

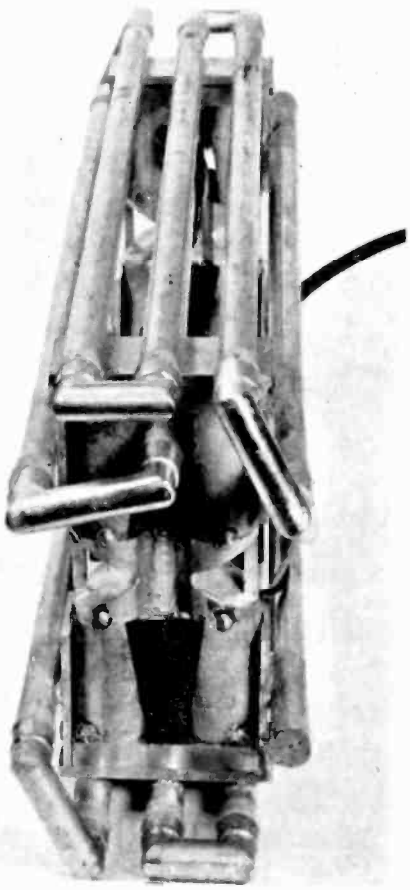

Fig. 2—Photograph taken from the front of the directional microphone with the screen case removed.

Description

The directional microphone employs two similar unidirectional units of the ribbon type as shown by the photographs of Figures 2 and 3. The damped pipe which forms a part of the compound acoustical termination at the back of the ribbon also serves as the frame. The damped pipe terminating the ribbon is quite long, being about 100 inches in length. This length is required in order to maintain phase relations in the low frequency range. The units must be very smooth and free of irregularities in response; furthermore, sensitivity of the two units must be the same within a fraction of a decibel over the entire operating frequency range. If these conditions are not maintained in the gradient frequency range, a high order of cancellation will not be obtained. These conditions have been obtained by special techniques developed for this type of microphone. It was decided

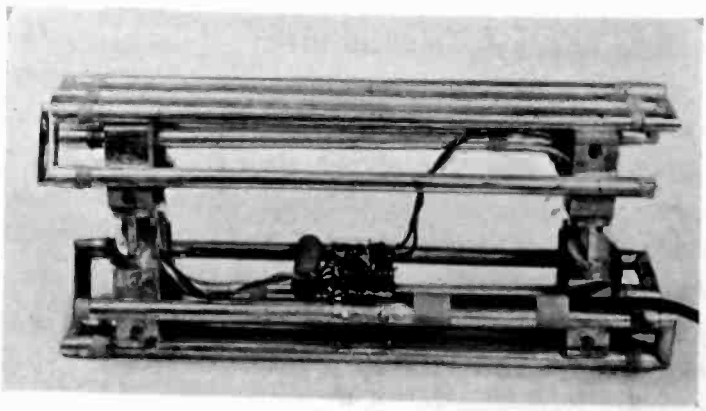

Fig. 3—Photograph taken from the side of the directional microphone with the screen case removed.

to place the two units 12 inches apart. The upper end of the operating range of the system as a second order gradient microphone is approximately 1000 cycles. In the overlap frequency band from 1000 to 2000 cycles, the system operates as a combination gradient and diffraction system. In the frequency range above 2000 cycles the front unit operates alone. The configuration of the magnet structure and the elements of the compound acoustical network which terminates the ribbon were chosen so that diffraction and the acoustical network conspired to form a directional system.

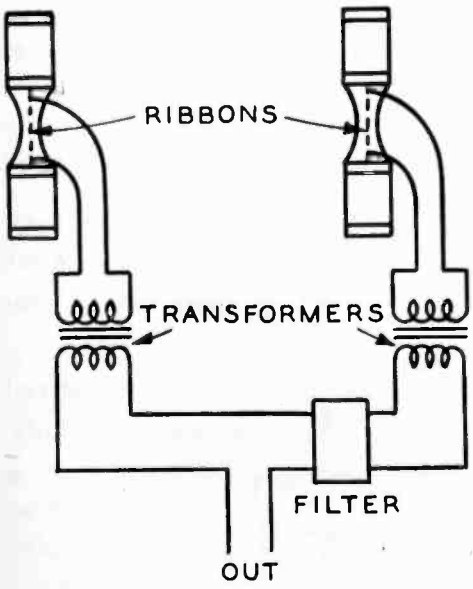

Fig. 4—Electrical circuit diagram of the directional microphone.

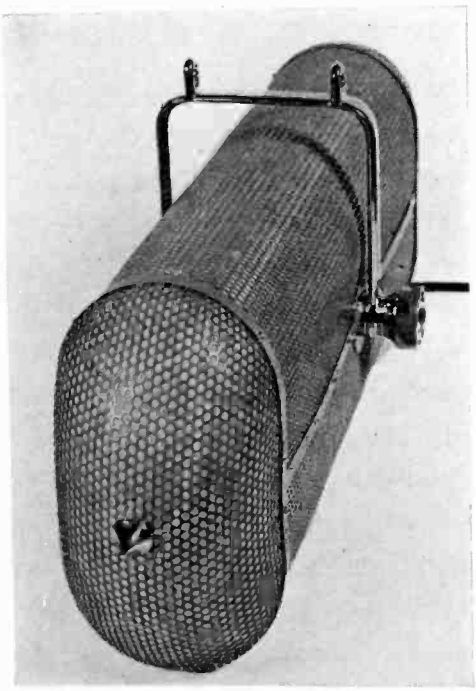

Fig. 5—Photograph taken from the front of the complete directional microphone.

The electrical circuit diagram is shown in Figure 4. The cross-over frequency range in which the output is transferred from the two units in opposition to the single front unit is between 1000 and 2000 cycles. The output impedance is approximately 250 ohms. This is normally raised to 30,000 ohms at the grid of the tube. Under these conditions, the variation in impedance due to the shift from two to one units is not serious. The transformers and electrical network are mounted on the frame between the two units.

A photograph of the complete microphone is shown in Figure 5.

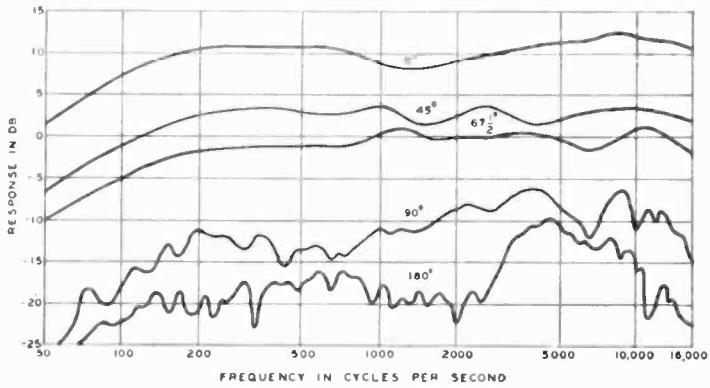

Fig. 6 — Response frequency characteristics of the directional microphone for angles of sound incidence of 0, 45, 67½, 90 and 180 degrees. Output impedance 250 ohms. 0 decibels = 100 microvolts per dyne per square centimeter.

Performance Characteristics

The response frequency characteristics of the complete microphone for various angles of the incident sound are shown in Figure 6. It will be seen that the output falls off rapidly beyond 45 degrees off the axis. The response at 90 degrees and in the rear hemisphere is attenuated 20 to 40 decibels. The sensitivity is about 6 decibels higher than conventional high quality microphones.

The polar directional patterns for 100, 500, 1000, 2000, 4000 and 8000 cycles are shown in Figure 7. These patterns show a high order of directivity. The total angle of reception for one-half energy response is about 60 degrees.

The ratio of energy response of a directional microphone compared to a nondirectional microphone, all directions being equally probable, is termed the directional efficiency. The directional efficiency of a microphone is given by

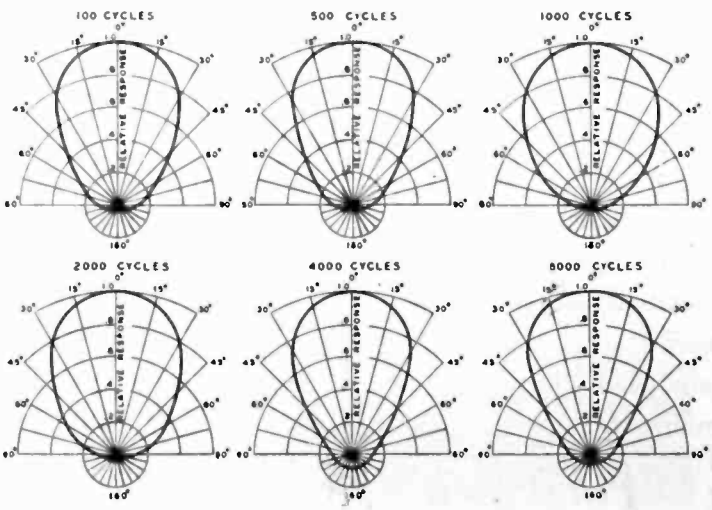

Fig. 7 — Directional characteristics of the directional microphone for 100, 500, 1000, 2000, 4000 and 8000 cycles.

$$\text{Directional Efficiency} = \frac{1}{4\pi} \int_0^{4\pi} f^2(\psi)\, d\Omega_\psi \qquad (3)$$

where $f(\psi)$ = ratio of the voltage output for incidence at the angle ψ to that for $\psi = 0$, and $d\Omega_\psi$ = element of solid angle at the angle ψ.

The directional efficiency of a microphone is a measure of the energy response to reverberation, and other random undesirable sound.

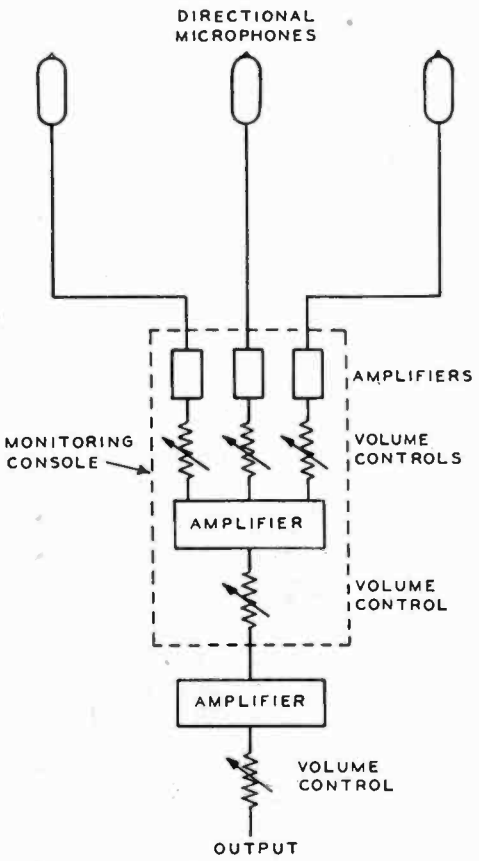

Fig. 8—Schematic diagram of the monitoring system for directional microphones.

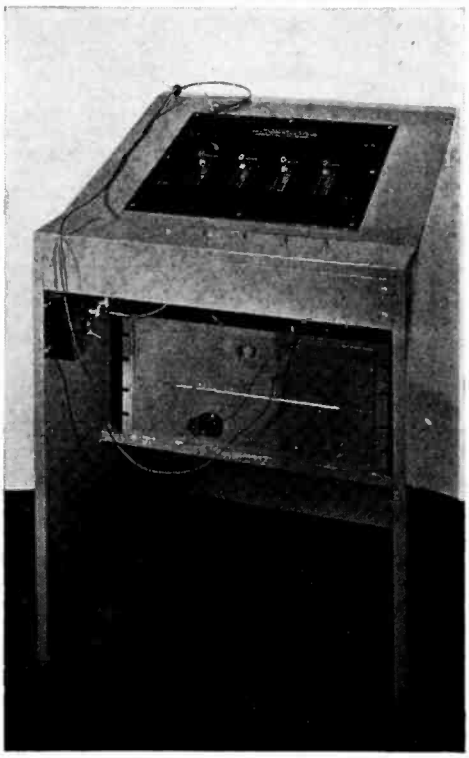

Fig. 9—Photograph of the monitoring console.

In this system, the experimentally determined directional pattern cannot be expressed in simple terms which can be integrated. Therefore, the directional efficiency was determined by numerical integration. The results thus obtained show that this microphone has a directional efficiency of 1/10. This means that for the same noise, reverberation and other undesirable sounds this microphone can be operated at 3.2 times the distance of a nondirectional microphone. This has been verified in subjective tests. In studios of the television and sound

motion picture type, sound pickup distances up to 12 feet on speech are possible without excessive reverberation.

Application of the Directional Microphone

A microphone with a small solid angle of sound pickup is useful in recording sound motion pictures, television, orchestras, radio, stage

Fig. 10 — Photograph of a set with three directional microphones and monitoring console.

productions and many applications in sound re-enforcing. One of the most important applications is that of sound pickup in television. The action in television covers a long period of time, a relatively large range of action with rapid changes in pickup points. In addition, it is becoming increasingly desirable that the microphone be kept out of the picture at all times. In the sound pickup system in use today, the microphone is mounted at the end of a boom which can be moved around by the operator to cover the action and at the same time keep the microphone out of the picture. This system is quite cumbersome and difficulty is experienced at times in covering the action. In the case of a microphone with a high order of directivity it is possible to use a number of fixed microphones arranged to cover the entire area

of action. As the action changes from one area to another, the appropriate microphone is brought into action. A schematic diagram of three microphones and a monitoring console is shown in Figure 8. A photograph of the monitoring console is shown in Figure 9. Slider type volume controls are used instead of rotating knobs to increase the speed of operation. A photograph of a set with three microphones and the monitoring console is shown in Figure 10. The operator at the monitoring console covers the action by fading to the appropriate microphone or microphones. The operator at the monitoring console takes the place of the boom operator. It appears from laboratory tests that the action can be covered in a more satisfactory manner than by means of a boom particularly when the action is complex and shifts rapidly from one part of the stage to another. With operating distances of twelve feet or more, it will be appreciated that the problem of microphone placement is reduced considerably in the case of activity covering the front to the back of the stage.

There is another outstanding advantage for the method of sound pickup shown in the photograph of Figure 10, namely, that the sound is picked up from the front of the stage rather than overhead as in the case of boom microphone pickup. The net result is better illusion, because the sound corresponds to the picture.

MECHANICAL FILTERS FOR RADIO FREQUENCIES*

By

Walter van B. Roberts and Leslie L. Burns, Jr.

Research Department, RCA Laboratories Division,
Princeton, N. J.

Summary—The high Q and small size of metal resonators make them desirable for use in multisection filters for low radio frequencies. This paper describes a simple type of band-pass filter composed of loosely coupled metal resonators with magnetostrictive drive and take-off. Filter characteristics with very sharp frequency discrimination may be obtained by employing a sufficiently large number of sections. Filters of this type are readily constructed for frequencies up to about half a megacycle and with bandwidths from about three per cent down to a small fraction of one per cent. The voltage gain of an amplifier stage utilizing such a filter is generally considerably lower than that of a stage employing electrical circuit coupling, especially at the higher frequencies and wide bands.

Theory and Mathematical Development of Mechanical Filters

A VIBRATING metal rod has a rather low decrement compared to an electrical circuit. For example, the Q of a mechanical resonator or "tank" is of the order of a few hundreds for nickel, several thousands for various steels, and as high as ten thousands for aluminum and its alloys. Furthermore, at radio frequencies the metal tank is small and cheap compared to the corresponding electrical tank so that many of them can be used in a filter.

An electrical circuit is simple compared to a high-frequency mechanically vibratory system. In the electrical case there is only one independently variable quantity, for example, the current. In the mechanical system, however, there may be vibrations in any of the three dimensions. Thus, while a long metal rod may carry longitudinal vibrations governed by the same equations as for an electrical transmission line, it may in addition carry waves of torsion, flexure, and other varieties. One has only to glance over the approximate treatment of the vibrations of a simple cylinder given in Section 199 of A. E. H. Love's A TREATISE ON THE MATHEMATICAL THEORY OF ELASTICITY, Fourth Edition, Cambridge University Press, 1927, in order to realize how complicated must be the vibration pattern in more elaborate structures such as are needed for filter operation. For these reasons it appears that the variety of structures providing filter

* Decimal Classification: R 386.1.

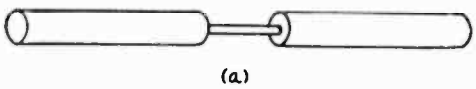

(a)

Fig. 1 (a)—Neck type single section filter; (b)—Slug type filter section.

(b)

characteristics is almost endless. In what follows, only such constructions will be considered as will, by virtue of symmetry and dimensions, operate in a substantially single mode of vibration analogous to the electrical transmission line. For this purpose the longitudinal mode will be chosen, although other modes, especially torsion, could be used.

The basic unit of the filters to be described is a single section filter composed of a pair of similar longitudinal resonators loosely coupled together so as to possess a pair of resonant frequencies marking the limits of its transmission band. Figure 1-a shows, as one way of making such a section, a pair of half-wavelength resonators connected together by a neck so thin as to act like a weak spring. Both ends of each resonator are motional loops at each of the resonant frequencies. On the other hand Figure 1-b shows a pair of quarter-wave resonators coupled by a "slug" which is relatively thick so that it acts somewhat as a heavy mass. In this case only the free ends of the resonators are motional loops. The band limits in either case can be determined by calculating the frequencies at which the tanks are resonant when vibrating in the same phase and in opposite phases. However, to obtain a more complete picture it is desirable to make use of the fact that these filter sections are mathematically equivalent to electrical filters composed of equal lengths of transmission line connected by a piece of line of different characteristic impedance.

Figure 2 shows the electrical filter section corresponding to Figure 1. Its tank portions have electrical length θ_1 and characteristic impedance Z_1 while the connecting portion has length θ_2 and impedance Z_2. The pass bands for a filter composed of any number of such sections connected end to end are the frequency ranges within which the iterative impedance of the section has a real component so that it can accept power from the driven end. The expression for the iterative impedance may be obtained by applying the definition of iterative

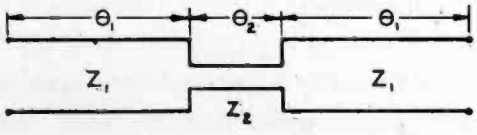

Fig. 2—Electrical filter section analog of Figure 1(a).

impedance, that is, by equating the unknown iterative impedance to the input impedance of the section when its output is connected to the same unknown impedance. It is perhaps simpler, however, to make use of the fact that the square of the iterative impedance is the product of the input impedances when the section is open circuited and short circuited at its center. By either method the square of the iterative impedance is found to be:

$$Z_1^2 \frac{(\tan \theta_1 + \phi \tan \tfrac{1}{2}\theta_2)(\phi \cot \tfrac{1}{2}\theta_2 - \tan \theta_1)}{(\cot \tfrac{1}{2}\theta_2 - \phi \tan \theta_1)(\tan \tfrac{1}{2}\theta_2 + \phi \tan \theta_1)}. \tag{1}$$

Which may also be written

$$\frac{Z_1^2}{\phi^2} \frac{\tan^2 \theta_1 - 2\phi \tan \theta_1 \cot \theta_2 - \phi^2}{\tan^2 \theta_1 - 2/\phi \tan \theta_1 \cot \theta_2 - 1/\phi^2} \tag{2}$$

in which expressions ϕ stands for the ratio Z_2/Z_1.

Since a pass band occurs in any range of θ_1 in which the above expressions are positive, it is evident that band limits are given by the roots of both the numerator and denominator of these expressions. If ϕ is either very small or very large the roots occur in closely spaced pairs. i.e., the pass bands are narrow. Within a pass band defined by a pair of roots of the numerator it is evident that the iterative impedance falls to zero at the band edges and has a maximum near midband. Denominator roots on the other hand define bands in which the iterative impedance rises to infinity at the band edges and is minimum at midband.

In a given structure the ratio θ_2/θ_1 is fixed so that Expressions (1) and (2) can be simplified for a number of particular values of this ratio. For example, if $\theta_2 = \theta_1$, a series of pairs of band edges is given by $\tan^2 \theta_1 = 2\phi + \phi^2$ and another series by $\tan^2 \theta_1 = \frac{2}{\phi} + \frac{1}{\phi^2}$. These expressions hold good for either neck-type or slug-type filters, the former type being defined as one having a value of ϕ small compared to unity, while the latter has ϕ large compared to unity. One of the important cases in practice to which the above equations apply is the slug-type filter with quarter-wave tanks. The first of the two equations is used since a large value of $\tan \theta_1$ is required. In this case the angular difference between the values of θ_1 satisfying the equa-

tion is readily determined to be approximately $\frac{2}{\phi}\left(1-\frac{1}{\phi}\right)$ for large values of ϕ. Since the angular length of the tanks is $\pi/2$ the fractional bandwidth, that is the ratio of bandwidth in cycles per second to the midband frequency in cycles per second, is $\frac{4}{\pi}\frac{1}{\phi}\left(1-\frac{1}{\phi}\right)$.

It may be noted in passing that the equations indicate the existence of pass bands when the elements are a multiple of a half wave in length, but that the fractional bandwidth in this case is determined by the square root of ϕ (or its reciprocal, according to the type of filter) so that an impractically great disparity between tank and coupler impedances is required to obtain a narrow band. This is the case treated for transmission line filters by Warren P. Mason in his book, ELECTRO-MECHANICAL TRANSDUCERS AND WAVE FILTERS, pages 75-77, D. Van Nostrand Co., 1942.

Another important case in practice is $\theta_2 = \frac{1}{2}\theta_1$ for which a straightforward solution gives an approximate fractional bandwidth $\frac{2}{\pi}\phi\left(1-\frac{\phi}{2}\right)$ for tanks a half-wave long and small ϕ. Again, there are other pass bands of lesser interest for the same structure.

One more particular case of importance is $\theta_2 = \frac{1}{3}\theta_1$. This covers a section composed of resonators three-quarter waves long coupled by a slug one quarter wave long. This is a desirable section for a magnetostriction driven slug-type filter because the drive and take-off resonators have motional nodes available for the coupling coils. The fractional band in this case is approximately $\frac{4}{3\pi}\frac{1}{\phi}\left(1-\frac{1}{3\phi}\right)$ for large values of ϕ. Comparing this band with the band previously found for a section with quarter-wave resonators coupled by quarter-wave slugs, it will be seen that the bandwidth is nearly, although perhaps not exactly, inversely proportional to the number of quarter waves composing the resonator.

While the bandwidth can be expressed explicitly for various simple relations between θ_1 and θ_2 as illustrated above, it can also be determined approximately in the general case, at least for the case of narrow bands. For referring back to Expressions (1) and (2), the roots of the numerator occur when $\tan \theta_1 = \phi \frac{\cos \theta_2 + 1}{\sin \theta_2}$, while roots

of the denominator occur when $\tan \theta_1 = \frac{1}{\phi} \frac{\cos \theta_2 + 1}{\sin \theta_2}$. If now the band is sufficiently narrow so that $\sin \theta_2$ can be considered as constant throughout the band, then the angular bands between roots are approximately $\frac{2\phi}{\sin \theta_2}$ for ϕ very small, and $\frac{2}{\phi} \frac{1}{\sin \theta_2}$ for ϕ very large. From these expressions it is evident that in every case the band is minimum when $\sin \theta_2 = 1$, i.e., when the coupling element is an odd multiple of a quarter-wave long. It will also be noted that considerable departure from the optimum length of coupler element is possible without much increase in bandwidth.

A reasonably convenient graphical solution for Expression (1) which applies to any ratio θ_2/θ_1 can be carried out as follows: Two circles are drawn with their centers at the origin, one with radius unity and the other with radius ϕ. Straight lines are drawn tangent to each circle at its top, bottom, and two sides. A line from the origin

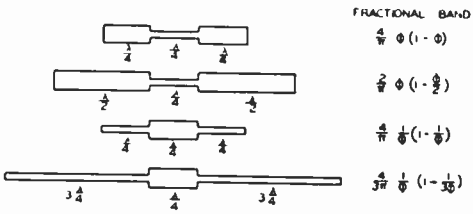

Fig. 3—Fractional bands produced by various practical single section filters.

at angle θ_1 intersects lines tangent to the unit circle at points proportional to $\tan \theta_1$ and $\cot \theta_1$. Another line at angle $\frac{1}{2}\theta_2$ intersects the ϕ circle tangent lines at points giving $\phi \tan \frac{1}{2}\theta_2$ and $\phi \cot \frac{1}{2}\theta_2$. By revolving the two lines from the origin while keeping the ratio of their angles constant the value of θ_1 may be determined which makes the numerator of Expression (1) vanish. The same construction will give all the roots. However, as this method of analysis is not likely to be required in view of the solutions already obtained for the more important practical cases it will not be elaborated in further detail. For convenient reference these practical cases are assembled in Figure 3. From this table approximate bandwidth for tanks of greater length can be inferred by assuming the bandwith to vary inversely as the tank length, while the band is substantially unaffected by the length of the coupling element so long as it is an odd multiple of a quarter wave.

Practical Limitations on Bandwidth

In a mechanical filter, the characteristic impedance of each portion is the product of its cross-sectional area and the intrinsic impedance

of the material of which it is made, the latter quantity being in turn the product of its density and the velocity of propagation of longitudinal waves along that portion. If all the filter is made of the same material, the quantity ϕ is simply the ratio of cross sections, assuming that the sections are small enough so that the velocity is the same in all portions. As has been demonstrated, ϕ or $1/\phi$ must be of the order of the desired fractional bandwidth. If a one per cent band is required, this means that a neck-type filter turned out of round stock must have a neck diameter only about one-tenth that of the tanks. It is easy to see that narrowness of band is limited by flimsiness of the structure. Matters are even worse if the filter is cut out of flat strip material (which would otherwise be a desirable construction because of the ease of punching such filters out in quantity) because in this case the neck width must be ϕ times the tank width. At this point it might be thought that while there is a limit to the smallness of ϕ practically obtainable in neck-type filters, ϕ could be made as large as desired in slug-type filters by simply making the slug large enough. Unfortunately, however, if the slug diameter is made too large it begins to vibrate in various undesired modes. Such undesired responses could perhaps be avoided by careful design or even employed to provide rejection points outside the pass band,[1] but for present purposes it appears preferable to keep the design as noncritical as possible by keeping all extraneous responses well away from the desired pass band.

A simple expedient for narrowing the band of the type of section heretofore discussed without changing the practically obtainable value of ϕ is to use longer tanks. This, however, cannot be carried too far as it results in an inconveniently long filter if many sections are employed, and also brings other pass bands too close to the desired band. A second expedient which applies to slug-type filters is to use thin walled tubing for the tanks so as to reduce their cross sectional area without a corresponding loss of sturdiness. In addition a material of higher intrinsic impedance may be used for the slugs than that used for the tanks. For example, steel slugs may be drilled and soldered to nickel plated aluminum rod or tube tanks. By the use of one or more of these expedients, bands sufficiently narrow for many purposes have been obtained without resulting in too flimsy a structure. One combination that has proved satisfactory employs steel ball bearings (annealed for easy drilling) soldered on thin wall nickel tubing. While this filter is not readily analyzed mathematically it has

[1] Mason, U. S. Patent 2,345,491, for example.

been found that a ball diameter of about a quarter wave is suitable, the bandwidth being controlled by the choice of tube diameter and wall thickness. It is thought that balls are less likely to develop extraneous resonances than the corresponding cylindrical slugs because the lowest natural frequency of a ball a quarter wave in diameter is nearly twice the operating frequency. The lowest frequency of a steel ball one inch in diameter is about 100 kilocycles, while for other sizes the frequency is inversely proportional to diameter.

Filters for Very Narrow Bands

From the foregoing it is evident that to obtain bands as narrow as the high Q of aluminum makes possible, or to obtain moderately narrow bands in the case of filters punched out of strip stock, some radically different method for obtaining sufficiently loose coupling is necessary. Many such methods have been tried with more or less success. For example, the coupling element may be connected between

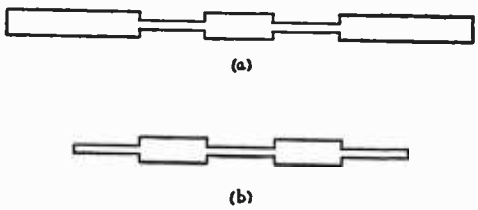

Fig. 4(a) — Twin quarter-wave neck-type of single-section filter; (b)—Twin quarter-wave slug-type of single-section filter.

points on the tanks near motional nodes where the same coupling element is less effective. Again, linear tanks may be coupled by inertia effects, for example, by one or more small steel ball bearings pressed between the sides of parallel tanks; the different kinetic energies imparted to the balls when the tanks vibrate in and out of phase produce two natural frequencies in the system and the bandwidth is less the nearer the balls are located to motional nodes of the tanks. But the simplest and most satisfactory method so far discovered for obtaining a very narrow band is to use what will be called multiple-neck or multiple-slug coupling elements. Figure 4 shows neck and slug-type sections coupled by twin elements. In Figure 4(a) two half-wave tanks are coupled by twin quarter-wave necks separated by a quarter-wave slug, while in Figure 4(b) two quarter-wave slugs are separated by a quarter-wave neck. A physical picture of the operation of these coupling systems may be had by considering one element adjacent to a tank as the actual coupling element while the other two act as two quarter-wave transformers in tandem which transform the impedance of the other tank to a value still further out of line with that

of the coupling element. The central element of these sections need not be of the same impedance as the tanks, but it facilitates analysis and is a convenient construction.

The pass bands and terminating impedance may be determined exactly as in the case of the simple coupling elements by obtaining an expression for the iterative impedance of the section. The derivation is, of course, more lengthy and leads to a more complicated expression for the square of the iterative impedance, namely,

$$\frac{Z_1^2 \quad \tan^4\theta - (\phi^4 + 2\phi^3 + 3\phi^2 + 4\phi)\tan^2\theta + (2\phi^3 + 3\phi^2)}{\phi^4 \tan^4\theta - (1/\phi^4 + 2/\phi^3 + 3/\phi^2 + 4/\phi)\tan^2\theta + (2/\phi^3 + 3/\phi^2)} \tag{3}$$

when all five elements of the section are of equal length. The bands of chief interest are those which occur when the elements are in the vicinity of a quarter-wave long, or odd multiple thereof. The bandwidth may be determined from the above expression, but for practical purposes it is sufficient to figure that the band is narrower by the factor ϕ (or $1/\phi$ for slug-type filters) as compared to the corresponding filter with a single coupling element. Another factor ϕ may be obtained by adding another pair of quarter-wave elements to form a triple-neck or triple-slug coupling. Thus, by using a sufficient number of elements in the coupler it is possible to obtain as narrow a band as desired without requiring ϕ to be impractically large or small. Another way of looking at the multiple coupler is to consider it as a low-pass filter operating above cutoff and hence attenuating, in a non-dissipative manner, vibrations passing through in either direction. From this point of view it seems probable that other forms of filters operating in an attenuating band could be employed as loose coupling means between tanks of the composite filter.

Choice of Materials

For the internal sections of any filter it is generally desirable to use a material of the highest possible Q. For this reason aluminum would be the unquestioned choice except for its large temperature coefficient of frequency, (about 200 parts per million per degree Centigrade). Where temperature stability is of primary importance, some isoelastic material such as the nickel alloy "Ni-Span C" may be used. This alloy has good magnetostrictive activity and better Q than nickel but is not as yet obtainable in thin walled tubing. It is available in standard wire gauges, and filters have been made by soldering steel balls on the wire. Although the Q of nickel is low compared to some

other metals, it is still high enough for filters that are not extremely narrow band and do not require extremely sharp cutoff. These three materials are the ones that have been mostly used. The steels have high Q but have much higher intrinsic impedance than aluminum which, as will be shown later, makes it more difficult to terminate the filter non-reflectively. Thin walled steel tubing however, might be a good choice in some cases. Table I shows some of the properties of interest in connection with filter design for a few common materials.

The data given were obtained from single samples three inches long, nickel plated where necessary to provide magnetostriction. The samples were inserted through a hole in a shield and small coils were placed on each end. In every case the coils were tuned off the resonant frequency of the sample to prevent loading. The signal generator was connected to one coil and a vacuum tube voltmeter to the other. The frequencies at which the output voltage dropped to 70.7 per cent of its maximum value were then determined and their difference divided into the center frequency to determine the Q of the sample.

Table I

Material	Density gms/cm³	Longitudinal Velocity in Thin Rod $\times 10^{-5}$ cm/sec	Intrinsic Impedance $\times 10^{-6}$	Q
1. Aluminum	2.73	5.11	1.39	4000
2. Armco Iron	7.76	5.13	3.98	850
3. Beryllium Copper	8.26	3.73	3.08	4900
4. Brass (Hard)	8.54	3.64	3.11	2500
5. Brass (Soft)	8.5	3.52	2.99	2000
6. Copper	8.95	3.72	3.33	1700
7. Dural	2.81	5.07	1.43	8000
8. Ferrite	4.46	5.58	2.49	1250
9. Invar	8.62	4.01	3.46	5000
10. Kovar	8.19	4.08	3.34	3500
11. Lead	11.3	1.49	1.68	40
12. Molybdenum	10.4	5.63	5.85	1700
13. Monel (K)	10.3	5.67	5.84	3300
14. Nickel	8.88	4.94	4.39	450
15. Ni-Span C	7.99	4.8	3.83	900
16. Phosphor Bronze	8.9	3.52	3.14	2000
17. Silver Solder (BT)	10.1	2.96	2.99	900
18. Solder (50-50)	8.84	2.08	1.84	72
19. Steel (Cold Rolled)	7.71	5.04	3.89	1100
20. Steel (Drill Rod)	7.86	5.13	4.03	900
21. Steel (Stainless)	7.94	4.97	3.95	1500

Drive and Take-Off Methods

For most purposes the mechanical filter must be driven from an electrical source and deliver power to an electrical load, and there seem to be only two methods of electromechanical conversion available that will operate at radio frequencies with reasonable efficiency. Perhaps the best in the long run, especially at frequencies above about 500 kilocycles, is the piezoelectric method. Permanently polarized barium titanate[2] appears particularly suitable for filter use. It can be applied in several ways. For the lower frequencies, a thin strip of titanate, silvered on both sides, may be soldered to the side of the end resonator of a filter. The application of radio-frequency voltage between the silver electrodes alternately stretches and contracts the strip in length, thus driving the resonator. Or the resonator may be cut transversely at a motional node and a thin wafer of titanate soldered between the cut portions. In this case the drive is effected by the change of thickness of the wafer when voltage is impressed across it. In both cases, of course, the composite resonator must be tuned after assembly. At very high frequencies the wafer may become a half wave long so as to be a resonator by itself, and replace a half wave of the original filter. Filters using the titanate have been made and tested sufficiently to indicate their possibilities but most of this filter work has employed the other method of drive and take-off, namely, magnetostriction. For this reason the present discussion will be limited to this type of operation, although the reason for using magnetostriction was chiefly that experimentation with the construction of the filter itself can be carried out most readily with the aid of magnetostriction. That is, by using magnetostrictive materials for the resonators or rendering them magnetostrictive by nickel plating them, the resonant frequency of any individual tank can be tested. Also if all the tanks are similar, including the tanks on the ends of the filter which cooperate with the drive and take-off coils, the filter can be made all in one piece and hence conform most accurately to theory.

Probably the main objection to magnetostrictive operation is the poor efficiency, especially at the higher frequencies, due to eddy current losses in the material, which is usually nickel or one of its alloys. This drawback can, however, be largely overcome by employing a material with very little losses. Ferrites, which are magnetic ceramic materials, have negligible eddy current losses and mechanical Q of the order of one or two thousand, and ferrites have been developed

[2] H. L. Donley, "Barium Titanate and Barium Strontium Titanate Resonators", *RCA Review*, Vol. IX, No. 2, pp. 218-228, June, 1948.

in the laboratory which have as large a magnetostrictive coefficient as nickel. If the end half waves of a filter be replaced by half waves of ferrite of the same characteristic impedance, a very efficient conversion is possible. Drive and take-off ferrite resonators may be cemented to the filter metal, or the ferrite may be copper plated at one end to permit soldering. The use of ferrites seems particularly desirable in broad-band filters when the highest conversion efficiency is required. For narrow-band operation nickel-plated aluminum is very satisfactory.

Figure 5 shows the drive and take-off arrangement typical of all the magnetostrictively-operated filters. A closely fitting coil is placed over the middle of the end half wave of the filter to provide magnetostrictive coupling. A permanent magnet (not shown) is located so as to magnetize the part of the filter under the coil in a longitudinal direction. The field is adjusted to give maximum drive, which requires that the material be something like half saturated. The shorter the piece of magnetostrictive material the stronger the field required. The impedance of the driving coil has a large resistive component due

Fig. 5 — Typical drive and take-off arrangement for magnetostrictively operated filters.

partly to losses in the material and partly to the motional reaction of the filter. The other coil and the condenser are chosen to constitute an L section matching network to match the driving coil to the source of electrical power, or to the grid of the following tube in the case of the take-off end of the filter. At the right-hand end in the figure is shown a unit comprising the network shown schematically at the left. The filter illustrated is a slug type with three-quarter-wave ends operating at 300 kilocycles with a band of 3 per cent. The tanks are thin wall nickel tubing and the slugs are 3/16-inch steel balls. As a refinement of this arrangement the tuning core shown at the left may consist of a ferrite rod whose length is chosen to give mechanical resonance just outside the transmission band. This steepens the cutoff considerably by destroying the impedance matching action of the network just outside the band. The ferrite must of course also be located in the magnet field but only a weak field is needed to produce the best results. Such rejector ferrites may be put at each end of the filter and in fact a bundle of slightly differently tuned ferrites may be used

to provide multiple rejection points, although this complication is not likely to be justified. The rejector ferrites are used as tuning cores also since their rejecting function is not much affected by their exact location in the coil.

Stage Gain

Since filters are normally used as a coupling means between two amplifier tubes, the gain of such a stage is a matter of some importance. However, since the gain is secondary to the prime function of selectivity not many gain measurements have been made. A few examples will give an idea of what can be expected. In the case of a ball on a nickel tube filter operating at 300 kilocycles with a 3 per cent band, a voltage gain of 9 was measured between 6SJ7 tube grids. A 100-kilocycle filter with band width 2.5 per cent and having ferrite drive and take-off elements gave a voltage gain approximately 70 per cent of that obtained from ordinary tuned-circuit coupling. The gains obtained appear to be less the higher the frequency as well as the broader the band.

Terminations

The least satisfactory thing about mechanical filters seems to be their termination. A filter should be terminated in a resistance equal to the iterative impedance of the section and this is not constant over the band, as has been noted. Without some form of damping in the filter the output consists of a series of peaks with deep valleys between. If the filter is made of relatively low Q material such as nickel, and is sufficiently narrow band, the peak-to-valley ratio may be satisfactory without any additional terminating resistance. The same is of course true of any material if the band be made narrow enough. But perhaps the only way to get a perfect termination without depending on losses within the filter is to extend the filter a few sections beyond the take-off point and introduce sufficient losses into these extra sections so that vibrations entering these sections are substantially damped out by the time they are reflected back to the pick-up point. This arrangement, however, allows most of the power transmitted to flow past the pick-up point and relatively little into the useful load. The best compromise method so far discovered is to provide the tightest possible megnetostrictive coupling between the drive and take-off filter elements and their associated coils, which assures maximum power transfer and also provides a corresponding amount of mechanical damping of the end resonators; and then if the peak-to-valley ratio is still too great, to add mechanical resistance until the best shaped response curve is obtained. One way to add damping is to coat the

end resonators with a viscous material such as vaseline or silicone oil, but it sometimes happens that this not only damps the resonator but also appreciably detunes it. A theoretically better way to add a pure mechanical resistance is to connect the end of the filter to a long rod of lossy material having characteristic impedance chosen (by giving it the correct diameter) to match the filter impedance somewhere inside the band. In practice a rather short rod-shaped piece of viscoloid cemented by its own solvent to the filter tip has been found to reduce very bad peak-to-valley ratios to an acceptable value. Tungsten loaded neoprene is even better. Of course, it is desirable to provide as great as possible a proportion of the required damping by the reaction of

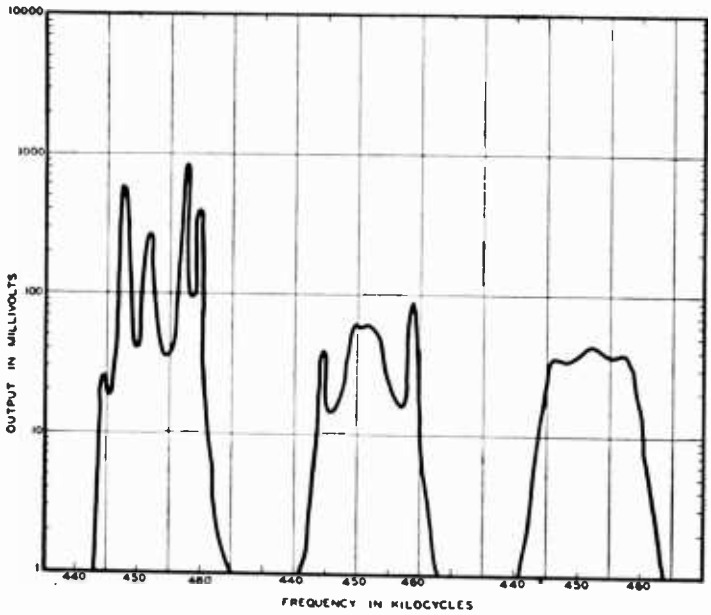

Fig. 6 — Effect of viscoloid end pieces on both ends, one end, and totally removed.

the drive and take-off circuits; for this reason the mechanical impedance of the tanks should be made as low as possible in proportion to the magnetostrictive coupling. For example, if the take-off tank is a nickel-plated aluminum tube of given diameter and thickness of plating, then the thinner the wall, the less the filter impedance and hence the less the terminating resistance required. Thus, since the reaction damping is constant, it should be possible to make the wall thin enough so that no extra damping is needed. On the other hand, if the end tank is nickel-plated solid rod, it will be seen that small diameter favors the ratio of magnetostrictive coupling to filter impedance. While the termination problem cannot be said to be solved in an entirely satisfactory manner, yet, by a certain amount of cut and try with a given filter, very useful performance can be obtained for bands as wide as commonly desired. Figure 6 shows three curves for

a four-section aluminum filter having a 15-kilocycle band centered on 452 kilocycles. The curve with the high peaks is without viscoloid end pieces, the smoothest curve is with pieces on both ends, while the middle curve has a piece on the output end only.

TUNING-UP METHODS

The individual resonators of a filter should be tuned to the same frequency. It is probable that commercially manufactured filters can be made to such close tolerances that no tune-up will be required, providing the bandwidth is large compared with the tolerance. However, very narrow band filters and experimental filters will usually require tuning up.

The bridge circuit of Figure 7 has been useful for this purpose. L_1 and L_2 are identical small universal wound coils. The output transformer is wound on a high permeability torus. The meter is a Ballantine vacuum tube voltmeter giving full scale deflection on ten millivolts input. The magnetostrictive resonator to be tested is placed in coil L_2

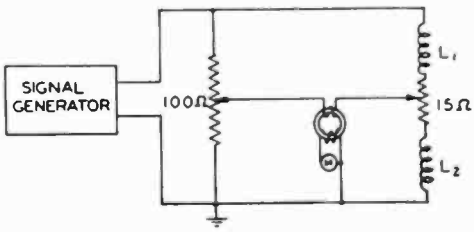

Fig. 7—Bridge circuit for tuning up mechanical filters.

and, preferably, a similar piece of material is placed in L_1. A polarizing magnet is placed near the specimen. The bridge is then brought near balance by means of the variable resistors. There should, however, be sufficient unbalance to give about half scale reading on the meter, and the unbalance should be with respect to the resistive component of the coil containing the specimen. Thus when the frequency of the source is adjusted to be the same as the resonant frequency of the sample the motional resistance produced in the coil by vibration of the sample shows up as a change in meter reading. With high Q resonators this dip or rise in reading is so sharp that the frequency of the generator must be changed very slowly to avoid passing over the response without noticing it. The bridge is a very sensitive indicator of mechanical resonance when operated near balance and with considerable input voltage. It will in fact indicate vibrations of metal discs and rings produced by the interaction of a magnet field with eddy currents set up in the disc or ring by coupling to the bridge coil. (For example, a new Roosevelt dime responds to 112-kilocycle excitation).

For the purpose of testing the tanks of a complete filter all the tanks not being tested must be so damped or detuned as to leave the frequency of the free tank in the test coil substantially unaffected by resonance of the others. This can usually be accomplished by putting tight fitting clamps on the adjacent tank or tanks. Gripping the adjacent tanks firmly between the fingers will sometimes be sufficient. When each resonator has been tested, if it is found that any one is too far out of line with the others, it is then tuned either up or down by filing. Filing away material at motional loops increases the frequency while filing at nodes decreases it. For decreasing the frequency of a neck-type filter it is more of a reversible operation to put a ring of solder around one or both ends of the resonator and then file solder off until the frequency is correct. This method of testing can be used for any filter, whether intended for magnetostrictive or piezoelectric operation, provided the resonators are made of magnetostrictive material or are nickel plated.

In the case of wide band filters there may be difficulty in sufficiently freeing the tank under test from effects of the adjacent tanks, because of the tight couplings. Of course, in the case of very wide bands the filter should not require tune-up because the tolerances are great enough to permit sufficiently accurate machining in the first place. However, it may be well to mention a type of filter construction that permits individual tune-up of each tank without difficulty. This method applies to single neck-type filters particularly. Each resonator is turned out separately with an eighth-wave tip wherever a neck should be. Then when the tips are butt welded or soldered together and excess solder filed off, the structure is indistinguishable from a one-piece filter, by eye at least. It is, of course, not nearly as solid. This method has been used with resonators turned out of nickel-plated aluminum rod stock which leaves the tips unplated and requires aluminum solder. The tips are first tinned and then sweated together in a jig that keeps them lined up. They must be tuned up before tinning. The amount of solder left in the joint after the ends are pushed tight together and the excess removed is so small that it has no apparent effect on the distribution of the resonant frequencies within the band. Filters made this way have been found to have resonances occurring very accurately at the intervals predicted by theory.

Torsion Filters

The propagation of torsional waves along a rod is governed by the same equations as for linear vibrations, except that the velocity is

only about 60 per cent as great. This makes low-frequency filters more compact but is undesirable for frequencies so high that tanks are inconveniently short. There is, however, one important difference in favor of torsional operation which is that the quantity corresponding to characteristic impedance is in the case of torsional operation proportional to the fourth power of the diameter rather than to the square as was the case for linear vibrators. Thus the same filter which gives a wide band when operated linearly will give a narrow band when operated in torsion. Or to put it another way, a narrow band torsion filter can be made without very great disparity in diameter between the tank and coupler portions.

In order to use a filter in the torsional mode some modification of the drive and take-off arrangement is necessary. While there are a number of ways in which torsion may be produced, it has been found

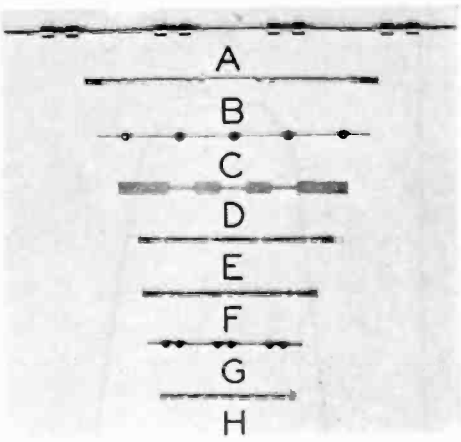

Fig. 8 — Examples of mechanical filters showing various constructions and coupling means. See Table II.

that the most simple and satisfactory method is to nickel plate only one half of the circumference of the drive and take-off tanks and to apply a transverse magnet field in the plane including the edges of the plating. The combination of the constant transverse magnetization with the alternating longitudinal magnetization produced by the driving coil gives a resultant magnetization which swings back and forth in direction about a mean position approximately transverse to the axis of the resonator, thus tending to twist the resonator ends first one way and then the other about the central plane. If the resonator being driven includes more than one half-wave, the adjacent half-waves may be plated on opposite sides of the resonator so that if the driving coil extends over both half-waves, the torques produced in the various half-waves will be additive in effect.

A particular application of the torsion filter is for extremely narrow band operation which can be achieved by the use of multiple-

neck coupling and which is made possible by the fact that magnesium has a uniquely high Q when operated in torsion,[3] namely about 100,000.

Some Illustrative Examples

In conclusion several filters are shown in the photograph Figure 8 to illustrate physical embodiments of the various types described. Table II gives the frequency and bandwidth of each of these.

Figures 9 and 10 show typical characteristic curves to give an idea

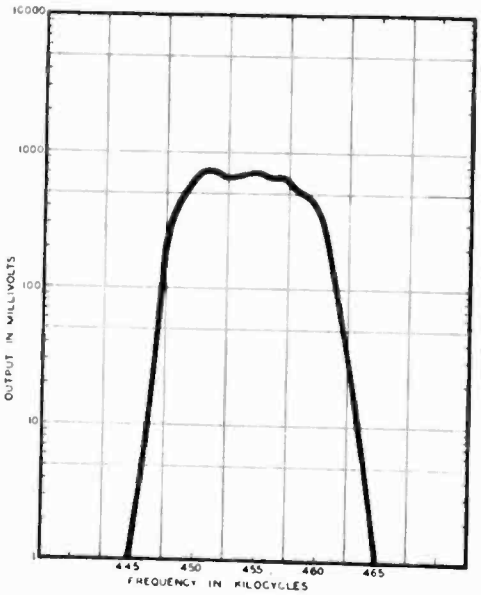

Fig. 9—Characteristic curve of an eight section filter employing steel balls on thin wall nickel tubing.

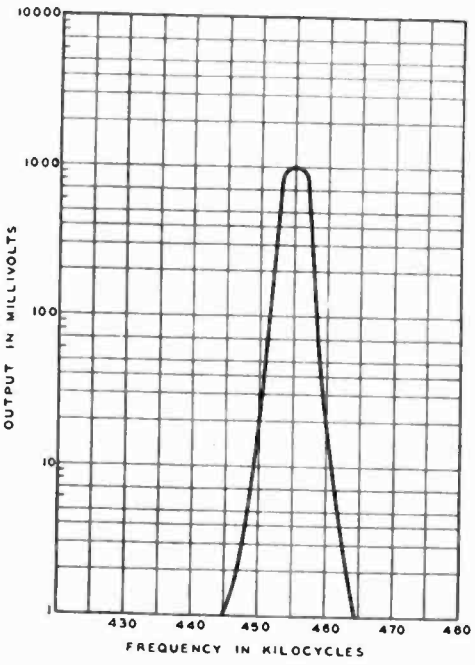

Fig. 10—Characteristic curve of a three section filter employing twin steel ball couplers on nickel tubing. Filter "G" of Figure 8.

of the performance possible. It should be remembered that the greater the precision of construction and tuning up and the more carefully the termination is worked out, the better will be the characteristic curve. The curve of Figure 9 could be improved by better termination.

Figure 11 shows one example of a complete unit. The drive and take-off coils are in the cans as are the coils and condensers of the

[3] W. P. Mason and H. J. McSkimin, "Energy Losses of Sound Waves in Metals Due to Scattering and Diffusion", *Jour. Appl. Phys.*, Vol. 19, No. 10, p. 945, October, 1948.

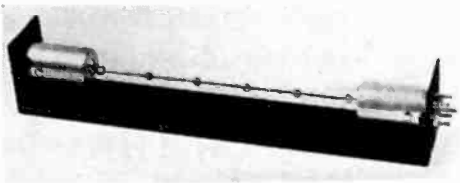

Fig. 11—Example of a complete unit. Drive and take-off coils as well as impedance matching networks are in the cans.

impedance matching networks. The magnets could be in the cans but were actually attached to the end balls that are gripped by the spring fingers.

Table II—Data on Filters Shown in Figure 8

Filter	No. of Sections	Type	Materials	Midband Frequency	Band
A	4	Twin Slug	Ni. plated Al. with steel slugs	200 Kc	300 cps
B	4	Twin Neck	Brass with Ferrite ends	260 Kc	12 Kc
C	5	Slug	Steel Balls on Ni-Span C Wire	300	9
D	1	Triple Neck	Strip Ni.	300	9
E	4	Neck	Al. with Ferrite & Viscoloid Ends	455	7
F	3	Twin Neck	Al. with $BaTiO_3$ Drive & Take-off	455	7
G	3	Twin Slug	Steel Balls on Ni. Tubing	455	4
H	8	Neck—Torsion Operation	Ni. Plated Al.	455	8

References

Other references to mechanical filters adapted to radio frequency operation include:

R. Adler, "Compact Electromechanical Filter," *Electronics*, Vol. 20, No. 4, p. 100, April, 1947.

Kinsley, U. S. Patent 2,342,869.

Mason, U. S. Patent 2,342,813.

THE IMAGE ISOCON — AN EXPERIMENTAL TELEVISION PICKUP TUBE BASED ON THE SCATTERING OF LOW VELOCITY ELECTRONS*

By

PAUL K. WEIMER

Research Department, RCA Laboratories Division,
Princeton, New Jersey

Summary—The image isocon is a new experimental television pickup tube similar in performance and physical appearance to an image orthicon. However, a novel method of generating the video signal is used giving an output signal of opposite polarity with the maximum current in the light. This results in an improved signal-to-noise ratio in the darker parts of the picture and freedom from spurious signals caused by multiplier dynode spots. The low-light sensitivity is comparable to that of the image orthicon, but a wider range of light levels can be accommodated without readjustment of the beam current. Resolution of experimental image isocons has been slightly inferior to the conventional image orthicons but this is partially compensated by their inherent freedom from dynode spots whose presence in the image orthicon occasionally requires deliberate defocusing of the beam. The more exact electron optical requirements of an image isocon place a greater burden on the skill and patience of the operating crew. Most experimental tubes have shown more objectionable time lag than found in an image orthicon. Closer tolerances in tube and coil design are required in an image isocon for consistent and reproducible results. Applications of the electron optical techniques used in the image isocon are suggested for storage tubes and pickup tubes for color.

INTRODUCTION

THE present trend toward high screen brightness for presentation of television pictures has made the observer increasingly aware of noise and other imperfections in the transmitted picture. At the same time, an expanding television service requires that high quality pictures be obtained at still lower illuminations on the original scene. The result is that greater demands are being made on the performance of the pickup tube particularly from the standpoint of sensitivity and signal-to-noise ratio.

The fluctuation noise associated with the incident light quanta falling on the photosentitive surface of a pickup device sets the upper limit of signal-to-noise ratio attainable in any given scene. All pickup

* Decimal Classification: R583.11.

tubes and even the eye itself fall short of transmitting the full information contained in the incident light. To attain this goal a pickup tube would require first, that the quantum efficiency of the photosurface be at least one electron per quanta, and second, that the generation of the video signal incur neither loss of signal nor addition of spurious noise. The present paper is concerned with an attempt to further improve the efficiency of generation of the video signal.

The iconoscope[1] represented a large increase in sensitivity over the image dissector[2] because the storage principle permitted the utilization of charge emitted throughout the entire frame time, instead of just that emitted during the fraction of a microsecond that the beam was on that particular picture element. However, the photoemission was not saturated by the low field at the target, and, furthermore, the video signal was partially masked by the shot noise in the input tube of the amplifier. By eliminating these defects the image orthicon,[3] now widely used in television broadcasting, has been able to obtain a hundredfold improvement in sensitivity over the iconoscope. A high field at the photoemitting surface succeeds in collecting all of the photoelectrons and an electron multiplier raises the output signal of the tube to such a level that amplifier noise is of no consequence. The sensitivity of the image orthicon exceeds that of super XX film and, for certain light ranges, approaches that of the human eye.[4] However, even the image orthicon is not completely efficient in converting the photoemission picture into a video signal. The scanning beam contributes noise which, in the darker parts of the scene, may exceed the inherent shot noise in the photocurrent. A brief examination of the operating cycle of the image orthicon will indicate that the excess beam noise is inherent in this method of discharge of the target and, under certain conditions, may represent a limitation to the sensitivity of this type of tube.

Referring to the cross-sectional diagram of Figure 1, the light from the scene to be televised is imaged on the semitransparent photocathode. The resulting photoelectrons are focused by the uniform

---

[1] V. K. Zworykin, G. A. Morton and L. E. Flory, "Theory and Performance of the Iconoscope", *Proc. I.R.E.*, Vol. 25, pp. 1071-1092, August, 1937.

[2] P. T. Farnsworth, "Television by Electron Image Scanning", *Jour. Frank. Inst.*, Vol. 218, pp. 411-444, October, 1934.

[3] A. Rose, P. K. Weimer and H. B. Law, "The Image Orthicon — a Sensitive Television Pickup Tube", *Proc. I.R.E.*, Vol. 34, pp. 424-432, July, 1946.

[4] A. Rose, "Television Pickup Tubes and the Problem of Vision", ADVANCES IN ELECTRONICS, Vol. I, pp. 131-166, Academic Press, 1948.

magnetic field to form an electron image on the thin glass target. Since these electrons strike the glass with an energy of several hundred volts, the secondary emission ratio of the glass is greater than unity, and the target becomes charged a volt or so more positive in the brightest parts of the picture. The target screen collects the secondary electrons and serves to limit the potential to which the glass may rise. A low velocity electron beam scans the opposite side of the target and deposits sufficient electrons to neutralize the positive charge accumulated during the preceding frame time. The conductivity of the glass is so chosen that in the 1/30 second between scans, most of the charge can leak through the glass, but only a negligible amount can spread transversely. The fraction of the beam not deposited on the glass returns to the gun where it is directed into an electron multiplier. Since the maximum beam is deposited in the bright (or positive) parts of the target, the output current is a minimum here and a maximum in the dark.

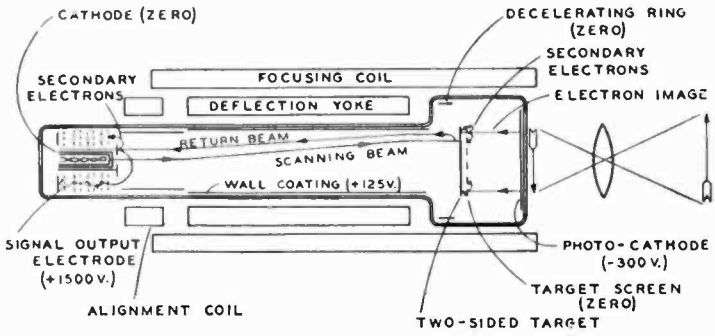

Fig. 1 — Cross-sectional diagram of the image orthicon.

In the output signal, the shot noise associated with the current in the return beam is superimposed on the noise inherent in the stored charge on the target. The reversed polarity of the signal (maximum current in the dark) causes the excess noise to appear most prominently in the darker parts of the picture.

An additional cause for spurious noise in the image orthicon is the low percentage modulation of output signal attainable in practice (20 to 30 per cent). The noise associated with the unmodulated part of the return beam appears in all parts of the picture and sets a further limit to low light sensitivity.

The relative prominence of the beam noise in the output signal of the image orthicon is obviously a function of the magnitude of the charge signal stored on the target. If this charge is sufficiently large the beam noise becomes negligible in comparison with the stored signal. In the new RCA 5655 studio type image orthicon, a higher capacity

target permits the storage of sufficient charge for a well-lighted scene so that the beam noise is not excessive even in the darker parts of the picture. However, under poor lighting conditions, the higher capacity target represents no advantage, and the output signal-to-noise ratio is limited by the beam noise.

It was the aim of the work to be described in this paper to develop a type of pickup tube in which the signal-to-noise ratio at all light levels should be limited only by the inherent shot noise in the primary photocurrent. While this goal has not been completely attained, a new method of video signal generation has been developed which does give improved noise characteristics over that used in the image orthicon. The word "isocon" has been coined to distinguish the new method of signal generation from the conventional orthicon. Following current pickup tube terminology an isocon possessing an image section will be called an "image isocon".†

The isocon method of signal generation is based upon the fact that the low velocity beam impinging on the target produces scattered electrons whose number is greatest in the positive (or bright) parts of the target. By means of electron optical techniques to be described, the scattered electrons may be separated from the bulk of the return beam and these alone admitted to the electron multiplier. The output signal current from an image isocon is thus of opposite polarity to that of the image orthicon and is free from the excess beam noise in the dark parts of the picture. In addition, the percentage modulation of the output signal can be made very high, thus reducing to a minimum the beam noise contribution in all parts of the picture. The isocon method of operation also results in other advantages as well as disadvantages. The performance of an experimental image isocon will be compared with that of the conventional image orthicon.

Electron Scattering at Low Velocity Bombardment

It is well known that an electron beam impinging on a metal plate or on an insulator with only a volt or two bombarding energy is not completely absorbed. The secondary emission ratio for metals instead of being zero is of the order of a few tenths,[5] and for insulators,[6] may be as high as eight or nine tenths. It has been found that true

---

† The name "isocon" has been added to an already overburdened nomenclature of electron tubes chiefly for convenience of reference.

[5] I. Gimple and O. Richardson, *Proc. Roy. Soc.*, A182, p. 61, 1943.

[6] O. Krenzien, "The Elementary Processes in the Secondary Electron Emission of Polar Crystals", *Wiss. Ver. Siem. Werk.*, 20, 91, 1942.

secondary emission does not occur unless the bombarding energy exceeds some critical voltage characteristic of the material of the order of 5 to 10 volts. For voltages below this value the electrons escaping from the surface are primary electrons which were reflected without energy loss.[5]

Measurements of secondary emission ratio (or more properly reflection coefficient) in the low voltage range is difficult because great care must be taken to ensure that the entire beam actually strikes the surface without simply being deflected before reaching it. The electron optical techniques used in the image orthicon for controlling the low velocity scanning beam have been found useful[7] for studying secondary emission and reflection at low bombarding voltages. Tests have shown that the electron reflection occurring from a glass surface need not be specular. An electron striking the surface normally will have an angle of reflection anywhere from zero up to ninety degrees. Accurate measurements of angular distribution of reflected electrons have not been made but inspection of the defocused disc of the return beam impinging upon a fluorescent screen indicates qualitatively that for one volt incident velocity all angles of reflection are equally probable.†

The term "scattered electrons" will be used in this paper to apply exclusively to the *non-specularly reflected* electrons obtained when a low velocity beam impinges on a surface. The scattered electrons are of particular interest in the design of the television pickup tube to be described in this paper and are so defined to distinguish them from the remainder of the returning electrons which will be called "reflected electrons". It should be noted that the term "reflected electrons" will also include those electrons which, having insufficient energy to reach the target surface are specularly reflected in the space in front of the target. In fact, the latter group may compose the bulk of the reflected electrons if the energy spread of the incident beam is as much as one volt or greater.

Use of Scattered Electrons for the Video Signal (Isocon Operation)

It was pointed out in the introduction that the signal-to-noise ratio and sensitivity of the image orthicon would be improved if the output current were a maximum in the light and fell to zero in the dark.

---

[7] P. K. Weimer, "Measurement of Secondary Emission of Insulators at Low Primary Energies", *Phys. Rev.*, 74, p. 1219, November 1, 1948.

† This result was obtained for reflection from fire polished lime glass,

Although it might conceivably be possible to reverse the polarity of the output signal by scanning at high velocity a target which was charged negatively in the light, the problem of poor percentage modulation of the output signal would remain unsolved. Moreover, the two-sided glass target used in the image orthicon with high velocity image section and low velocity scanning had already demonstrated the desirable properties of freedom from shading and stability over a wide range of light levels.

It has been found that these features could be retained and the preferred positive polarity of output signal obtained with an image orthicon target at low velocity scanning if, instead of using the entire return beam for the video signal, the scattered fraction alone is admitted to the multiplier. As shown in Figure 2 the number of scattered electrons are a maximum in the lighted or positive parts of the target and substantially zero in the dark. The reflected portion of the return beam can be prevented from entering the multiplier by means of apertures.

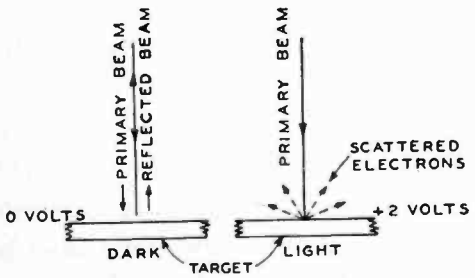

Fig. 2 — A simplified picture of electron scattering at the target of the image isocon.

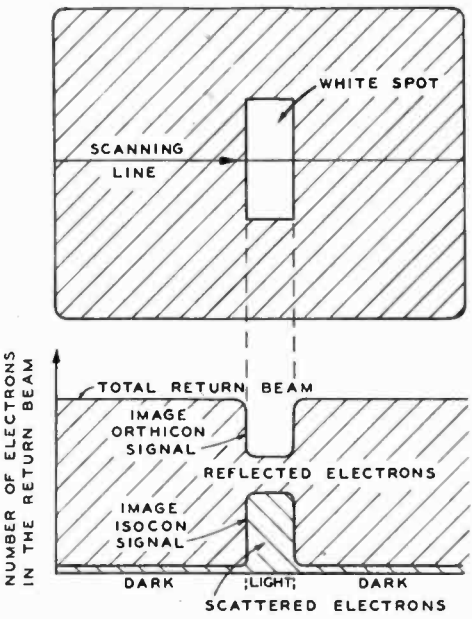

Fig. 3—Comparison of the output signals of the image isocon and the image orthicon.

Figure 3 shows the relative fractions of scattered and reflected electrons in the return beam when it scans across a white spot on a black background. Although the total return beam is a minimum in the bright areas where electrons have been deposited on the target, the number of the *scattered* electrons is a maximum. Also, it will be noted that the percentage modulation of the scattered electrons is very much greater than the percentage modulation for the total return beam.

In forming the video signal from the scattered electrons, the assumption has been made that in scanning a given charge on the

target, the number of scattered electrons produced will be proportional to the magnitude of the charge. Experience has shown this to be at least approximately true and a satisfactory rendition of half tones is obtained.

It may be noted that the optimum secondary emission ratio of the glass target is somewhat different for the isocon type of operation as compared with the conventional image orthicon. In the latter, the ratio should be as low as possible in order to keep down the excess beam noise which accompanies a poorly modulated output signal. For isocon operation, however, the higher the ratio the greater the output signal. For satisfactory discharge of the target it should not greatly exceed 0.7. Measurements have indicated that the ratio of lime glass falls between 0.5 and 0.8.

A Method for Separating the Scattered and Reflected Electrons

The separation of the scattered electrons from the reflected electrons is not as simple as might be suggested by Figure 2. The complicating factor is that the primary beam is actually of a conical shape with the electrons converging to a focus at the target. Consequently, both the reflected and scattered electrons will diverge upon leaving the target with almost complete intermingling of the two groups unless special precautions are taken.

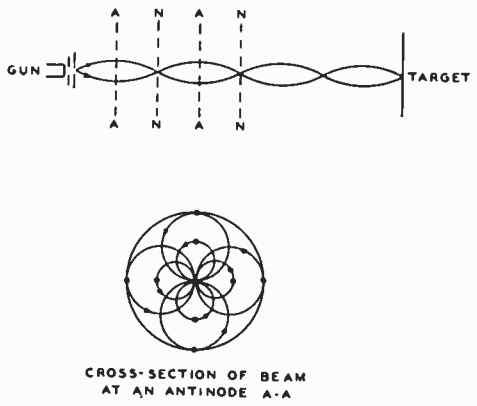

Fig. 4 — Electron paths in a uniform magnetic field.

The uniform magnetic field, which is used for focusing purposes in the image orthicon, may also be employed to advantage for separating the scattered electrons. Figure 4 shows the electron paths within the scanning beam of the image orthicon. The electrons emerge at high velocity from the defining aperture of the gun in a direction which is substantially parallel to the magnetic lines. However, there is a slight divergence of the emerging beam and most of the electrons will possess small transverse velocity components corresponding to an energy ranging from zero up to a volt or more. Each electron describes a helix in the magnetic field and the beam converges to a focus at several nodal points between the gun and the target. The cross section of the beam at an antinode is a disc whose diameter is approximately 0.090 inch for a maximum transverse energy of one volt and a mag-

netic field of 60 gausses. The electrons proceed down the axis of the tube with a longitudinal energy of several hundred volts but are decelerated in the space immediately in front of the target.

If the beam finds the target potential slightly negative with respect to the gun cathode, all of the electrons return to the gun in a beam whose characteristics are similar to those of the primary beam. If the target is say one volt positive those electrons whose transverse energy does not exceed one volt will possess sufficient longitudinal energy to strike the target and be scattered. However, the maximum transverse energy, which can be acquired in the scattering process, is no more than the total energy of the bombarding electron or target voltage which in this case is one volt. The scattered electrons are therefore completely indistinguishable from the reflected electrons unless the energy spread in the incident beam is considerably less than the one volt target potential assumed here.

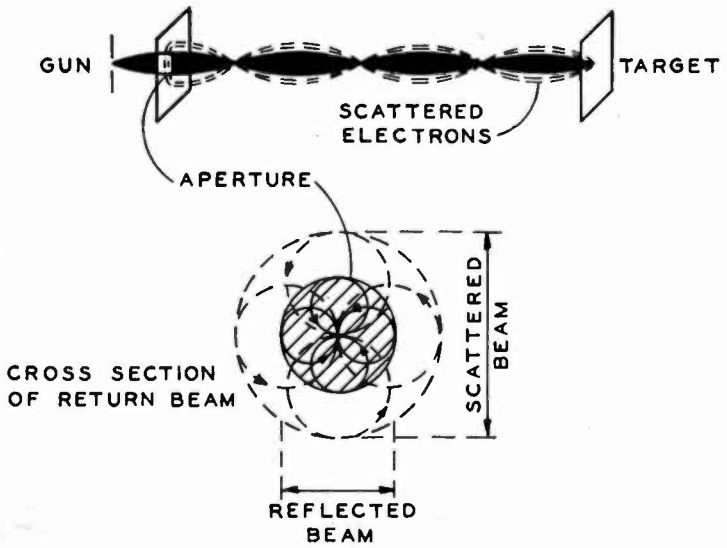

Fig. 5 — Scattered electrons around a well-aligned beam.

In case the target potential does exceed the energy spread in the incident beam, some of the scattered electrons will be found in the space surrounding the reflected electrons in the return beam as shown in Figure 5. A possible method for separating these widely scattered electrons by means of an aperture is suggested by Figure 5, but such a method is inefficient and gives a nonlinear output unless the primary energy spread is extremely small.

A much more efficient method for separating the scattered and reflected electrons is illustrated in Figure 6. This consists of deliberately introducing additional helical motion into the primary beam so that the scattered electrons of the return beam are all found on

one side of the reflected electrons. In Figure 6 the excess helical motion is produced by a set of short deflection plates mounted close to the gun, but obviously other methods are applicable. The plates give a fixed transverse velocity to all the primary electrons which, when superimposed on their own random velocities, results in the helical paths whose cross section is shown in somewhat exaggerated form in Figure 6B. Electrons now approach the target obliquely along helices whose diameters may range from *OA* to *OB*. The transverse energy of electrons in the primary beam may range from one volt up to four or more.† Since this transverse energy is acquired at the expense of the longitudinal energy, the "cut-off" or black potential of the target is raised by a volt positive with respect to the gun cathode potential.

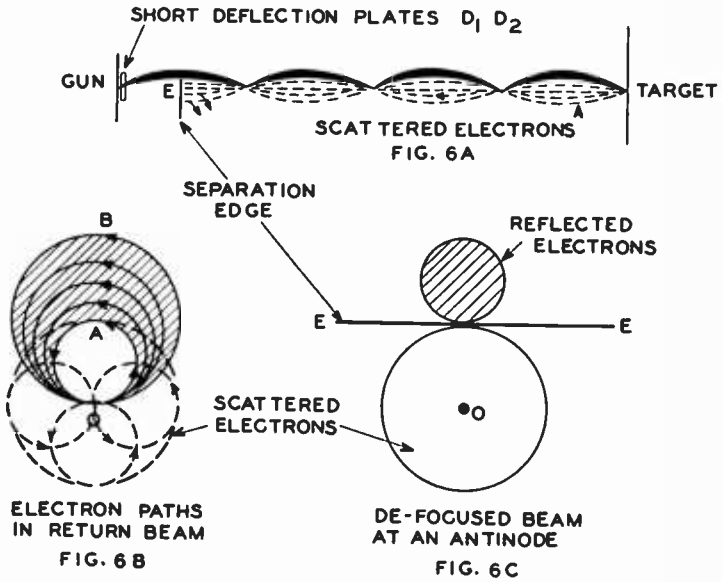

Fig. 6—Helical motion method of separating scattered and reflected electrons.

Now consider what happens when a small amount of light falls on the tube raising the target slightly above its cut-off potential. The first group of electrons now able to land on the target will be those with the least helical energy. These electrons execute helical motion of a diameter indicated by *OA* in Figure 6B. On striking the target they will be scattered in all directions forming many helices whose diameters may be any size from zero up to *OA*. Since all the primary electrons were focused on the point *O* at the instant of impact, the magnetic line through this point forms the central axis of the scattered beam. Figure 6C shows the cross section of the return beam at an antinode. It will be noted that at the antinodes all of the scattered electrons fall below the line E-E for the low target potential specified,

† The addition of a fixed transverse velocity to all the electrons in the beam increases the existing energy spread of the beam several fold.

while the reflected electrons are all found above this line. The two groups may be completely separated as shown in Figure 6A by placing an electrode so that it intercepts the scattered electrons, letting the unwanted reflected electrons go on by. Or, a better method which is used in the experimental image isocon in Figure 7, is to admit the scattered electrons into an electron multiplier while intercepting the reflected electrons on the edge of the multiplier aperture.

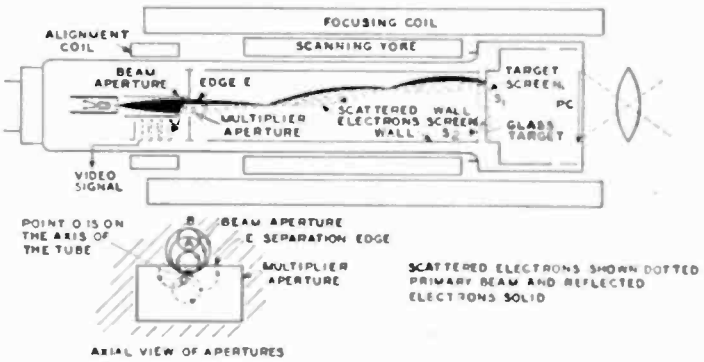

Fig. 7 — Cross-sectional diagram of an experimental image isocon.

For higher target potentials, corresponding to the brightest parts of the picture, a small fraction of the scattered electrons fall above the line E-E and are lost. This is the consequence of the wider scattering produced by the increased energy of impact. In practice, it has been found advisable, for reasons to be discussed later, to operate† so that the separation edge E-E passes approximately through *O*, the center of the scattered beam. Under these conditions at all light levels half of the scattered electrons are utilized and the linearity of response is preserved.

Description of an Experimental Image Isocon

Figure 7 shows a cross-sectional diagram of an experimental image isocon which has been designed to operate on the electron scattering principle. This form of tube is very similar in external appearance to the image orthicon. It may be operated in an image orthicon camera without modification of the camera other than that necessitated by the output polarity reversal. Although many variations in tube structure and operating technique have been tested, the arrangement shown in Figure 7 has several advantages to offer.

† In some of the experimental image isocons, electrostatic deflection plates were used to position the return beam in any manner desired relative to the separation edge. In the tube shown in Figure 7 the multiplier aperture was located relative to the beam aperture so that this condition should be automatically assured.

The helical motion of the primary beam necessary for separation of scattered electrons is obtained in Figure 7 by positioning the aperture labeled "beam aperture" slightly off the axis of the tube. This aperture is approximately forty mils in diameter and is located at an antinode in the beam. The beam emerging from the defining aperture is made up of electrons having all directions of helical motion (See Figure 4). The beam aperture at the first antinode selects out a group of electrons to form a primary beam having the proper helical motion for separation of the scattered electrons. A second aperture labeled "multiplier aperture" is also in the plane of the antinode and located relative to the beam aperture so that it passes only the scattered electrons in the return beam. The first stage of the multiplier is mounted immediately behind the multiplier aperture. The upper edge of the multiplier aperture serves as the separation edge E-E referred to in the preceding section. The reflected electrons are intercepted on this edge of the multiplier aperture and do not enter the multiplier. The output signal from the multiplier is modulated with the opposite polarity to that of the image orthicon, having maximum current in the light instead of in the dark.

In addition to the special apertures for the gun and multiplier, the wall screen, S_2, forms an essential part of the tube. This screen is of fine mesh, and, being mounted at an out-of-focus position, is not resolved by the beam. The strong uniform electric field produced in front of the target by this screen is necessary for two reasons: to minimize the residual scan of the return beam, and to reduce beam bending in the vicinity of the target. The latter effect may give rise to spurious edges in the transmitted picture.

The need for restricting the scan of the return beam is essential to successful separation of the scattered electrons by the method described above. If the return beam moves appreciably relative to the separation edge E some of the reflected electrons may enter the multiplier and give spurious shading. Inasmuch as the deflection fields serve only to bend the magnetic lines of the focusing field, it might be expected that the return beam would exactly retrace the path of the incident beam. However, such is not the case in the standard image orthicon where the return beam may scan on the multiplier an area of ¼ to ½ inch diameter. The principal cause of the lack of retrace in the image orthicon is the electrostatic lens action of the deceleration field in front of the target. A fine mesh screen attached to the wall cylinder has been found the most convenient method of descanning by

removing its cause, but other dynamic methods of immobilizing the return beam have also been used.

The need for a higher electric field in front of the target of an image isocon than is required for an image orthicon is a consequence of the method of separating the scattered electrons. As indicated in Figure 8 an electron approaching the target at a boundary between a white and dark area will be deflected toward the more positive area. This transverse impulse at the target causes the electrons to follow a different diameter helix on their return path and results in their displacement relative to the separation edge. For certain orientations of the black and white boundary at the target, the reflected electrons may be deflected into the multiplier aperture giving a spurious bright edge on the boundary in the transmitted picture. In order to minimize this effect the electric field in front of the target should be at least

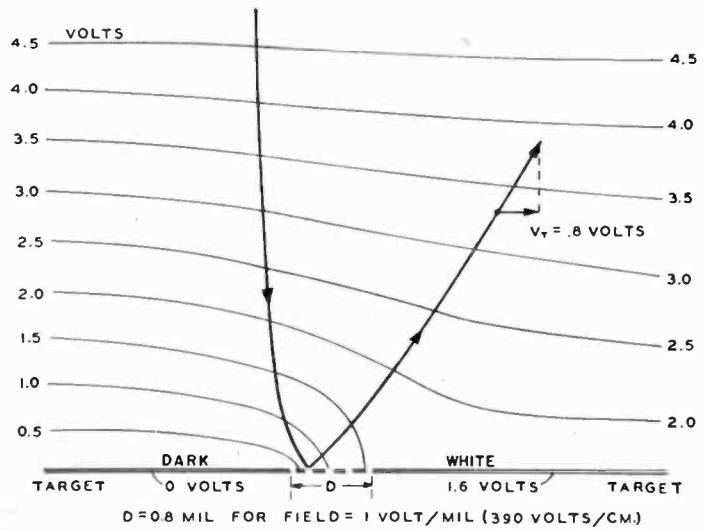

Fig. 8 — Electron path in the neighborhood of the target (low velocity scanning). The path length shown is only a few thousandths of an inch in length and the effect of the magnetic field over this distance is negligible.

five hundred volts per centimeter. Even with this field some beam deflection will occur and the transmitted picture will appear slightly differentiated if the selection edge E is located as shown in Figure 6C. In order to prevent the reflected electrons from being deflected into the multiplier, it has been found desirable to locate the separation edge so that it passes approximately through point *O* in Figure 6C. This procedure eliminates the spurious edge effect but reduces the output signal by one half.

Comparison of Performance of an Experimental Image Isocon With a Conventional Image Orthicon

Experimental image isocons of several different designs have been

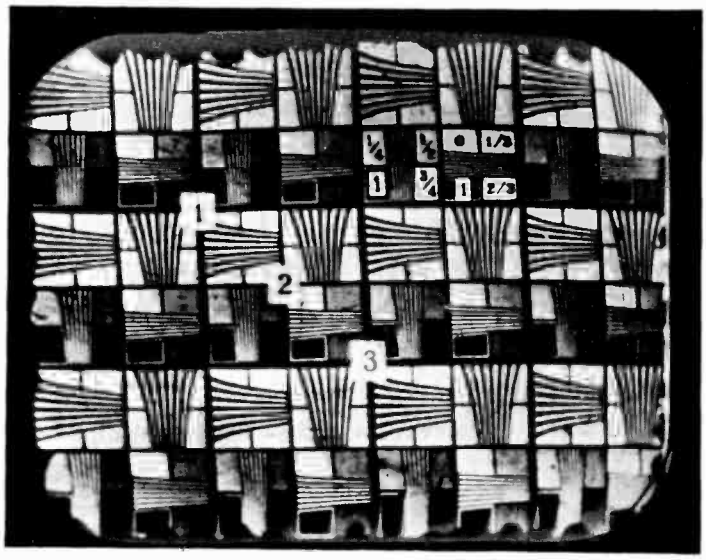

Fig. 9—Test pattern transmitted by an experimental image isocon.

built and tested to date. Some of these have been operated in modified image orthicon cameras in studio tests where the performance could be compared directly with that of standard image orthicons focused on the same scene. The scattered electron tubes have demonstrated certain advantages as well as disadvantages as compared to the conventional tubes. Many factors enter into a complete evaluation and the following statements can at best be considered only tentative. Figures 9 and 10 show photographs of television pictures transmitted by an experimental image isocon.

The principal advantage of the image isocon is its greater freedom from noise, particularly in the darker parts of the scene. The noise characteristics are discussed in some detail in the following section. An additional improvement has been gained in eliminating the

Fig. 10—Half tone transmitted by an experimental image isocon.

"dynode spots" often found in the image orthicon pictures. In the latter tube the return beam scans the first stage of the multiplier in sharp focus with the result that a secondary emission picture of that electrode is superimposed on the output signal. Any nonuniformities in secondary emission ratio, as well as the dynode aperture itself are often clearly visible in the transmitted picture. In the image isocon the return beam striking the multiplier is descanned and defocused, thus, removing this source of spurious signal. A further advantage of the scattered electron tube is that the greatly diminished beam noise in the output signal permits a wider range of light levels to be transmitted without readjusting the beam current. For example, if the camera is swung from a bright scene to a dimly lit scene, the full sensitivity of the image orthicon ordinarily cannot be realized unless the beam current is decreased to reduce the beam noise. Care must be taken in decreasing the beam current lest a bright spot will "charge up" and cause comet effects. The superior performance of the scattered electron operation under these conditions may be readily demonstrated.

The principal disadvantage of the experimental scattered electron pickup tubes has been found to be the criticalness of initial adjustment. The more exact electron optical requirements place a greater burden on the skill and patience of the operating crew. Some of the problems connected with the initial adjustments are described under OPERATING ADJUSTMENTS. Once the correct voltages and magnetic fields have been found there is no need to change them during operation assuming no drift in the power supplies. However, effects of slight misadjustment are more apparent in the output signal than for an image orthicon. For example, spurious edge effects, poor resolution, time lag, nonuniform picture or even complete reversal of signal polarity may be the consequence of slight misadjustment.

Assuming optimum electron optical adjustment the experimental image isocons were inferior from the standpoint of resolution and time lag. Where a conventional 3-inch image orthicon under best conditions may transmit a limiting resolution of 1200 to 1500 lines, the corresponding image isocon would give only about 900. This deterioration is mostly due to the necessity for giving the scanning beam excess helical motion. The greater time lag observed in the image isocon at low light levels is also due to this excess helical motion making the beam less efficient in discharging the target. The lower maximum resolution in the image isocon is partially compensated by the fact that there is no need to partially defocus the beam to

eliminate multiplier spots as is often necessary in a conventional image orthicon.

Signal-to-Noise Ratio

The electron current emitted by a photocathode has a fundamental shot noise associated with it given by the formula:

$$I_{ns} = (2e\,I\,\Delta f)^{1/2} \qquad (1)$$

where I_{ns} is the root-mean-square noise current in amperes,

e is the electronic charge in coulombs,

I is the total emitted current in amperes,

Δf is the frequency bandwidth.

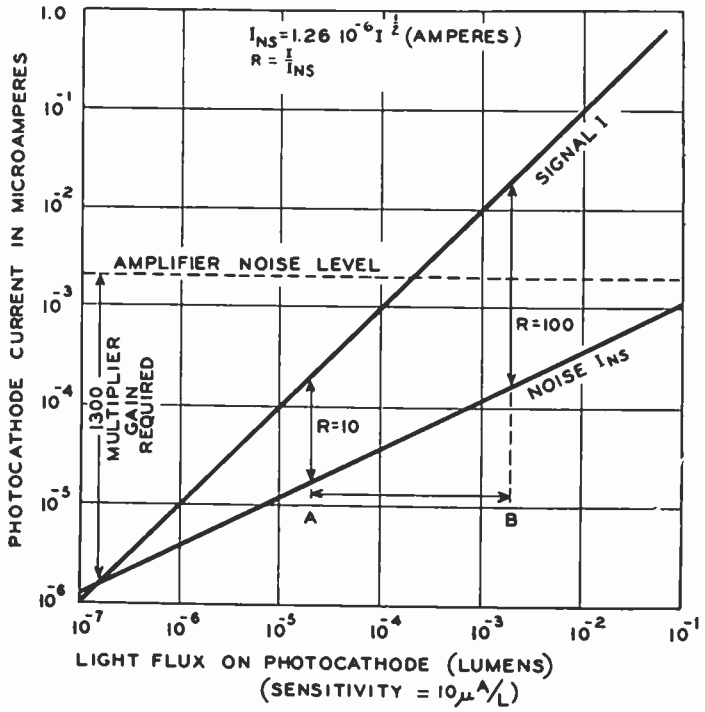

Fig. 11—Noise characteristics for an ideal pickup tube.

Figure 11 shows a plot of the signal current and associated noise as given by (1). An ideal pickup tube should transmit at all light levels no more noise than indicated by I_{ns}. However, the input circuit of the camera amplifier contributes additional noise whose magnitude is indicated for a 5 megacycle pass band. In order for I_{ns} to represent the limiting noise in the output signal, it is necessary that some type of noiseless amplifier be incorporated into the tube to raise the signal level to such a value that its associated noise exceeds the amplifier

noise. A gain of about 1300 is required. An electron multiplier offers a convenient way of obtaining this gain. In the ensuing discussion it will be assumed that adequate multiplier gain is available to allow one to neglect amplifier noise. The small amount of noise introduced by the multiplier itself will be neglected.

A quantitative comparison of the actual signal-to-noise ratio improvement realized by the use of scattered electrons may be calculated as follows: Consider a typical scene whose light range falls between the values A and B in Figure 11. Assuming the photocathode sensitivity to be 10 microamperes per lumen, the signal-to-noise ratio† R in the high lights would be 100 and in the low lights 10. The signal-to-

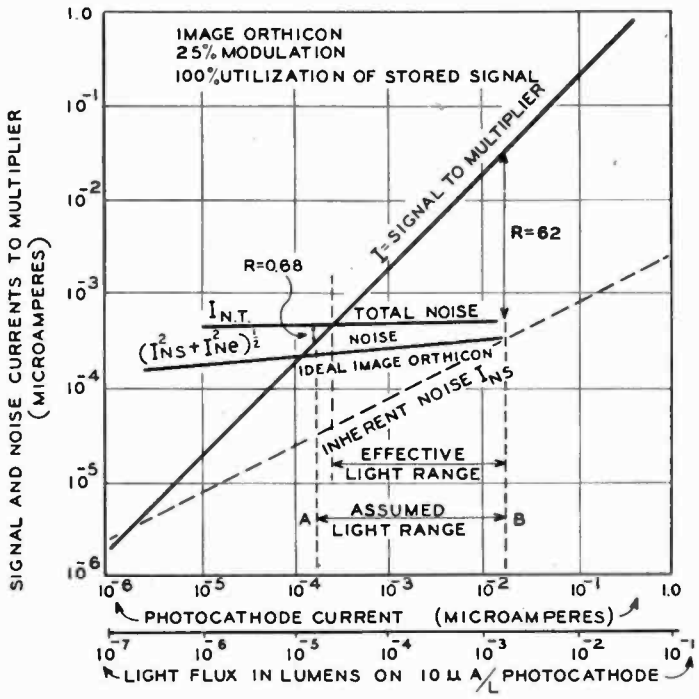

Fig. 12—Signal and noise currents to the multiplier of an image orthicon with the beam current adjusted for the assumed light range AB.

noise ratios obtainable in typical image orthicons and image isocons have been calculated for this light range and the results indicated in Figures 12 and 13.

The signal entering the multiplier of the image orthicon is plotted in Figure 12 as being twice the total photocathode current (full storage range). The factor of two gain is derived from the secondary emission on the picture side of the target which multiplies both the stored charge and its associated noise by two. The total noise entering the multiplier of the image orthicon is made up of three components whose sum is given by:

† Peak-to-peak signal divided by root-mean-square noise current.

$$I_{nt} = (I_{ns}^2 + I_{nb}^2 + I_{ne}^2)^{1/2} \quad (2)$$

where I_{ns} is the inherent signal noise stored on the target,

I_{ne} is the beam noise associated with the part of the beam which is effective in discharging the target. By definition $I_{ne} = 0$ in the brightest area and is a maximum in the dark.

I_{nb} is the constant background noise associated with the part of the beam which fails to land on the target at any light level.

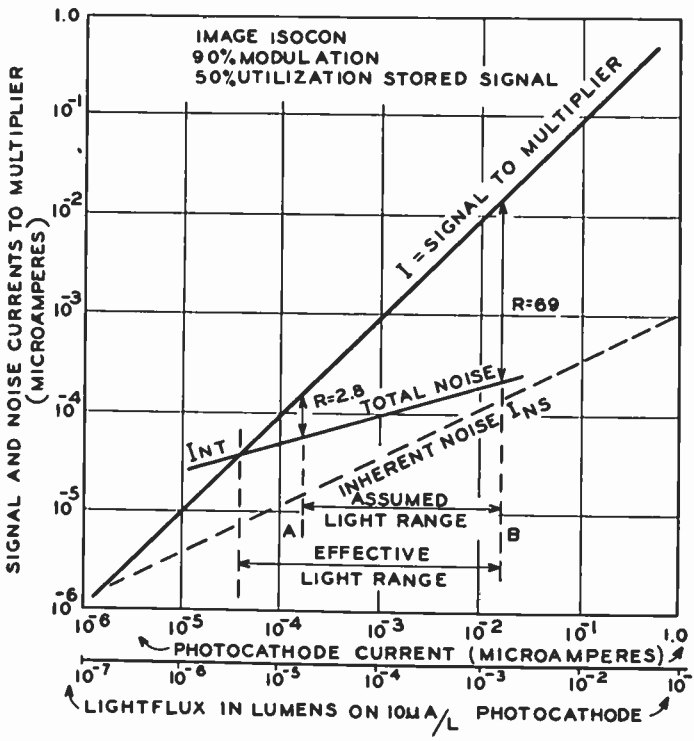

Fig. 13—Signal and noise currents to the multiplier of an image isocon with the beam current adjusted for the assumed light range AB.

In an ideal image orthicon having 100 per cent modulation of output signal, I_{nb} would be zero. However, the usual image orthicon has a modulation of about 25 per cent. Taking this value of modulation, I_{nb} can be calculated, and I_{nt}, the total noise, found from Equation (2). The value of the noise currents are plotted in Figure 12. It is seen that for the light range AB the signal-to-noise ratio is 62 for the high lights and 0.68 for the low lights.

A similar calculation has been made for the image isocon signal and is illustrated in Figure 13. Here one must take into account the fact that the signal current entering the multiplier is not necessarily

equal to the charge stored on the target, but may be greater or less depending on the reflection coefficient of the glass (on the scanned side) and the efficiency of collection of the scattered electrons. A reflection coefficient of 0.66 would give a signal gain of two at the target but about 50 per cent of the scattered electrons are absorbed by the wall screen S_2 and another 50 per cent are intercepted on the edge of the multiplier. The net signal is thus 50 per cent of the stored charge or approximately equal to the total photocathode current.

The total noise entering the multiplier aperture of the image isocon is given by,

$$I_{nt} = (2I_{ns}^2 + I_{nb}^2)^{1/2} \tag{3}$$

where I_{ns} is the noise associated with the utilized part of the signal stored on the target. The factor 2 is used to take into account also the equal but independent noise associated with the utilized part of the scattered electrons.

I_{nb} is the background noise resulting from stray electrons getting into the multiplier. I_{nb} is constant at all light levels.

The background current giving rise to I_{nb} is not inherent in the scattered electron signal but has been observed to be present in all the experimental tubes tested. Fortunately this excess beam noise can be made much smaller than the excess noise in the image orthicon as evidenced by the much higher percentage modulation obtainable here. (As high as 97 per cent in the image isocon signal compared to 25 per cent for the image orthicon signal.) Assuming 90 per cent as a typical modulation, the total noise has been calculated according to Equation (3) and plotted in Figure 13. For the light range AB, the signal-to-noise ratio R is 69 for the high lights and 2.8 for the low lights. The corresponding values for the image orthicon as given in Figure 12 were 62 and 0.68 respectively, indicating that the use of the scattered electrons gave an improvement of 1.1 in the high lights and 4.1 in the low lights. While the improvement in the high lights is not striking, the decreased noise in the dark parts of the picture and the extended low light range *for fixed beam current* is noticeably superior to the image orthicon.

Although the image isocon represents a closer approach to the limitation provided by the inherent signal noise, reference to Figure

13 will indicate that there is still considerable margin for improvement. A still higher percentage modulation of the signal entering the multiplier would be desirable. On the other hand, if the excess current entering the multiplier were great enough to drop the modulation much below 50 per cent, there would be very little advantage gained by inverting the output signal polarity.

Operating Adjustments

In principle, the scattered-electron tube shown in Figure 7 should not require any special adjustments when first inserted in the camera coil and turned on. The multiplier aperture is so located relative to the beam aperture that only scattered electrons should enter the multiplier giving immediately the proper polarity signal. Unfortunately, the electron optical conditions are sufficiently critical that a slight misadjustment may produce either no picture at all or a picture of wrong polarity over a part or all of it. The most likely causes for a poor initial picture are (1) bad mechanical alignment of the tube or coil, (2) improper voltages or fields to give an antinode in the plane of the separation aperture, or (3) too much residual scan in the return beam.

In the experimental tubes misalignment was the principal offender, the tolerances being considerably more severe than for an image orthicon. An alignment coil (see Figure 7) over the gun giving a small transverse field of variable direction and magnitude was found to be the most satisfactory means of correcting for existing misalignments. As in the image orthicon the alignment coil was adjusted while watching the picture although the electron optical function of the coil was somewhat different. In this case, it is desirable that the alignment coil is located further into the focusing coil than is usual for the image orthicon. Its principal effect is therefore to center the beam properly over the beam aperture, rather than to give the beam helical motion. A widely diverging beam from the defining aperture is necessary to be sure that when the beam is properly positioned over the aperture to select the electrons of correct helical motion that there will be some electrons having that motion.

The present method of separation of scattered electrons is based on having an antinode in the beam in the plane of the separation edge Thus, a particular ratio of gun voltage to magnetic field strength is required to match the tube dimensions.

Nonuniform shading in the video signal of the image isocon electrons can nearly always be traced to too much residual scan in the

return beam. Although the decelerating screen S_2 in Figure 7 greatly reduces this scan, it may still be excessive unless proper operating precautions are taken. The beam on its initial and return passage along the curved magnetic lines of the deflection coil will acquire additional helical motion which may cause the return beam to scan over the edge of the multiplier aperture. This scan may be eliminated by adjusting the distance of the deflection coil from the target so that the helical motion induced in the incident beam by the deflection coil will be cancelled by the effect of the deflection coil on the return beam.

Other Applications

The electron optical method used in separating the scattered electrons may also be used for other forms of pickup tubes or storage

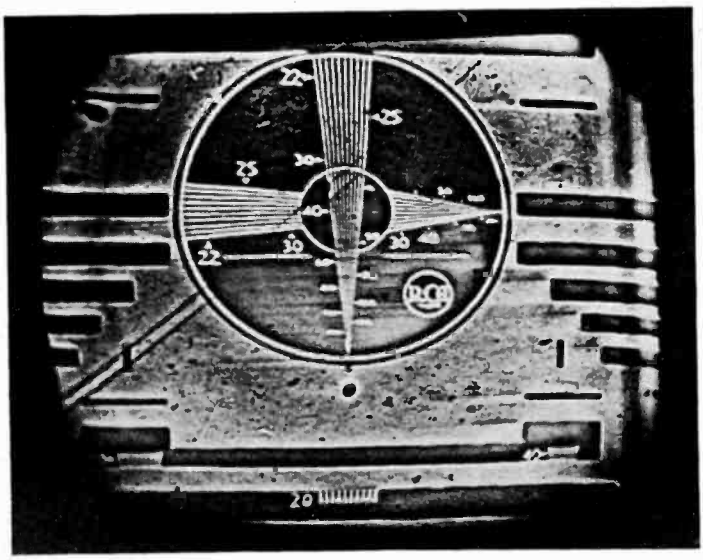

Fig. 14 — Test pattern transmitted by an experimental beam deflection storage tube. Inasmuch as the video signal is generated without requiring that the beam discharge the target, a picture may be stored for a considerable time while being continuously scanned.

tubes. For example, one application might be in a pickup tube for simultaneous color television where it is desired to separate the three video signals from a single return beam. Another application is for a storage tube in which the beam is deflected by the charges on the target without actually discharging the target. The amount of deflection is readily detected by passing the return beam over an edge placed at an antinode in the beam. Figure 14 shows a beam deflection picture obtained by a beam approaching to within a few mils of the target before it is reflected. The differentiated character of the signal would be unsatisfactory for broadcasting, but could well be useful for transmitting information such as maps or meter readings, etc.

ACKNOWLEDGMENTS

The writer has profited greatly from the interest and advice of V. K. Zworykin[8] and Albert Rose.[8] The construction and evaluation of experimental tubes has been greatly aided by the cooperation and assistance of H. B. Law,[8] P. G. Herkart,[8] A. C. Schroeder,[8] R. C. Webb,[8] R. B. Janes[9] and R. E. Johnson.[9]

[8] RCA Laboratories Division, Princeton, N. J.
[9] RCA Victor Division, Lancaster, Pa.

THE USE OF FERRITE-CORED COILS AS CONVERTERS, AMPLIFIERS AND OSCILLATORS*

By

V. D. Landon

Research Department, RCA Laboratories Division,
Princeton, New Jersey

Summary—The availability of various ferrites as magnetic core materials makes it possible to use non-linear inductors as frequency converters at frequencies up to a few megacycles. If the oscillator frequency is greater than the signal radio frequency and the intermediate frequency, the circuit regenerates. If the oscillator excitation is sufficient, the circuit may oscillate at radio frequency and intermediate frequency simultaneously. If either the radio-frequency circuit or the intermediate-frequency circuit is tuned higher than the oscillator frequency, the circuit is degenerative. This is shown theoretically and experimentally.

Introduction

THE use of saturating cores as magnetic amplifiers is not new. Fitzgerald[1,2] shows the use of saturating reactors as direct-current amplifiers. This art has had considerable commercial application. The signal, in the form of a direct current, is applied to one winding on the core partially saturating it. A second winding (uncoupled by balancing) is placed in series with a 60-cycle voltage source and a rectifying load. The amount of 60-cycle current passed is a function of the degree of saturation of the core. The direct-current output of the rectifier is an amplified function of the direct-current signal current.

In this case the amplification seems to depend on the difference in frequency between the signal and the 60-cycle exciter voltage. Obviously a higher frequency exciter voltage may be used and then the frequency of the signals may be increased.

The use of ferrite-cored coils permits the use of exciter frequencies up to a few megacycles.

---

* Decimal Classification: R363.

[1] Alan S. Fitzgerald, "Some Notes on the Design of Magnetic Amplifiers", *Jour. Frank. Inst.*, Vol. 244, Nos. 4, 5 and 6, pp. 249-265, 323-362, 415-439, October, November, December, 1947.

[2] A more complete bibliography on magnetic amplifiers will be found in *Electronics*, Vol. 21, No. 1, pp. 194-195, January, 1948. However, the following pertinent patents are not included in the *Electronics* bibliography: Turner 2,026,758. Alexanderson 1,206,643. Elmen 1,544,381. Slepian 1,645,302. Hartley 1,287,982. Peterson 1,884,844.

Ferrite Cores

Various ferrites have been used as radio-frequency magnetic core material for some time. For example, in January, 1909 a Dr. Siegfried Hilpert was granted German patent #226347 concerning the use of copper ferrite. The work was not followed up at the time.

Recent work in Holland[3] and at RCA Laboratories has indicated that ferrites may find wide commercial application in the near future. They have a higher permeability at frequencies up to a few megacycles than any other available materials. At the same time moderately high Q is obtained.

An additional feature is the unusual characteristic of retaining a high Q when partially saturated with direct current.

It is evident that such a material should be usable in magnetic amplifier circuits utilizing higher frequencies than heretofore.

Certain other improvements in magnetic amplifier design are fairly obvious.

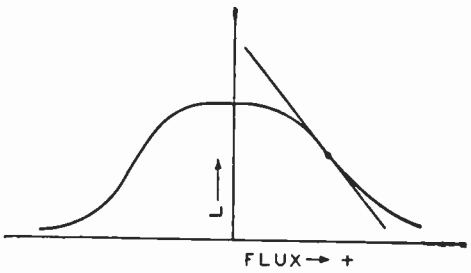

Fig. 1—Effective inductance as a function of direct-current flow.

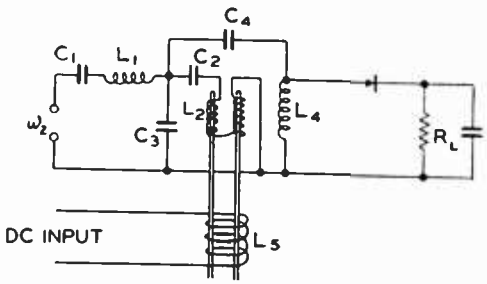

Fig. 2 — Circuit for steepening input-output curve.

Biasing the Core

A curve of the effective small-signal inductance as a function of the direct-current flux has the general form of the curve shown in Figure 1. Obviously the circuit will be most sensitive as an amplifier if the direct-current flux is adjusted to the point where a given alternating-current power input produces the greatest percentage change in inductance. This may be accomplished with direct current in one of the windings or with a permanent magnet. A permanent magnet was used in all the circuits discussed below.

Use of a Slope Filter

A circuit such as that of Figure 2 may be used to increase the

[3] J. L. Snoek, NEW DEVELOPMENTS IN FERROMAGNETIC MATERIALS, Elsevier Publishing Co., Inc., New York, 1947.

variation in output resulting from a given small change in reactance.

In Figure 2, L_1C_1 is resonant to the excitation frequency ω_2. The mesh L_4C_4 is also resonant to ω_2. The coupling between L_1C_1 and L_4C_4 consists of $L_2C_2C_3$.

The mesh L_2C_2 is also resonant to ω_2 for one value of flux. For a slightly smaller value of flux, $L_2C_2C_3$ is parallel resonant to ω_2. Since C_3 is much larger than C_2, the series and parallel resonant conditions are obtained with only a slight difference in flux. The resulting curve of response versus flux is plotted in Figure 3. By using a direct-current biasing flux to bias the curve to the center of the steep straight portion, the greatest sensitivity will be obtained. A small current in L_5 will then produce a larger current in the load resistor R_L.

Use as a Frequency Converter

Since the current in L_4C_4 of Figure 2 is a modulated signal it is evident that side bands are generated in the non-linear inductance.

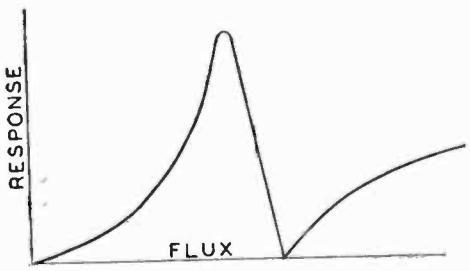

Fig. 3 — Input-output curve for Figure 2.

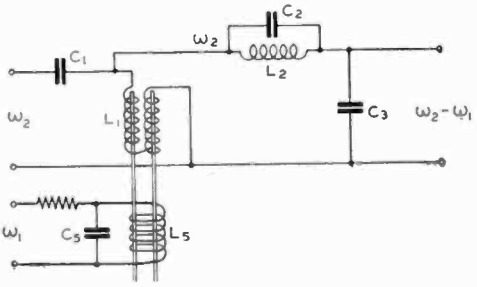

Fig. 4—Circuit for an oscillating transformer.

If the signal in L_5 is at high frequency, a separate circuit may be resonated to one of the side bands and we then have a frequency converter.

The special coupling arrangement of Figure 2 of $L_2C_2C_3$ is then not needed. The circuit becomes that of Figure 4.

In Figure 4, the oscillator voltage at ω_2 is applied to L_1C_1, which may be resonant to ω_2. The mesh L_2C_2 is a wave trap resonant to ω_2 to keep current of that frequency out of the intermediate-frequency circuit. The circuit $L_1C_1L_2C_2C_3$ is resonant to the intermediate frequency $\omega_2 - \omega_1$. The signal ω_1 is applied to L_5C_5 which is resonant to it. The inductance L_5 is wound over both halves of L_1. See Specification of the Transformer below.

The Oscillating Transformer

Mathematics predicts and experiment has proved that the circuit

of Figure 4 regenerates and even oscillates if the oscillator excitation at ω_2 is sufficient. That is to say, ω_1 beats with ω_2 to produce voltage at $\omega_2 - \omega_1$. A resonant circuit at $\omega_2 - \omega_1$ produces a high current at that frequency. This beats with ω_2 to reproduce ω_1. Since a circuit is also resonant to ω_1, the resulting current may exceed the causative current and oscillation results at ω_1 and $\omega_2 - \omega_1$ simultaneously. Obviously the power is supplied by the exciter current at ω_2.

Mathematics of the Oscillating Transformer

For the purpose of this analysis it will be assumed that there is only a single non-linear inductance which is resonated simultaneouly to ω_2, ω_1 and $\omega_2 - \omega_1$ by means of an external network. This assumption does not change the results qualitatively. The practical expedient of winding L_1 and L_5 separately and balancing out their coupling is to make it possible to tune the circuits separately without reaction on each other.

It is possible to build up a circuit utilizing a balance of this sort in a manner that would cause the voltage at $\omega_2 - \omega_1$ to be balanced out. This should be avoided. There are four frequency components of interest namely, ω_1, ω_2, $\omega_2 - \omega_1$ and direct current. If the flux in half the core is reversed for any one of these alone, the contribution of that half the core at frequency $\omega_2 - \omega_1$ is reversed and the output is zero. However, if any two of these components are reversed simultaneously in one half the core (as in Figure 4, where ω_2 and $\omega_2 - \omega_1$ are reversed in one half) the two reversals cancel out and operation is the same as in a single coil.

The assumption is made that the voltage and current in the non-linear inductance are related in the following manner.

$$e = \frac{di}{dt}(L_0 + L_1 i) \tag{1}$$

where L_0 is the small-signal inductance, and L_1 is a constant.

It should be understood that the equation can only be accurate over a limited region where $L_1 i < L_0$.

Assume a current of the form,

$$i = a \sin \omega_1 t + b \sin \omega_2 t.$$

The term $b \sin \omega_2 t$ should be thought of as a large exciter current having a function similar to the B supply of a tube. The term $a \sin \omega_1 t$ is the signal input.

Now if $$i = a \sin \omega_1 t + b \sin \omega_2 t, \tag{2}$$

then $$\frac{di}{dt} = a\omega_1 \cos \omega_1 t + b\omega_2 \cos \omega_2 t, \tag{3}$$

and

$$L_1 i \frac{di}{dt} = L_1 [a^2 \omega_1 \sin \omega_1 t \cos \omega_1 t + b^2 \omega_2 \sin \omega_2 t \cos \omega_2 t + ab\omega_2 \sin \omega_1 t \cos \omega_2 t + ab\omega_1 \sin \omega_2 t \cos \omega_1 t]. \tag{4}$$

The first two terms of the bracket of Equation (4) lead to second harmonic components that are not of interest at the moment. The last two terms may be transformed as follows:

$$L_1 ab\omega_2 \sin \omega_1 t \cos \omega_2 t = \frac{L_1 ab}{2} [\omega_2 \sin (\omega_2 + \omega_1) t - \omega_2 \sin (\omega_2 - \omega_1) t]$$

$$L_1 ab\omega_1 \sin \omega_2 t \cos \omega_1 t = \frac{L_1 ab}{2} [\omega_1 \sin (\omega_2 + \omega_1) t + \omega_1 \sin (\omega_2 - \omega_1) t].$$

Adding:

$$e_s = \frac{L_1 ab}{2} [(\omega_2 + \omega_1) \sin (\omega_2 + \omega_1) t - (\omega_2 - \omega_1) \sin (\omega_2 - \omega_1) t]. \tag{5}$$

If the circuit resonates to $\omega_2 - \omega_1$ the current at $\omega_2 - \omega_1$ is found by dividing by the resistance.

$$i_{2-1} = \frac{L_1 ab}{2R_{2-1}} (\omega_2 - \omega_1) \sin (\omega_2 - \omega_1) t,$$

where R_{2-1} is the resistance of the circuit at frequency $\omega_2 - \omega_1$.

The ratio of output current to input current is,

$$\frac{i_{2-1}}{i_1} = \frac{-L_1 ab}{2aR_{2-1}} (\omega_2 - \omega_1) \frac{\sin (\omega_2 - \omega_1) t}{\sin \omega_1 t}. \tag{6}$$

The ratio of peak currents is,

$$\frac{I_{2-1}}{I_1} = \frac{L_1 b}{2R_{2-1}} (\omega_2 - \omega_1),$$

or

$$\frac{I_{2-1}}{I_1} = \frac{(\omega_2 - \omega_1)\, L_0}{R_{2-1}} \frac{L_1 b}{2L_0} = Q_{2-1} \frac{L_1 b}{2L_0}.$$

Q_{2-1} is the ratio of the reactance of L_0 at $\omega_2 - \omega_1$ to the *resistance of the whole resonant circuit* at $\omega_2 - \omega_1$.

The term $L_1 b/2L_0$ is a factor which must have a value less than unity. It probably lies in the region between ¼ and ⅛ in a practical case.

The Feedback Effect

If i_1 (which equals $a \sin \omega_1 t$) produces i_{2-1} (which equals $\frac{-L_1 ab\ (\omega_2 - \omega_1)}{2 R_{2-1}} \sin (\omega_2 - \omega_1)\, t$), then it is evident that i_{2-1} will produce a current i_f at the frequency $\omega_2 - (\omega_2 - \omega_1)$ or at ω_1. This current has the value

$$i_f = a\, Q_{2-1} \frac{L_1 b}{2L_0} Q_1 \frac{L_1 b}{2L_0} \sin \omega_1 t$$

$$= a\, Q_{2-1}\, Q_1 \left(\frac{L_1 b}{2L_0} \right)^2 \sin \omega_1 t$$

In a steady state condition it must be remembered that the actual input current i_1 includes i_f as part of itself. The current which would have flowed if the feedback effect were not present is $i_1 - i_f$. The voltage required to produce i_1 in the presence of feedback is less than that without feedback by the ratio $\frac{i_1 - i_f}{i_1}$.

If $Q_{2-1}\, Q_1 \left(\frac{L_1 b}{2L_0} \right)^2 > 1$, the circuit will oscillate at $\omega_2 - \omega_1$.

This is a condition quite easy to obtain since it is easy to obtain a Q of the order of 50 when using a partially saturated ferrite core.

Of course, the tendency to oscillate can be overcome by resistance or by reducing the excitation at ω_2. Such a circuit can be used as a regenerative converter. To the extent that it is regenerative it is also an amplifying converter. Unfortunately no method has been devised for disconnecting or neutralizing the feedback. If this could be done, the circuit could be used as a non-regenerative amplifying converter.

Degeneration Using a Circuit Resonant to $\omega_2 + \omega_1$

As pointed out in Equation (5) the action of ω_2 and ω_1 in the non-linear inductance, produces a component at frequency $\omega_2 + \omega_1$. It should be noted however that the sign of this term is positive while the sign of the term at $\omega_2 - \omega_1$ is negative.

This component at $\omega_2 + \omega_1$, beats with ω_2 to produce feedback at ω_1 also. Because of the above mentioned difference in sign however, the feedback is degenerative in this case. This has been checked experimentally using the circuit of Figure 5. In using this circuit, if L_2C_2 is tuned to 780 kilocycles corresponding to $\omega_2 - \omega_1$, oscillation occurs at ω_1 and $\omega_2 - \omega_1$. However if L_2C_2 is tuned to 1220 kilocycles, corresponding to $\omega_2 + \omega_1$, the circuit tuned to 220 kilocycles is degenerated. Or rather it acts as though another circuit tuned to 220

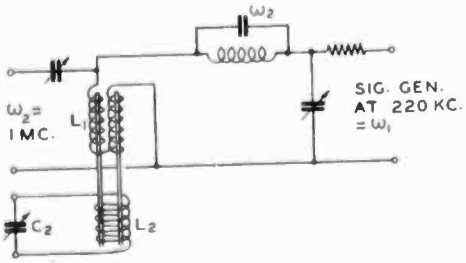

Fig. 5—Circuit for a degenerative converter.

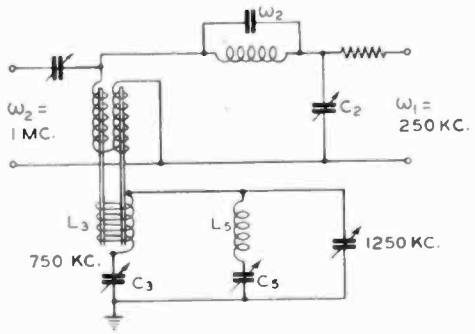

Fig. 6—Oscillator using $2\omega_2 - \omega_1$.

kilocycles were coupled to it. The depth of the valley between peaks may be made to go to as low as 10 per cent of peak response.

Oscillation Above the Excitation Frequency

An attempt was made to neutralize the positive regeneration caused by the circuit tuned to $\omega_2 - \omega_1$ by using simultaneously a circuit tuned to $\omega_2 + \omega_1$ to produce negative regeneration. This was not wholly successful because of critical tuning and regeneration of another sort which is of some interest.

The circuit used was that of Figure 6. In operation the meshes of C_3L_3 and C_5L_5 were separately resonated to 750 kilocycles so that L_3C_3 L_5C_5 was resonant to 750 kilocycles and would be unaffected by the setting of C_4. The capacitor C_4 was left at minimum and C_2 was tuned to 250 kilocycles. Oscillation then occurred at 250 kilocycles and 750 kilocycles. At this point C_4 was tuned so that $L_3L_5C_3C_5C_4$ was resonant to 1250 kilocycles and for very critical tuning, oscillation stopped. However, the circuit was highly regenerative at adjacent frequencies.

At this point the capacitor C_2 was open circuited, eliminating the circuit tuned to 250 kilocycles. Oscillation then occurred at 750 and 1250 kilocycles. If 750 kilocycles is now called ω_1, then 1250 kilocycles is $2\omega_2 - \omega_1$. Changes in frequency were made to show that this is the actual relationship. This corresponds to ω_1 beating with the second harmonic of ω_2. This is probably the actual process in operation because a strong second harmonic is present even though no resonant circuit is present at that frequency. Somewhat stronger excitation is required for oscillation to occur with this circuit than with that of Figure 4 or Figure 5.

Maximizing Stable Amplification

It should be noted that the actuating means is ampere turns. If it is assumed that the best Q obtainable is independent of frequency, then the power input required for a given number of ampere turns is proportional to frequency. This means that the lower the input frequency the higher the gain (the output frequency being held constant). Similarly the higher the output frequency the higher the gain (the input frequency being held constant).

If the input frequency is ω_1 and the output $\omega_2 + \omega_1$, ω_2 being the oscillator, and if the excitation may be adjusted to where the circuits at ω_1 and $\omega_2 + \omega_1$ act like a pair of coupled circuits, the power gain will be exactly $\frac{\omega_2 + \omega_1}{\omega_1}$ compared to equivalent selectivity performance obtained with two circuits tuned to ω_1. If $\omega_2 - \omega_1$ is used instead of $\omega_2 + \omega_1$, some regenerative gain may be obtained in addition to the factor $\frac{\omega_2 - \omega_1}{\omega_1}$. Excitation must be kept below the point of oscillation.

To maximize the gain, then, the excitation and output frequencies should be increased as much as practical. Unfortunately the approximation that the Q is independent of frequency, breaks down when frequencies above a megacycle are used. It seems likely that with presently available cores, 5 megacycles is as high as there is any advantage in going.

Experimental Amplifier

To check the above theory, an amplifying converter, like that shown in Figure 7, was set up.

In operation L_1C_1 was tuned to ω_2. The mesh L_2C_2 was tuned near to ω_2 but was mistuned sufficiently to allow enough voltage at this fre-

quency to appear on the crystal. The circuit $L_2C_2L_3C_3$ was tuned to $\omega_2 - \omega_1$, or $\omega_2 + \omega_1$ by varying C_3. The circuits L_5C_5 and L_4C_4 were tuned to ω_1. A signal at ω_1 was applied to L_5C_5. An amplified component at ω_1 could be observed in the tube voltmeter across C_4. It was difficult to determine the extent of the non-regenerative gain because it was found that the frequencies $\omega_2 + \omega_1$, ω_2 and $\omega_2 - \omega_1$ were so close together that the circuits L_1C_1, $L_2C_2L_3C_3$ responded to all three simultaneously. However favoring $\omega_2 - \omega_1$ caused regeneration or even oscillation while favoring $\omega_2 + \omega_1$ caused degeneration. Not only the circuit $L_3C_3L_2C_2$ but also the circuit $L_2C_2L_1C_1$ could cause oscillation by being tuned to $\omega_2 - \omega_1$, since the excitation at ω_2 was only slightly reduced by this degree of mistuning.

Amplification of the predicted amount could be obtained by a critical adjustment of the tuning but probably some regeneration was present.

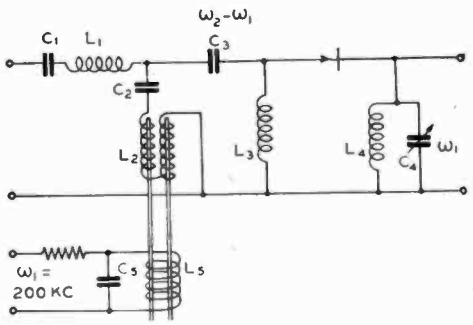

Fig. 7—Experimental amplifier.

Oscillating Non-Linear Capacitor

For all the functions mentioned in the preceding section, a non-linear capacitor should be just as effective as a non-linear inductance. A disadvantage is that there is no trick corresponding to the balanced windings on the non-linear core. Another difference is that, in the capacitor, the non-linearity may be a function of the frequency.

Non-linear capacitors may be made from various titanates. Considerable work has already been done along this line.[4]

Specification of the Transformer

In order to keep the required excitation power at a small value, it was found desirable to keep the size of the saturating part of the core quite small.

The dimensions of the ferrite cores are given in Figure 8. Two such cores are used in one transformer. The arrangement of L_1 is shown in Figure 9. The arrangement of L_2 is shown in Figure 10. For the circuits of Figures 4 and 5 the coil L_1 had 45 turns on each

[4] H. L. Donley, "Effect of Field Strength on the Dielectric Properties of Barium Strontium Titanate", *RCA Review*, Vol. VIII, No. 3, pp. 539-553, September, 1947.

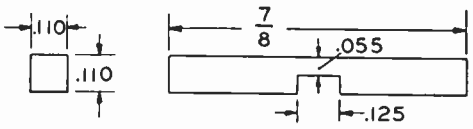

Fig. 8 — Core specifications for Figure 4.

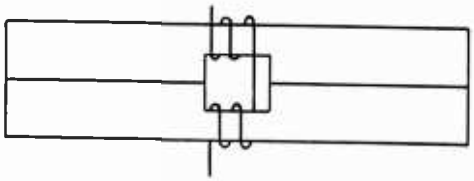

Fig. 9—Winding L_1 for Figure 4.

side of the core and tuned to 1 megacycle with about 300 micromicrofarads with the magnet properly positioned. The coil L_2 had 85 turns and tuned to 450 kilocycles with about 350 micromicrofarads. The size of the wire is not critical since most of the loss is in the core.

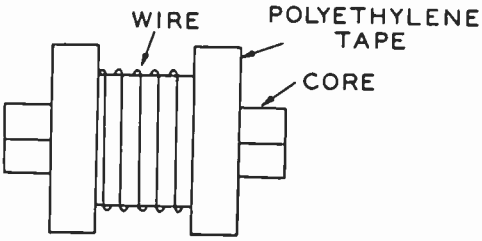

Fig. 10—Winding L_2 for Figure 4.

For Figure 7, L_1 has 10 turns of 7-41 litz on each side and L_2 has 400 turns of #40 silk enamel copper wire.

Conclusion

The developments disclosed include several novel ideas, which could be incorporated in practical apparatus. It has not been definitely decided whether any of these possible applications would have practical advantages over accomplishing the same results with vacuum tubes. The possible uses that have been considered are the following:

1. Converter for a superheterodyne receiver in the broadcast band.
2. A completely tubeless receiver, using one or more germanium crystal oscillators for exciter power.
3. A frequency standard, using a quartz crystal oscillator and its harmonics as a primary standard. Generate the frequencies between harmonics by a magnetic oscillator using the harmonics as exciting current.
4. A flip flop counter using two magnetic amplifier transformers to replace a double triode.

TRANSIENT RESPONSE OF FILTERS*

By

MURLAN S. CORRINGTON

Home Instrument Department, RCA Victor Division,
Camden, N. J.

Summary—*The ideal low-pass filter is defined as one which is perfectly flat for frequencies from zero to cutoff and attenuates at a fixed number of decibels per decade beyond. The transient response of such a filter has been computed and it is shown that such a characteristic is not necessarily desirable when the time of rise and amount of overshoot are important. From this basic transient response it is possible to derive many solutions for selectivity curves composed of straight line segments. These can be used for comparative purposes when designing practical circuits.*

There are often simple relations between the transient response of a low-pass filter and that of the corresponding high-pass filter. Many curves are given to show these responses, as well as the effect of peaking and rolloff near cutoff.

INTRODUCTION

IN MANY engineering departments of the electronic industry it is believed that the ideal low-pass amplifier, such as an audio or video amplifier, should have as flat a selectivity curve as possible up to the cutoff frequency, and should attenuate smoothly beyond. The contention is that if the amplitude bandwidth is sufficient to pass the highest frequency component of the incoming signal without appreciable attenuation, the output signal will contain negligible distortion.

The analysis which follows will show that in addition to the waveform distortion that can be produced in such an amplifier, due to phase shift near cutoff, there is a transient overshoot and subsequent ringing of the circuit that may be objectionable. The effect on the transient of varying such a flat response near cutoff by peaking and by rolloff will also be discussed. Similar properties of the high-pass filter will be given. By analogy the results for the low-pass filter can be applied to the envelope of the transient oscillation in the band-pass filter, and a similar analogy relates the envelope of the transient oscillation of a band-elimination filter to the response of a high-pass filter.

IDEALIZED RESPONSE CURVES

In order to obtain equations for a low-pass filter which can be

* Decimal Classification: R143.2.

integrated readily, it is customary to assume a flat amplitude characteristic and linear phase shift, as shown by Figure 1. Using the Fourier integral for the response due to a unit step function[1]

$$e = \tfrac{1}{2} A(0) + \frac{1}{\pi} \int_0^\infty \frac{A(\omega)}{\omega} \sin [\omega t - \theta(\omega)] \, d\omega \qquad (1)$$

on this characteristic, the result is

$$e = \tfrac{1}{2} + \frac{1}{\pi} \int_0^{\omega_0} \frac{\sin \omega (t - t_d)}{\omega} \, d\omega = \tfrac{1}{2} + \frac{1}{\pi} \operatorname{Si} \omega_0 (t - t_d). \qquad (2)$$

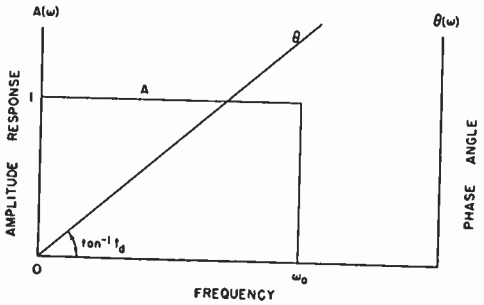

Fig. 1—Idealized characteristic.

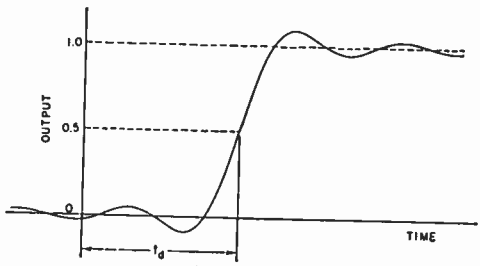

Fig. 2—Response to unit step function.

The startling result, shown by Figure 2, is that the circuit starts to respond before the disturbing force is applied. This inconsistency is caused by the fact that it is mathematically impossible to assign arbitrary and independent amplitude and phase characteristics to a minimum net phase shift network.[2,3]

The relations between the two characteristics that must be satisfied are well known, and many examples have been given by Bode.[4] As soon as the amplitude characteristic is specified over the entire range of frequencies, the phase curve can be computed directly. From these two characteristics the Fourier integral can be used to determine the transient response to any applied wave form. Thus the transient

---

[1] W. L. Sullivan, "Analysis of Systems with Known Transmission-Frequency Characteristics by Fourier Integrals," *Elec. Eng.*, Vol. 61, No. 5, pp. 248-256, May, 1942.

[2] K. Küpfmüller, "Über Beziehungen zwischen Frequenzcharakteristiken und Ausgleichsvorgängen in linearen Systemen," *Elektrische Nachrichten-Technik*, Vol. 5, pp. 18-32, January, 1928.

[3] E. A. Guillemin, COMMUNICATION NETWORKS, Vol. II, pp. 480, 501-504; John Wiley & Sons, New York, N. Y., 1935.

[4] Hendrik W. Bode, NETWORK ANALYSIS AND FEEDBACK AMPLIFIER DESIGN, Chapters 13, 14, 15; D. van Nostrand Company, Inc., New York, N. Y., 1945.

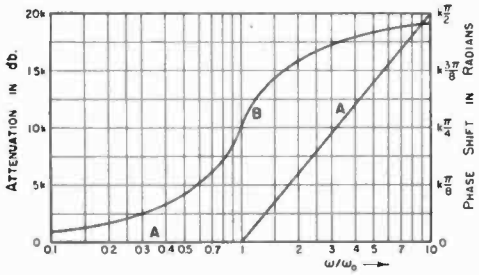

Fig. 3—Semi-infinite constant slope characteristic.

response and the selectivity curve are merely two equivalent ways of observing the characteristics of a given circuit. Either one completely determines the other. In the example of Figure 1, the rate of cutoff at ω_0 is infinite. This requires an infinite number of sections of filter, and the phase shift will also be infinite. This means that such a circuit could not pass a signal in a finite time, and the precursory response of Figure 2 is therefore meaningless, but merely shows how an impossible assumption leads to an impossible conclusion.

In the following section the characteristic of Figure 1 will be modified so the attenuation beyond cutoff is a constant number of decibels per decade, and the corresponding phase curve will then be as shown by Figure 3. This is a physically realizable case and will transmit a signal in a finite time. It is a particularly important ideal case since a large number of characteristics composed of straight line segments can be obtained from it by integration and convolution.

Transient Response of Idealized Low-Pass Filter

The response of a network having the transfer characteristic of Figure 3 can be computed by the formulas in the Appendix. k corresponds to the number of circuits in cascade required for a given characteristic. For example, for a single circuit $k = 1$, and the attenuation beyond cutoff is 20 decibels per decade (approximately 6 decibels per octave).

The time delay curve for this characteristic is shown by Figure 4. It was determined by dividing the phase shift, curve B of Figure 3, by the normalized frequency ω/ω_0. For low frequencies, $\omega/\omega_0 << 1$,

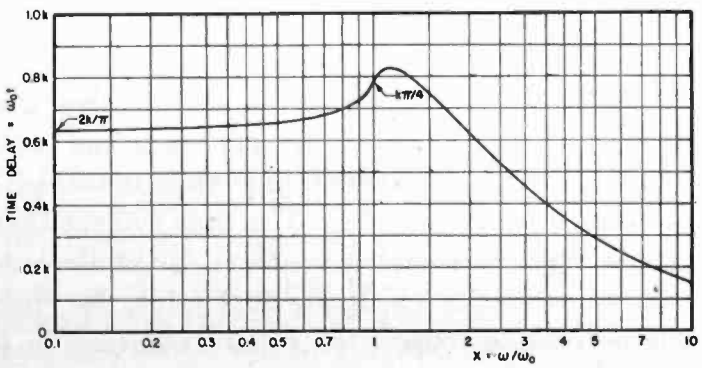

Fig. 4—Time delay curve for semi-infinite constant slope low-pass filter.

the time delay is nearly constant, but there is a substantial peak just beyond cutoff, following which the delay decreases smoothly toward zero.

For a unit impulse the response is $h_1(\alpha)$ shown by Figure 5. The subscript indicates a low-pass filter of one section. The variable $\alpha = \omega_0 t$ corresponds to time and $\alpha = 2\pi$ is equivalent to the time required for a complete oscillation at the cutoff frequency ω_0.

For a single circuit, $h_1(\alpha)$, the output rises suddenly to unity and then drops smoothly, oscillating with gradually decreasing amplitude, with the period increasing gradually toward $\alpha = 2\pi$. The response to a unit step function, shown by Figure 6, is the integral of the response to a unit impulse, thus

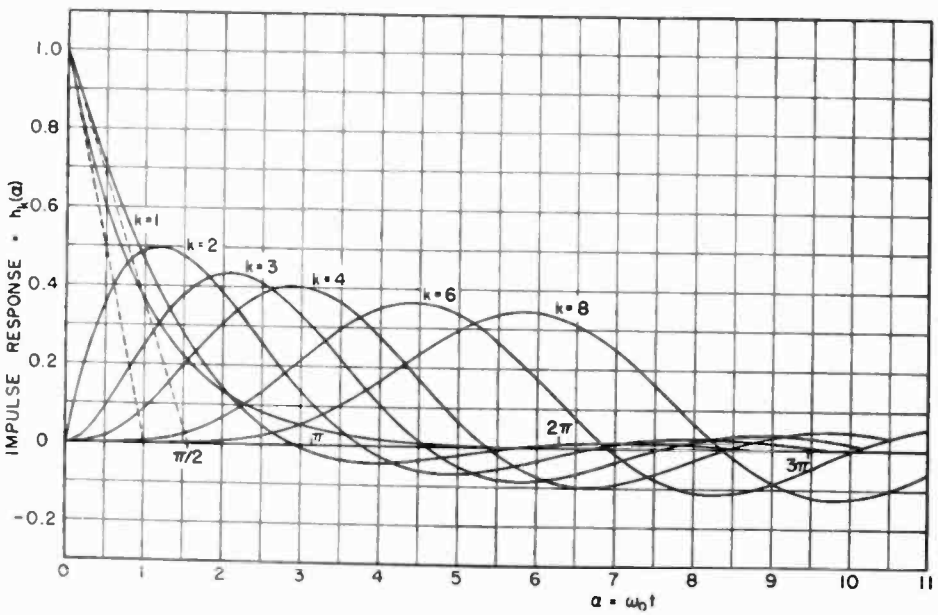

Fig. 5—Impulse response of semi-infinite constant slope low-pass filter.

$$A_1(\alpha) = \int_0^{\alpha} h_1(\alpha)\, d\alpha. \tag{3}$$

The step function response output rises almost linearly at first, overshoots approximately six per cent, and oscillates about the final value of unity with decreasing amplitude and the period gradually increasing toward $\alpha = 2\pi$. It is thus evident that such a flat amplifier cannot reproduce a step function faithfully but must "ring" with a damped oscillation about the final value, the ringing frequency gradually decreasing toward the cutoff frequency in the limit.

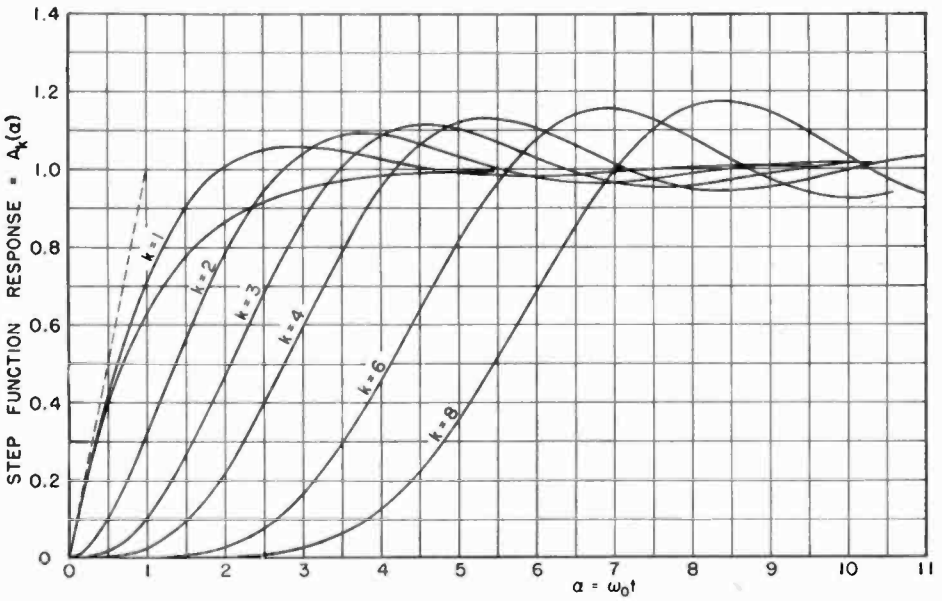

Fig. 6—Step function response of semi-infinite constant slope low-pass filter.

Application of Convolution Theorem

The response of the network to an infinitely short pulse, the unit impulse, is one of the most fundamental quantities of the theory of transients.[5,6] From this property the response to any other wave form can be computed directly. Thus if $h(t)$ is the impulse response and $e(t)$ is any applied wave form, the response to $e(t)$ is[7]

$$i(t) = \int_0^t h(\lambda)\, e(t-\lambda)\, d\lambda. \tag{4}$$

The integral can be evaluated analytically or by numerical integration.

Consider two identical low-pass circuits in cascade, each with responses $h_1(\alpha)$ and $A_1(\alpha)$. By Equation (4) the response to a unit step function, for the two circuits in cascade, will be

$$A_2(\alpha) = \int_0^\alpha A_1(\alpha-\lambda)\, h_1(\lambda)\, d\lambda \tag{5}$$

---

[5] J. R. Carson and O. J. Zobel, "Transient Oscillations in Electric Wave Filters," *Bell Sys. Tech. Jour.*, Vol. 2, pp. 1-52, July, 1923.

[6] E. C. Cherry, "Pulse Response: a New Approach to A.C. Electric-Network Theory and Measurement," *Journal of the Institution of Electrical Engineers*, Part III, Vol. 92, pp. 183-196, September, 1945.

[7] Vannevar Bush, OPERATIONAL CIRCUIT ANALYSIS, p. 68, Eq. (102); John Wiley & Sons, Inc., New York, N. Y., 1929, 1937.

and for a unit impulse

$$h_2(\alpha) = \frac{d}{d\alpha} A_2(\alpha) = \int_0^\alpha h_1(\alpha - \lambda)\, h_1(\lambda)\, d\lambda \qquad (6)$$

since the output of the first circuit forms the input voltage for the second. This process can be continued to give corresponding $h_k(\alpha)$ and $A_k(\alpha)$ for higher values of k.

The curves of Figure 5 show how the impulse response depends upon the rate of cutoff of the filter. For large values of k (many circuits in cascade) the response at the output is delayed while it passes through the network. The first maximum is the greatest one, and the circuit then oscillates with decreasing amplitude, and the frequency decreases as it approaches the cutoff frequency ω_0. The overshoot in the negative direction increases with the number of circuits, as more of the energy stored in the preceding circuits is discharged into the output circuit.

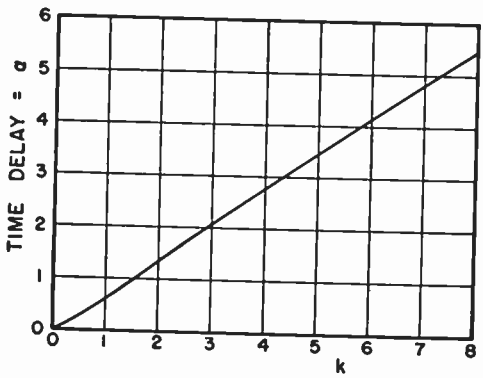

Fig. 7—Time delay of response.

The response to a unit step function is the integral of the impulse response, as shown by Figure 6. The circuits cause an overshoot and damped ringing of frequency ω_o. The overshoot is approximately six per cent for one circuit, rising to nearly 18 per cent for eight circuits. The maximum rate of rise is given by the height of the first loop of Figure 5 and as the number of circuits is increased the speed of response gradually decreases. If the time delay is taken as the time required to reach the fifty per cent point, the delay increases almost linearly with the number of circuits, k, as shown by Figure 7.

Since the cutoff frequency is the same for each filter, it is seen that the more rapidly the filter cuts off, the greater the overshoot. The region beyond cutoff must be considered as part of the design problem, since it determines the phase shift of the network just before cutoff, as well as the overshoot.

Effect of High-Frequency Peaking and Roll Off on a Low-Pass Filter

A low-pass filter with simple shunt peaking can be obtained by

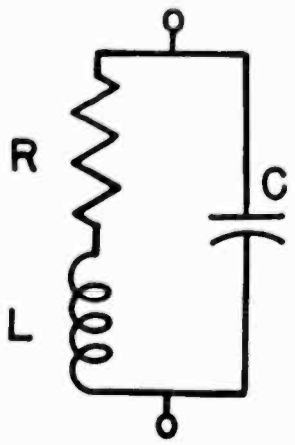

Fig. 8 — Low-pass filter with shunt peaking coil.

driving the circuit of Figure 8 with a high-impedance tube and taking the output voltage from the capacitor. This circuit is used for comparison because it is simple and is nearly as good as most other circuits, even though others may be more complicated.[8] The rate of attenuation for high frequencies is 6 decibels per octave, corresponding to $k = 1$, rather than 12 decibels per octave for the series-peaking coil. It can thus be compared with a single circuit with characteristic shown by Figure 3. The normalized impedance is

$$\frac{Z}{R} = \frac{1 + pL/R}{1 + pRC + p^2LC} \tag{7}$$

Let $\omega_0 = 1/RC$, $\dfrac{\omega}{\omega_0} = x$, and $\dfrac{\omega_0 L}{R} = Q$. Then

$$\frac{Z}{R} = \frac{1 + iQx}{1 - Qx^2 + ix}. \tag{8}$$

If the Q of the circuit is varied by changing the inductance, L, of the peaking coil, the selectivity curves will be as shown by Figure 9.

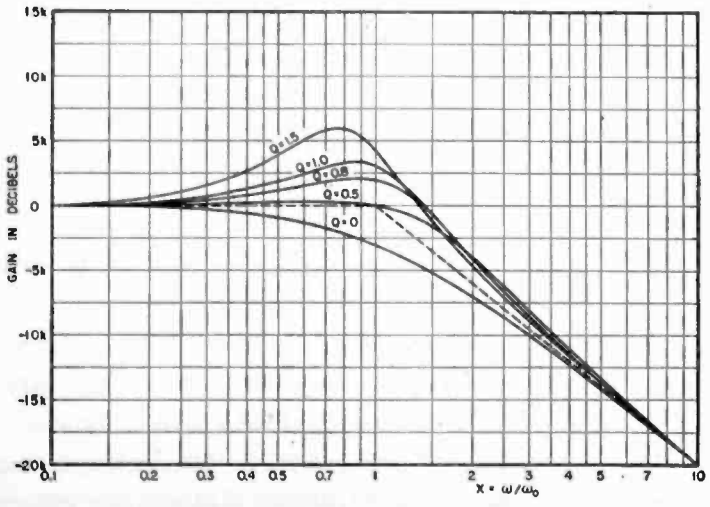

Fig. 9 — Amplitude characteristics for low-pass filter.

[8] Heinz E. Kallmann and Rolf E. Spencer, "Transient Response," with mathematical appendix by Charles P. Singer, *Proc. I.R.E.*, Vol. 33, No. 3, pp. 169-195, March, 1945. This paper discusses this case as well as many others, and obtains a measure of performance for each.

For a single circuit $k = 1$. $Q = 0$ corresponds to $L = 0$ and is the usual RC characteristic. All curves start out flat, and are asymptotic to the same line of unit slope (20 decibels per decade) going through unit gain at $x = 1$. The frequency of greatest gain decreases as Q increases, since the LC product increases with L.

By means of the usual Laplace transform tables,[9] the response of the above circuits to a unit impulse function and a unit step function can be computed from the above Equation (8) for the normalized impedance. When this is done the curves of Figures 10 and 11 are obtained.

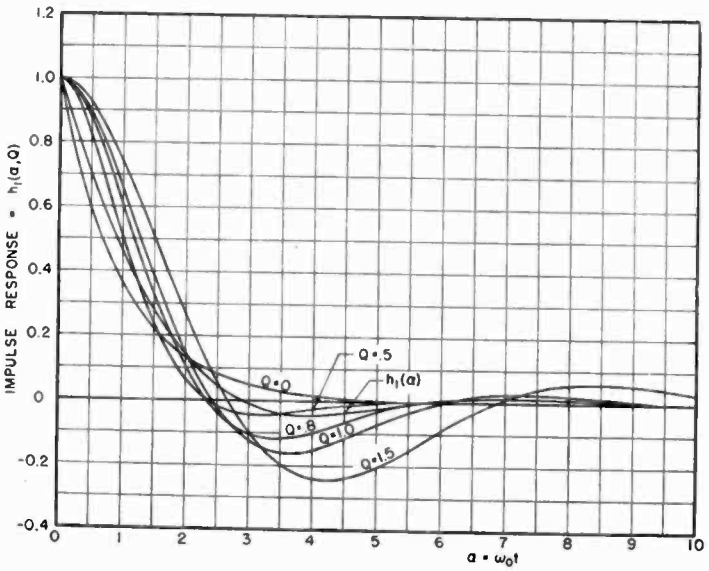

Fig. 10—Response to unit impulse, $h_1(\alpha, Q)$, low-pass filter.

The results of Figure 10 show that when a unit impulse is applied to the circuit of Figure 8 the capacitor is instantaneously charged up to unit voltage by an infinite surge of current. This current then discharges through the coil. If the circuit is not heavily damped (Q large) it will oscillate with an exponentially decaying sine wave, with frequency approximately equal to the frequency of maximum response on the selectivity curve of Figure 9.

For zero inductance, $Q = 0$, the usual RC discharge curve is obtained. When $Q = \frac{1}{2}$ the voltage does not begin to drop as fast, but then drops rapidly and overshoots approximately four per cent in the negative direction, with an oscillation that is quickly damped out because of the relatively high dissipation in the resistor. If Q is increased to 1, there is a longer delay before the voltage begins to drop rapidly, and it overshoots approximately sixteen per cent in the negative direc-

[9] Murray F. Gardner and John L. Barnes, TRANSIENTS IN LINEAR SYSTEMS, Appendix A, pp. 332-356, Vol. I; John Wiley & Sons, Inc., New York, N. Y., 1942.

tion. The curve is not as heavily damped as before. Reducing the damping still further gives a similar curve, $Q = 1.5$. In each case the oscillation decreases in proportion to the factor $e^{-\alpha/2Q}$. For no damping, $R = 0$, or $Q = \infty$, the impulse response will be a cosine wave, continuing to infinity.

The response of the semi-infinite constant-slope characteristic, $h_1(\alpha)$ is shown for comparison. The initial rate of decrease is rapid, but the rate is not maintained. The overshoot is approximately the same as for $Q = \frac{1}{2}$. If a compromise between rate of decrease to zero and amount of overshoot is required, it is then evident that an absolutely flat amplifier is not necessarily optimum. Slight peaking such as $Q = \frac{1}{2}$ may be better.

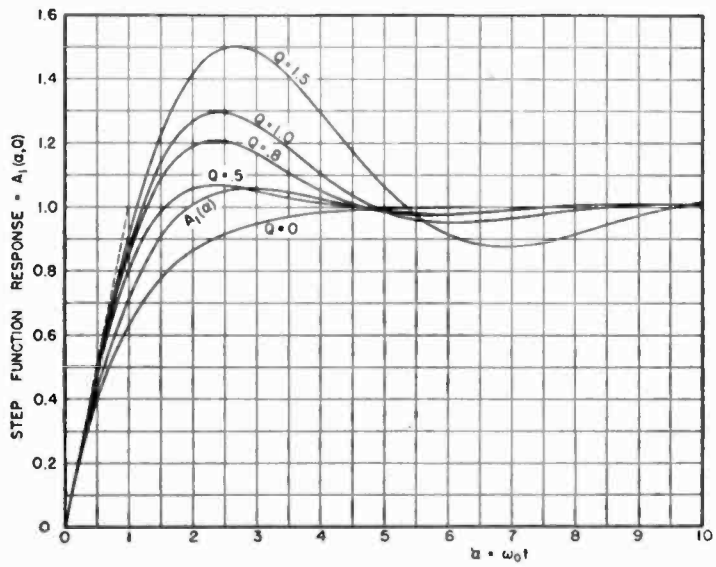

Fig. 11—Response to unit step function, $A_1(\alpha, Q)$, low-pass filter.

The response to a unit step function is shown by Figure 11. $Q = 0$ is the usual *RC* charging curve which, like all the others, starts out with unit slope. As Q is raised, the overshoot increases rapidly; the ringing becomes more and more pronounced. The curve of $A_1(\alpha)$ does not rise as rapidly as for $Q = \frac{1}{2}$, but the overshoot is nearly the same.

It is evident that the initial rate of rise is determined by the asymptotic rate of attenuation beyond cutoff. For a single circuit, $k = 1$, the curves are nearly linear at the origin and have unit slope. The additional gain near cutoff, due to peaking, causes greater overshoot and more rapid rise to unity, but the ringing has less damping and may be objectionable. The curves of Figure 9 show that for $Q = \frac{1}{2}$ there is actually a greater bandwidth than for the semi-infinite constant-slope characteristic, so the greater rate of rise is to be expected, since

more of the higher frequencies are passed without appreciable attenuation.

Effect of Cascading Low-Pass Filters

The effect of cascading the circuits can be computed by an application of the convolution theorem, Equation (4), or by a direct application of the Laplace transform tables. The curves of Figures 5 and 6 show the results for a semi-infinite constant-slope characteristic, and Figures 12 and 13 show the results for the selectivity curves of Figure 9, with $k = 2$.

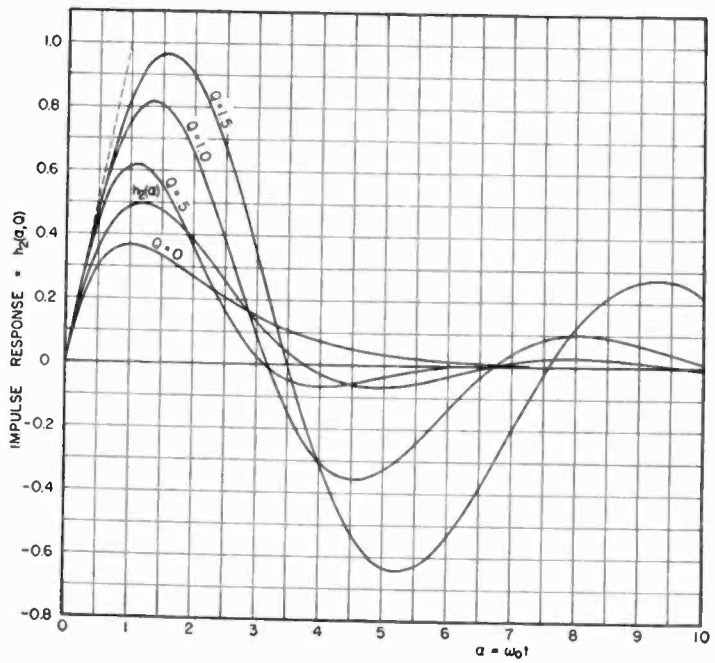

Fig. 12—Response to unit impulse, $h_2(\alpha, Q)$, low-pass filter.

Comparison of Figure 12 with Figure 10 shows that when two circuits are cascaded the impulse response no longer starts at unity at the origin, but passes through zero and has unit slope. The height of the first loop rises uniformly with increasing Q. The damping factor is $e^{-\alpha/2Q}$, which is the same as for a single circuit. The frequency of the oscillation is the same as for a single circuit, but the negative overshoot is greater in proportion. As Q is increased by increasing L, the resonant frequency determined by LC decreases, so that a longer time is required to complete an oscillation for higher values of Q. The curve of $h_2(\alpha)$ is also shown for comparison, and although the initial rate of rise is the same as for the other circuits, the decay is much less rapid.

Integration of the curves of Figure 12 results in the response to a unit step function, shown by Figure 13. The curves all start out like parabolas, rather than with constant slopes. If the input to the first

stage is a unit step, the output of the first stage will start out with unit slope, in accord with Figure 11. This unit slope input to the second stage is then changed over to a parabola by the same process. If there were three circuits in cascade, the curve would start out like a cubic equation, etc.

Comparison of Figures 11 and 13 shows that the first overshoot is approximately doubled for two circuits in cascade, but the damping factor and frequency of oscillations remains unchanged. It is evident that the Q must remain much less than unity for most video amplifiers. If the overshoot and subsequent oscillation for a single stage is appreciable, it becomes worse when the circuits are cascaded.

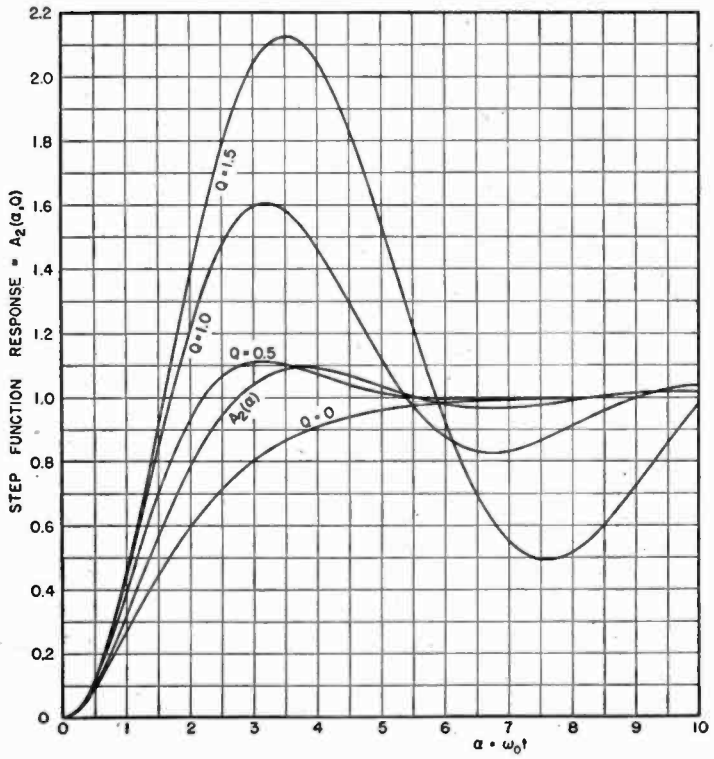

Fig. 13—Response to unit step function, $A_2(\alpha, Q)$, low-pass filter.

Transient Response of Idealized High-Pass Filter

The characteristic curve of a semi-infinite constant-slope high-pass filter is shown by Figure 14. The transfer characteristic is unity from $\omega = \omega_0$ to infinity, and drops at a uniform rate of $20k$ decibels per decade for frequencies between zero and ω_0.

Let the characteristics be defined as follows:

$$A(\omega) = x^k \qquad \theta(\omega) = k\{B(x) - \pi/2\} \qquad 0 \leq x \leq 1 \tag{9}$$

$$A(\omega) = 1 \qquad \theta(\omega) = -k\,B(1/x) \qquad 1 \leq x < \infty \tag{10}$$

where $$B(x) = \frac{2}{\pi}\int_0^x \tanh^{-1} t\, dt/t \text{ and } x = \omega/\omega_0.$$

The Fourier integral expression for the response to a unit step function can be written

$$A^k(\alpha) = \frac{1}{\pi}\int_0^1 x^{k-1} \sin\{\alpha x + \tfrac{1}{2}k\pi - kB(x)\}\, dx$$

$$+ \frac{1}{\pi}\int_1^\infty \frac{1}{x} \sin\{\alpha x + kB(1/x)\}\, dx \qquad (11)$$

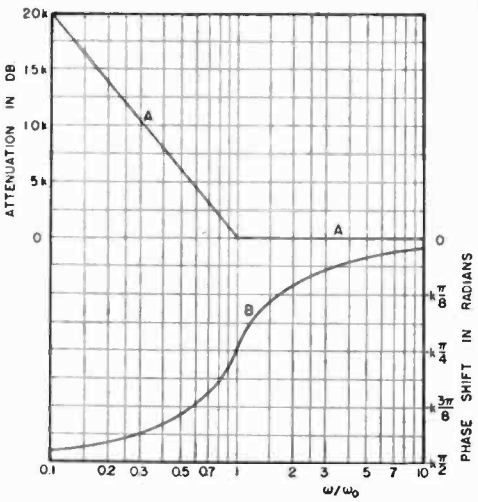

Fig. 14—High-pass filter.

where $A^k(\alpha)$ means the response to a unit step function for a semi-infinite constant-slope high-pass filter. It can be shown by successive differentiation of the Fourier integral for $A_k(\alpha)$, Equation (28) of appendix I, that

$$A^k(\alpha) = \frac{d^k}{d\alpha^k} A_k(\alpha). \qquad (12)$$

This leads to the relations

$$A^1(\alpha) = h_1(\alpha) \qquad (13) \qquad \text{and} \qquad h^1(\alpha) = \frac{d}{d\alpha} h_1(\alpha). \qquad (14)$$

This means that the curves for the high-pass filter can be obtained from those of the low-pass filter, Figures 5 and 6, by numerical differentiation with a difference table, or by convolution from the lower-order curves, remembering to add the contribution of the unit impulses to the integral.

Figure 15 shows the transient response for the high-pass filter $h^k(\alpha)$. A positive unit impulse occurs at the origin, after which the response suddenly drops to the negative value $-2k/\pi$. From this point there is a uniform rise, followed by an overshoot in the positive direction and a decaying ripple with frequency gradually approaching ω_o in the limit. As usual the more circuits in cascade, the greater the

overshoot in both directions and the less damping on the resulting ripple.

If each of these curves is integrated with respect to α, the curves $A^k(\alpha)$ are obtained as shown by Figure 16. Because of the initial unit impulse on each $h^k(\alpha)$, all the $A^k(\alpha)$ start at unity, decreasing rapidly and oscillating about the final value of zero, since such a filter cannot pass direct current.

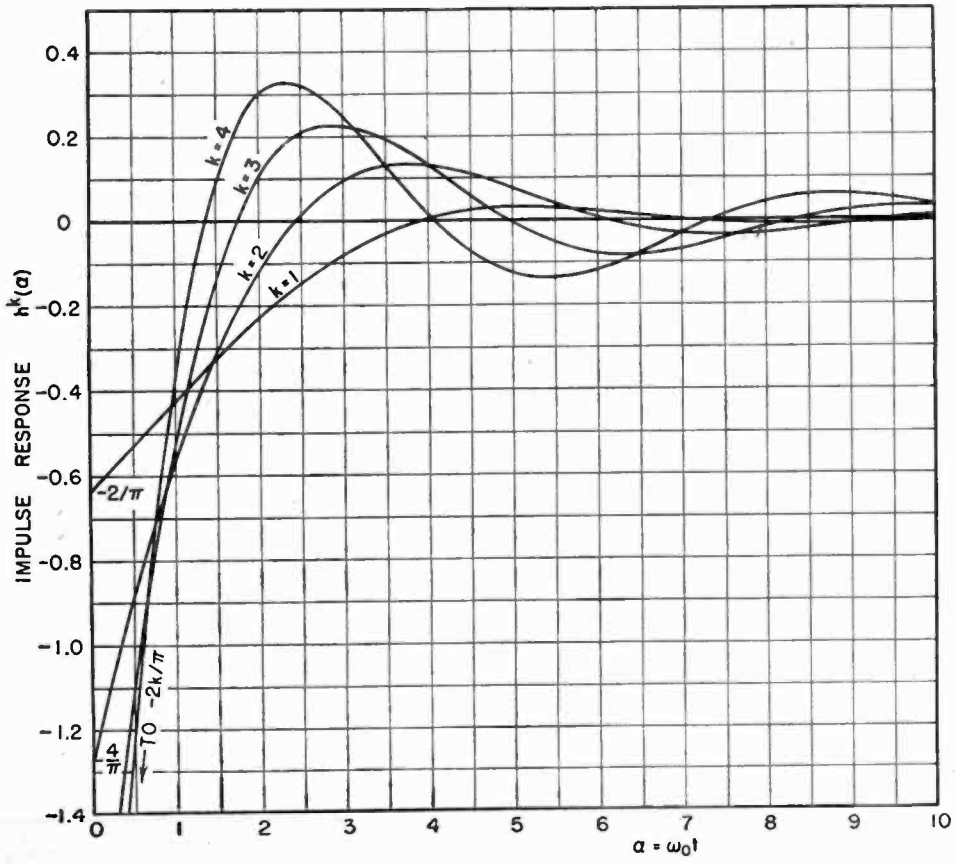

Fig. 15—Impulse response of semi-infinite constant slope high-pass filter.

Effect of Peaking and Roll Off Near the Cutoff Frequency of a High-Pass Filter

In order to compare the response of a high-pass filter with that of a low-pass filter, invert the attenuation curves of Figure 9 about the point $x = 1$ as shown by Figure 17. This is done by replacing p by $1/p$ in the equation for the normalized impedance. This is equivalent to replacing each capacitor with an inductor and each inductor with a capacitor. The circuit of Figure 8 then becomes that of Figure 18.

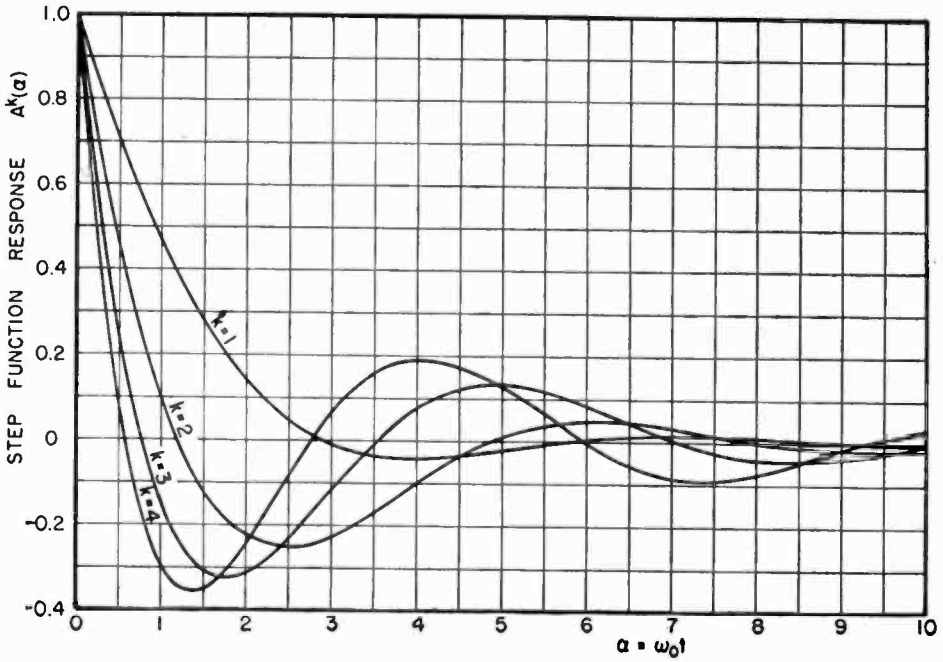

Fig. 16—Step function response of semi-infinite constant slope high-pass filter.

$$\frac{1}{Z} = \frac{1}{pL} + \frac{1}{R + 1/pC} \tag{15}$$

$$\frac{Z}{R} = \frac{p\,(p + 1/RC)}{p^2 + p\,\dfrac{R}{L} + \dfrac{1}{LC}} = \frac{ix\,(ix + Q)}{-x^2 + ix + Q} \tag{16}$$

where $Q = 1/\omega_0 RC,\ \omega_0 = R/L,\ x = \omega/\omega_0.$

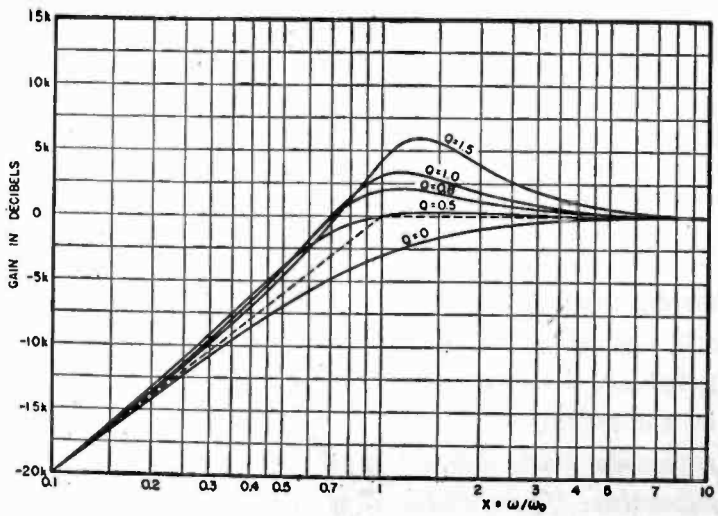

Fig. 17—Amplitude characteristics for high-pass filter.

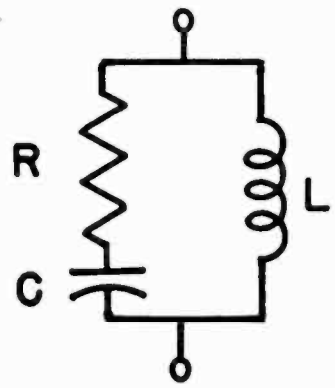

Fig. 18—High-pass filter.

All the attenuation curves start at zero at the origin since the inductance L is a short circuit for direct current. At high frequencies the circuit behaves like a resistance R. Q is varied in each case by changing the peaking capacitor C.

Starting with the operational form for the normalized impedance, the transient responses can be derived from the usual tables of Laplace transforms. Figure 19 shows the impulse response for various amounts of peaking. Each of the curves starts with a positive unit impulse, following which the curve drops to an initial value of $Q - 1$.

Some of these curves are very simply related to those for a low-pass filter. Thus

$$h^1(\alpha) = \frac{d}{d\alpha} h_1(\alpha). \tag{17}$$

$$\text{For } Q = 0,\ h^1(\alpha, 0) = \frac{d}{d\alpha} h_1(\alpha, 0). \tag{18}$$

$$\text{For } Q = \tfrac{1}{2},\ h^1(\alpha, 0.5) = -\tfrac{1}{2}\, h_1\,(\tfrac{1}{2}\,\alpha, 0.5). \tag{19}$$

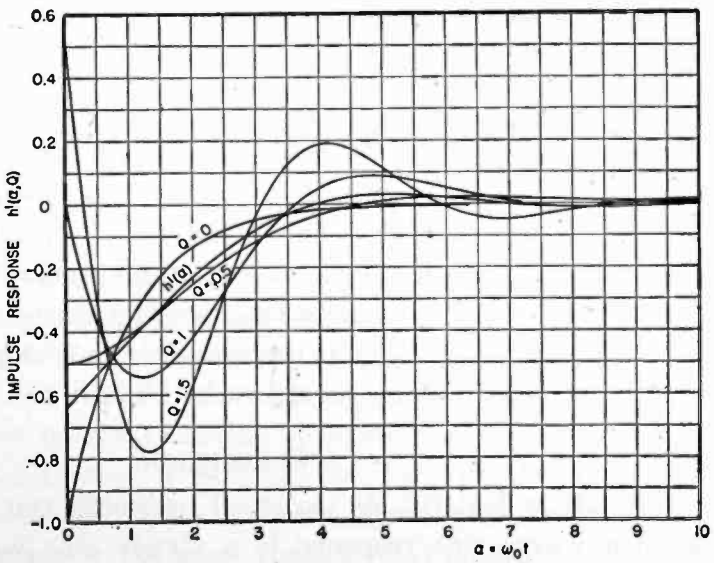

Fig. 19—Response to unit impulse, $h^1(\alpha, Q)$, high-pass filter.

$$\text{For } Q = 1,\ h^1(\alpha, 1) = \frac{d}{d\alpha} h_1(\alpha, 1). \tag{20}$$

$$\text{For } Q = 1.5,\ h^1(\alpha, 1.5) = 2\frac{d}{d\alpha} h_1\left(\tfrac{3}{2}\alpha, 1.5\right) + \tfrac{1}{2} h_1\left(\tfrac{3}{2}\alpha, 1.5\right). \tag{21}$$

There are corresponding relations between the A's.

As the Q is increased the frequency of maximum gain increases, as shown by Figure 17. This is also shown by the increased frequency of the transient response, Figure 19.

The integral curves give the response to a unit-step function, as shown by Figure 20. As before the frequency of response increases with Q, since the Q is raised by decreasing the capacitance, C. The initial value is always unity.

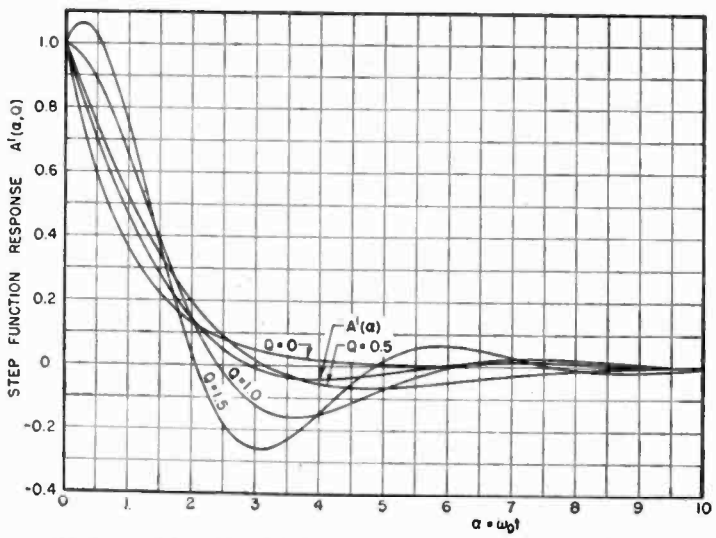

Fig. 20—Response to unit step function, $A^1(\alpha, Q)$, high-pass filter.

If two identical stages are cascaded, the response is modified. The frequency of oscillation does not change, but the initial value and the amount of overshoot increases. Figure 21 shows the impulse response for two stages in cascade. The initial value following the positive unit impulse at the origin is doubled, and the overshoot is also approximately doubled. For all cases the damping factor is $e^{-\frac{1}{2}\alpha}$, for a single stage or for two stages. The response to a unit step function is similar to that of a single stage, as shown by Figure 22.

Conclusions

The characteristics of electrical networks can be specified in two common ways. The response to a steady sine wave gives the usual

selectivity curve, and the response to a unit impulse or to a unit step function gives the transient response. These two properties are directly related and are merely two equivalent ways of observing the same phenomenon. Either one can be computed directly from the other.

There is a great need for the development of circuit theory that does not deal with sine waves. In modern circuit applications such as radar, pulse modulation, television, etc., many of the signals are not sine waves but are of a discontinuous nature. The usual steady state analysis has a very limited usefulness in these studies and the transient response is becoming more and more important. An extensive catalog

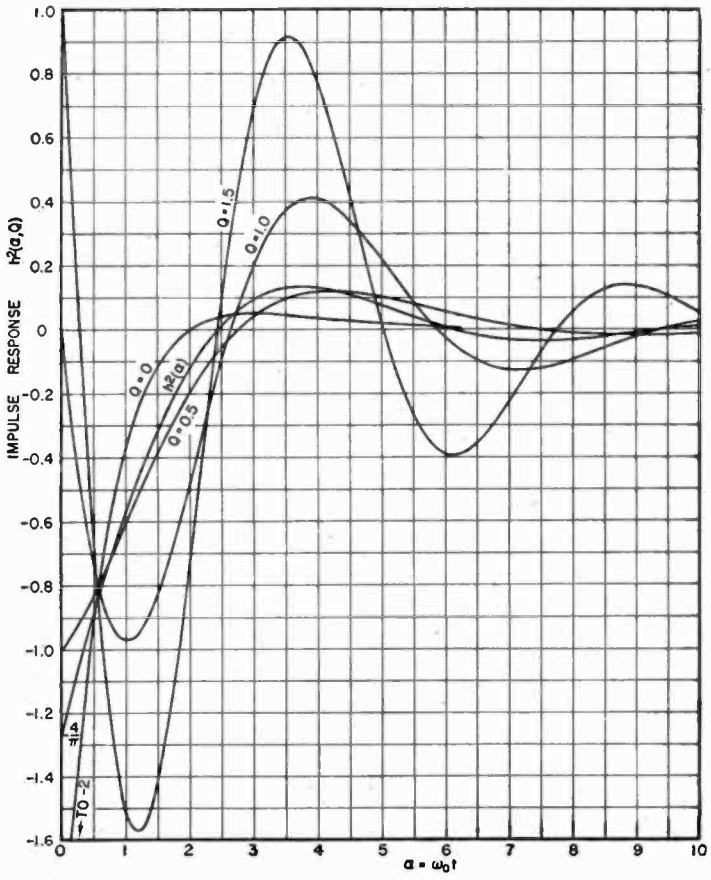

Fig. 21—Response to unit impulse, $h^2(\alpha, Q)$, high-pass filter.

of such responses is needed. This paper gives many such curves, and shows that the ideal flat amplifier is not necessarily desirable when the time of rise and amount of overshoot are important. There are many examples to show the effect of rate cutoff and the effect of peaking and rolloff near cutoff on the transient response. When such circuits are cascaded the signal wave is delayed, the time of rise increases, and any overshoot increases rapidly with the number of sections.

The impulse response is the most fundamental quantity. From it

the response to any other wave form can be computed by simple integration. The mathematical analysis leading to such a solution is normally very complex. One completely new solution has been computed numerically and is tabulated. It is very basic and many solutions for selectivity curves composed of straight line segments can be derived from it. This permits the computation of a catalog of idealized characteristics that can be used for comparative purposes when designing practical circuits.

A low-pass filter will oscillate at approximately the cutoff frequency when a transient is applied. If there is peaking near cutoff the frequency will be approximately that of maximum gain. The initial rate

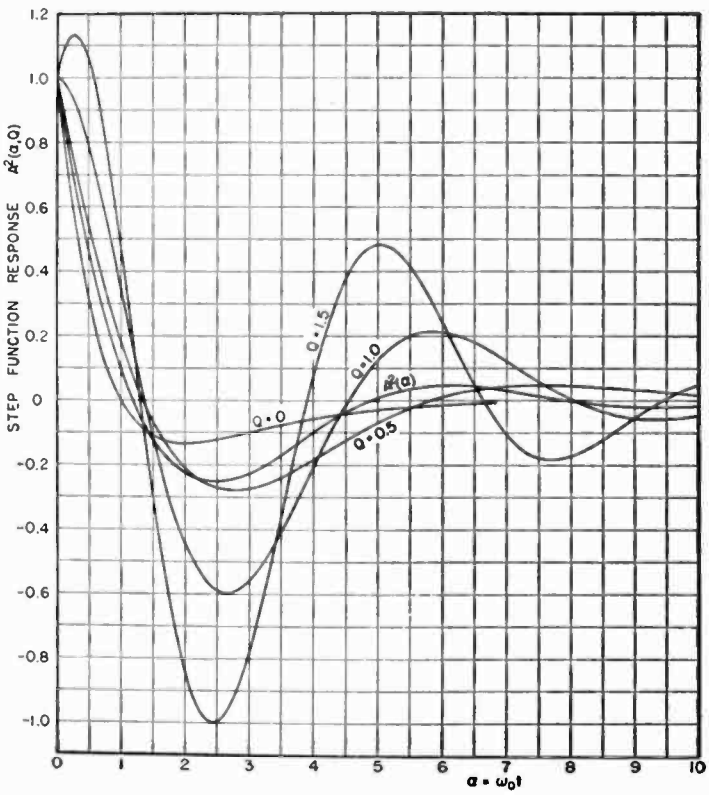

Fig. 22—Response to unit step function, $A^2(\alpha, Q)$, high-pass filter.

of rise is determined by the rate of cutoff. For a single section (cutoff at 20 decibels per decade) the initial rate of rise is unity. For two sections the rise is delayed considerably because the wave must pass through each section in turn. The build-up time from 10 per cent to 90 per cent, the time delay, and the amount of overshoot increases with the number of sections in cascade. By a well known analogy these results also apply to a band pass filter if the filter is symmetrical about the center frequency. In this case the envelope of the modulated carrier wave corresponds to the response of the low pass filter.

The speed of response or the velocity of propagation of a high-pass filter is infinite since the high frequencies are passed without attenuation. The applied unit impulse causes an infinite surge of current which charges up the circuit. This charge then discharges through the circuit elements; it will oscillate if the loading is not too heavy. For the examples shown the damping is independent of the Q or the number of circuits in cascade. The frequency of oscillation is approximately the cutoff frequency of the filter, although it will be more nearly equal to the frequency of maximum gain if there is peaking near cutoff. In many cases there is a simple relation between the response of a high-pass filter and the corresponding low-pass case. By a known analogy the response of a band elimination filter is similar to that of a high pass filter if there is symmetry about the center frequency. The envelope of the modulated carrier corresponds to the response of the analogous high-pass filter.

APPENDIX

Derivation of Power Series Expansion

Consider the semi-infinite constant-slope characteristic of a minimum net phase shift circuit, shown by Figure 3.

The filter characteristic is flat for $0 \leq \omega/\omega_0 \leq 1$ and cuts off at the uniform rate of $20k$ decibels per decade for frequencies $1 \leq \omega/\omega_0 < \infty$.

The phase curve B is uniquely determined* and tables have been published.[10,11] The attenuation, A, is an even function of frequency and the phase, B, is an odd function of frequency.

$$\text{Then } A(\omega) = 1 \qquad 0 \leq \omega/\omega_0 \leq 1 \qquad (22)$$

$$= (\omega/\omega_0)^{-k} \qquad 1 \leq \omega/\omega_0 < \infty \qquad (23)$$

and the phase angle

$$\theta(\omega) = k\,B(\omega/\omega_0) \qquad 0 \leq \omega/\omega_0 \leq 1 \qquad (24)$$

---

* Reference 4, p. 341.

[10] Murlan S. Corrington, "Table of the Integral $\frac{2}{\pi}\int_0^x \tanh^{-1} t\,dt/t$," *RCA Review*, Vol. 7, No. 3, pp. 432-437, September, 1946. [$x = 0(.01).97(.005).99(.002)\ 1$; $5D$]

[11] D. E. Thomas, "Tables of Phase Associated With a Semi-Infinite Unit Slope of Attenuation," *Bell Sys. Tech. Jour.*, Vol. 26, pp. 870-899, October, 1947. [$B(x)$ in degrees and radians, x, $1/x = 0(.001).996(.0005).998(.0001)\ 1$; $5S$].

$$= k\{\tfrac{1}{2}\pi - B(\omega_0/\omega)\} \qquad 1 \leq \omega/\omega_0 < \infty \tag{25}$$

where $B(x) = \dfrac{2}{\pi}\displaystyle\int_0^x \tanh^{-1} t\, dt/t \qquad x^2 \leq 1.$ (26)

The Fourier-integral expression for the response to a unit step function is the indicial admittance $A(t)$, or[1]

$$A_k(t) = \tfrac{1}{2}A(0) + \frac{1}{\pi}\int_0^\infty \frac{A(\omega)}{\omega}\sin[\omega t - \theta(\omega)]\, d\omega$$

$$= \tfrac{1}{2} + \frac{1}{\pi}\int_0^{\omega_0} \frac{1}{\omega}\sin[\omega t - kB(\omega/\omega_0)]\, d\omega$$

$$+ \frac{1}{\pi}\int_{\omega_0}^\infty \frac{(\omega/\omega_0) - k}{\omega}\sin[\omega t - \tfrac{1}{2}k\pi + kB(\omega_0/\omega)]\, d\omega. \tag{27}$$

Let $\omega/\omega_0 = x$, $\omega_0 t = \alpha$, where $\alpha = 2\pi$ corresponds to one cycle at the cutoff frequency.

Then $A_k(\alpha) = \tfrac{1}{2} + \dfrac{1}{\pi}\displaystyle\int_0^1 \frac{1}{x}\sin[\alpha x - kB(x)]\, dx$

$$+ \frac{1}{\pi}\int_1^\infty \frac{1}{x^{k+1}}\sin[\alpha x - \tfrac{1}{2}k\pi + kB(1/x)]\, dx. \tag{28}$$

Since the response to a unit impulse $h_k(t)$ is the derivative with respect to time of the response to a unit step function, $h_k(t) = \dfrac{d}{dt}A_k(t)$,

$$h_k(\alpha) = \frac{1}{\pi}\int_0^1 \cos[\alpha x - kB(x)]\, dx$$

$$+ \frac{1}{\pi}\int_1^\infty \frac{1}{x^k}\cos[\alpha x - \tfrac{1}{2}k\pi + kB(1/x)]\, dx. \tag{29}$$

FOURIER INTEGRAL FOR $k = 1$

For the case of a single circuit $k = 1$, Equation (29) becomes

$$h_1(\alpha) = \frac{1}{\pi}\int_0^1 \cos\left[\alpha x + B(x)\right] dx + \frac{1}{\pi}\int_1^\infty \frac{1}{x}\sin\left[\alpha x + B(1/x)\right] dx \qquad (30)$$

where the subscript indicates a single circuit low-pass filter.

Since the response is zero before the impulse is applied at $t = 0$,

$$h_1(-\alpha) = \frac{1}{\pi}\int_0^1 \cos\left[\alpha x - B(x)\right] dx - \frac{1}{\pi}\int_1^\infty \frac{1}{x}\sin\left[\alpha x - B(1/x)\right] dx = 0. \qquad (31)$$

Expand Equations (30) and (31) by the trigonometric formulas for functions of the sum and difference of two angles.
Then

$$h_1(\alpha) = \frac{1}{\pi}\int_0^1 \cos\alpha x \cos B(x)\, dx + \frac{1}{\pi}\int_0^1 \sin\alpha x \sin B(x)\, dx + \frac{1}{\pi}\int_1^\infty \frac{1}{x}\sin\alpha x \cos B(1/x)\, dx + \frac{1}{\pi}\int_1^\infty \frac{1}{x}\cos\alpha x \sin B(1/x)\, dx \qquad (32)$$

$$h_1(-\alpha) = \frac{1}{\pi}\int_0^1 \cos\alpha x \cos B(x)\, dx - \frac{1}{\pi}\int_0^1 \sin\alpha x \sin B(x)\, dx - \frac{1}{\pi}\int_1^\infty \frac{1}{x}\sin\alpha x \cos B(1/x)\, dx + \frac{1}{\pi}\int_1^\infty \frac{1}{x}\cos\alpha x \sin B(1/x)\, dx = 0. \qquad (33)$$

Adding Equations (32) and (33),

$$h_1(\alpha) = \frac{2}{\pi}\int_0^1 \cos \alpha x \cos B(x)\, dx + \frac{2}{\pi}\int_1^\infty \frac{1}{x} \cos \alpha x \sin B(1/x)\, dx. \quad (34)$$

Subtracting Equations (32) and (33),

$$h_1(\alpha) = \frac{2}{\pi}\int_0^1 \sin \alpha x \sin B(x)\, dx + \frac{2}{\pi}\int_1^\infty \frac{1}{x} \sin \alpha x \cos B(1/x)\, dx. \quad (35)$$

Either Equation (34) or Equation (35) is in a form suitable for the evaluation for various values of α, since the α appears only in the sine and cosine terms of the integrands.

Series Expansion of Second Integral

The following derivation will be based on the second integral of Equation (35). During the numerical computation the final result was checked at various points with Equation (34). Great care is required in this derivation to obtain integrands at each step that do not contain poles, since numerical integration must be used later to compute the coefficients of the series. The second member of Equation (35) can be computed as follows:

Consider the integral

$$I = \int_1^\infty \sin \alpha x \{1 - \cos B(1/x)\}\, dx/x = \int_1^\infty \sin \alpha x\, dx/x - \int_1^\infty \sin \alpha x \cos B(1/x)\, dx/x. \quad (36)$$

Integrate by parts

$$I = \left[\sin \alpha x \left\{ \int_x^\infty \frac{1 - \cos B(1/t)}{t}\, dt \right\} \right]_1^\infty$$

$$-\alpha\int_1^\infty \cos\alpha x\left\{\int_x^\infty \frac{1-\cos B(1/t)}{t}\,dt\right\}dx$$

$$=-\sin\alpha\int_1^\infty \frac{1-\cos B(1/t)}{t}\,dt$$

$$-\alpha\left[\cos\alpha x\int_x^\infty\int_u^\infty \frac{1-\cos B(1/t)}{t}\,dt\,du\right]_1^\infty$$

$$-\alpha^2\int_1^\infty\left[\int_\bullet^\infty\int_u^\infty \frac{1-\cos B(1/t)-A_2/t^2}{t}\,dt\,du\right]\sin\alpha x\,dx$$

$$-\alpha^2\int_1^\infty\left[\int_x^\infty\int_u^\infty \frac{A_2}{t^3}\,dt\,du\right]\sin\alpha x\,dx$$

$$=-\sin\alpha\int_1^\infty \frac{1-\cos B(1/t)}{t}\,dt$$

$$+\alpha\cos\alpha\int_1^\infty\int_u^\infty \frac{1-\cos B(1/t)}{t}\,dt\,du$$

$$-\alpha^2\left[\sin\alpha x\int_x^\infty\int_v^\infty\int_u^\infty \frac{1-\cos B(1/t)-A_2/t^2}{t}\,dt\,du\,dv\right]_1^\infty$$

$$-\frac{A_2\alpha^2}{2}\left[\frac{\pi}{2}-\mathrm{Si}\,\alpha\right]$$

$$+\alpha^3\int_1^\infty\cos\alpha x\left\{\int_x^\infty\int_v^\infty\int_u^\infty \frac{1-\cos B(1/t)-A_2/t^2}{t}\,dt\,du\,dv\right\}dx \tag{37}$$

where $1-\cos B(t)=A_2t^2+A_4t^4+A_6t^6+\cdots$ (38)

and $\mathrm{Si}\,\alpha=\int_0^1 \sin\alpha x\,dx/x=\int_0^\alpha \sin x\,dx/x$ (39)

is the customary sine integral.

Integral Representations for the Coefficients

The first coefficient is

$$C_0 = \int_1^\infty \frac{1 - \cos B(1/t)}{t}\, dt. \tag{40}$$

Apply the reciprocal transformation $1/t = s$. Then

$$C_0 = \int_0^1 \frac{1 - \cos B(s)}{s}\, ds = +\,0.1161\,3332 \tag{41}$$

by numerical integration.
The next coefficient is

$$D_1 = \int_1^\infty \int_u^\infty \frac{1 - \cos B(1/t)}{t}\, dt\, du. \tag{42}$$

Apply the reciprocal transformation twice

$$D_1 = \int_0^1 \int_0^v \frac{1 - \cos B(s)}{s}\, ds\, \frac{dv}{v^2}. \tag{43}$$

Use the identity that is obvious from Figure 23.

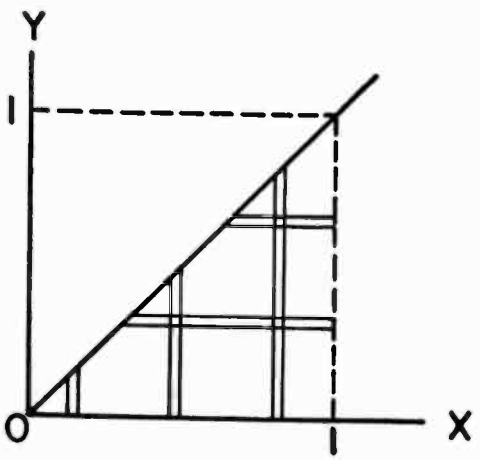

Fig. 23—Inversion of order of integration.

$$\int_0^1 dx \int_0^x f(x,y)\, dy = \int_0^1 dy \int_y^1 f(x,y)\, dx \tag{44}$$

$$D_1 = \int_0^1 \left[\frac{1-\cos B(s)}{s}\right] ds \int_s^1 \frac{dv}{v^2}$$

$$= \frac{1}{1!}\int_0^1 \left[1-\cos B(s)\right]\frac{1-s}{s^2}\, ds = +\,0.1053\ 0825 \tag{45}$$

by numerical integration.

By a similar process, the next coefficient is

$$C_2 = \int_1^\infty \int_v^\infty \int_u^\infty \frac{1-\cos B(1/t) - A_2/t^2}{t}\, dt\, du\, dv$$

$$= \int_0^1 \left[\int_0^r \int_0^s \frac{1-\cos B(t) - A_2 t^2}{t}\, dt \frac{ds}{s^2}\right] \frac{dr}{r^2} \tag{46}$$

Invert the order of integration in the brackets and integrate once. This leaves a double integral. Invert this order of integration, and reduce to the single integral.

$$C_2 = \frac{1}{2!}\int_0^1 \left[1-\cos B(t) - A_2 t^2\right] \frac{(1-t)^2}{t^3}\, dt$$

$$= +\,0.0017\ 6070\ 48. \tag{47}$$

By a similar process

$$D_3 = \frac{1}{3!}\int_0^1 \left[1-\cos B(t) - A_2 t^2\right] \frac{(1-t)^3}{t^4}\, dt$$

$$= +\,0.0016\ 4158\ 30 \tag{48}$$

$$C_4 = \frac{1}{4!}\int_0^1 \left[1-\cos B(t) - A_2 t^2 - A_4 t^4\right] \frac{(1-t)^4}{t^5}\, dt$$

$$= +\,0.0000\ 2339\ 5690. \tag{49}$$

A continuation of the process of partial integration, starting with Equation (37) leads to the result

$$\int_1^\infty \sin \alpha x \cos B(1/x)\, dx/x$$

$$= \left[\frac{\pi}{2} - \mathrm{Si}\ \alpha\right] \left[1 + \frac{A_2}{2}\alpha^2 - \frac{A_4}{4}\alpha^4 + \frac{A_6}{6}\alpha^6 - \cdots\right]$$

$$+ \sin \alpha \left[C_0 - C_2 \alpha^2 + C_4 \alpha^4 - \cdots\right]$$

$$- \cos \alpha \left[D_1 \alpha - D_3 \alpha^3 + D_5 \alpha^5 - \cdots\right]. \qquad (50)$$

Series Expansions for the Coefficients

The above method for determining the coefficients is unsatisfactory for determining the high-order coefficients of the series because of the difficulty in obtaining accurate enough values of cos $B(x)$ to use in the numerical integration, so the following supplementary method was used. Starting with Equation (36), and applying Equation (38),

$$I = \int_1^\infty \{1 - \cos B(1/x)\} \sin \alpha x \frac{dx}{x}$$

$$= A_2 \int_1^\infty \sin \alpha x \frac{dx}{x^3} + A_4 \int_1^\infty \sin \alpha x \frac{dx}{x^5}$$

$$+ A_6 \int_1^\infty \sin \alpha x \frac{dx}{x^7} + A_8 \int_1^\infty \sin \alpha x \frac{dx}{x^9} + \cdots$$

$$= \frac{A_2}{2!}\left[\sin \alpha + \alpha \cos \alpha + \alpha^2 \mathrm{si}\ \alpha\right]$$

$$+ \frac{A_4}{4!}\left[(3! - \alpha^2) \sin \alpha + (2! - \alpha^2)\, \alpha \cos \alpha - \alpha^4 \mathrm{si}\ \alpha\right]$$

$$+ \frac{A_6}{6!}\left[(5! - 3!\,\alpha^2 + \alpha^4) \sin \alpha + (4! - 2!\,\alpha^2 + \alpha^4)\, \alpha \cos \alpha + \alpha^6 \mathrm{si}\ \alpha\right]$$

$$+ \frac{A_8}{8!}\left[(7! - 5!\,\alpha^2 + 3!\,\alpha^4 - \alpha^6) \sin \alpha + (6! - 4!\,\alpha^2 + 2!\,\alpha^4 - \alpha^6)\right.$$

$$\left. \alpha \cos \alpha - \alpha^8 \mathrm{si}\ \alpha\right] + \cdots \qquad (51)$$

where $\operatorname{si}\alpha = \operatorname{Si}\alpha - \frac{\pi}{2}$. (52)

The coefficient of $\sin\alpha$ in Equation (51) is

$$\left[\frac{A_2}{2!} + \frac{3!}{4!}A_4 + \frac{5!}{6!}A_6 + \frac{7!}{8!}A_8 + \cdots\right]$$

$$-\alpha^2\left[\frac{A_4}{4!} + \frac{3!}{6!}A_6 + \frac{5!}{8!}A_8 + \frac{7!}{10!}A_{10} + \cdots\right]$$

$$+\alpha^4\left[\frac{A_6}{6!} + \frac{3!}{8!}A_8 + \frac{5!}{10!}A_{10} + \frac{7!}{12!}A_{12} + \cdots\right]$$

$$-\alpha^6\left[\frac{A_8}{8!} + \frac{3!}{10!}A_{10} + \frac{5!}{12!}A_{12} + \frac{7!}{14!}A_{14} + \cdots\right]$$

$$+\cdots \tag{53}$$

Which shows that

$$C_0 = \sum_{n=1}^{\infty} \frac{(2n-1)!}{(2n)!}A_{2n} \tag{54}$$

$$C_2 = \sum_{n=1}^{\infty} \frac{(2n-1)!}{(2n+2)!}A_{2n+2} \tag{55}$$

$$C_4 = \sum_{n=1}^{\infty} \frac{(2n-1)!}{(2n+4)!}A_{2n+4} \tag{56}$$

$$C_{2r} = \sum_{n=1}^{\infty} \frac{(2n-1)!}{(2n+2r)!}A_{2n+2r} \tag{57}$$

by comparison with Equation (50).

In a similar manner

$$D_1 = -\sum_{n=1}^{\infty} \frac{(2n-2)!}{(2n)!}A_{2n} \tag{58}$$

$$D_3 = -\sum_{n=1}^{\infty} \frac{(2n-2)!}{(2n+2)!} A_{2n+2} \tag{59}$$

$$D_{2r-1} = -\sum_{n=1}^{\infty} \frac{(2n-2)!}{(2n+2r-2)!} A_{2n+2r-2} \tag{60}$$

When r becomes a fairly high integer, it is obvious that the denominators of Equations (57) and (60) are much larger than the numerators and convergence is rapid. For small values of r Equations (41) to (49) are satisfactory. The A_{2r} of Equation (38) are the key to the entire computation. They can be evaluated as follows.

The series for $B(x)$ is known to be*

$$B(x) = \frac{2}{\pi}\left\{x + \frac{1}{3^2}x^3 + \frac{1}{5^2}x^5 + \frac{1}{7^2}x^7 + \cdots\right\} \tag{61}$$

The power series of Equation (61), as far as the term in x^{40}, was raised to even powers, $B^2(x)$, $B^4(x)$, $B^6(x)$, etc. as high as $B^{12}(x)$. The series for

$$1 - \cos B(x) = B^2(x) - \frac{B^4(x)}{4!} + \frac{B^6(x)}{6!} - \cdots$$

$$= A_2x^2 + A_4x^4 + A_6x^6 + \cdots \tag{62}$$

was then used to determine the A_{2r}. The sliding strip method[12] is a very systematic procedure to use with a calculating machine when multiplying series.

Evaluation of First Integral

The first integral of Equation (35) can be evaluated as follows. Let

$$\sin B(x) = \sum_{n=1}^{\infty} a_{2n-1}\, x^{2n-1} \tag{63}$$

which defines the a's. Then

---

* Reference 9, Equation (5).

[12] H. Chernoff, "A Note on the Inversion of Power Series," Mathematical Tables and other Aids to Computation, Vol. 2, pp. 331-335, October, 1947.

$$I = \int_0^1 \sin \alpha x \sin B(x)\, dx$$

$$= a_1 I_1 + a_3 I_3 + a_5 I_5 + \cdots \tag{64}$$

where $I_n = \int_0^1 x^n \sin \alpha x\, dx.$ (65)

Two integrations of Equation (65) by parts leads to the recurrence relation

$$I_n = \frac{1}{n+1} \sin \alpha - \frac{\alpha}{(n+1)(n+2)} \cos \alpha - \frac{\alpha^2}{(n+1)(n+2)} I_{n+2}. \tag{66}$$

Applying Equation (66) repeatedly, it can be shown that

$$I_1 = 1! \left\{ \sin \alpha \left(\frac{1}{2!} - \frac{\alpha^2}{4!} + \frac{\alpha^4}{6!} - \frac{\alpha^6}{8!} + \cdots \right) \right.$$

$$\left. - \cos \alpha \left(\frac{\alpha}{3!} - \frac{\alpha^3}{5!} + \frac{\alpha^5}{7!} - \frac{\alpha^7}{9!} + \cdots \right) \right\} \tag{67}$$

$$I_3 = 3! \left\{ \sin \alpha \left(\frac{1}{4!} - \frac{\alpha^2}{6!} + \frac{\alpha^4}{8!} - \frac{\alpha^6}{10!} + \cdots \right) \right.$$

$$\left. - \cos \alpha \left(\frac{\alpha}{5!} - \frac{\alpha^3}{7!} + \frac{\alpha^5}{9!} - \frac{\alpha^7}{11!} + \cdots \right) \right\} \tag{68}$$

$$I_5 = 5! \left\{ \sin \alpha \left(\frac{1}{6!} - \frac{\alpha^2}{8!} + \frac{\alpha^4}{10!} - \frac{\alpha^6}{12!} + \cdots \right) \right.$$

$$\left. - \cos \alpha \left(\frac{\alpha}{7!} - \frac{\alpha^3}{9!} + \frac{\alpha^5}{11!} - \frac{\alpha^7}{13!} + \cdots \right) \right\} \tag{69}$$

since $I_{2n-1} \to 0$ as $n \to \infty$.

Substituting Equations (67), (68), (69) and similar higher order ones into Equation (64) and collecting terms gives

$$I = \sin \alpha \left[b_0 - b_2 \alpha^2 + b_4 \alpha^4 - b_6 \alpha^6 + \cdots \right]$$

$$-\cos\alpha\,[b_1\alpha - b_3\alpha^3 + b_5\alpha^5 - b_7\alpha^7 + \cdots] \tag{70}$$

where

$$b_0 = \sum_{n=1}^{\infty} \frac{(2n-1)!}{(2n)!}\, a_{2n-1} = \int_0^1 \sin B(x)\, dx \tag{71}$$

$$b_1 = \sum_{n=1}^{\infty} \frac{(2n-1)!}{(2n+1)!}\, a_{2n-1} = \int_0^1 (1-x)\sin B(x)\, dx \tag{72}$$

$$b_2 = \sum_{n=1}^{\infty} \frac{(2n-1)!}{(2n+2)!}\, a_{2n-1} = \frac{1}{2!}\int_0^1 (1-x)^2 \sin B(x)\, dx \tag{73}$$

$$b_r = \sum_{n=1}^{\infty} \frac{(2n-1)!}{(2n+r)!}\, a_{2n-1} = \frac{1}{r!}\int_0^1 (1-x)^r \sin B(x)\, dx. \tag{74}$$

The integral representations for the b_r can be obtained as follows:

$$\int_0^1 \sin \alpha x \sin B(x)\, dx = \int_0^1 \sin\{\alpha - (1-x)\alpha\} \sin B(x)\, dx$$

$$= \sin\alpha \int_0^1 \cos(1-x)\alpha \sin B(x)\, dx$$

$$-\cos\alpha \int_0^1 \sin(1-x)\alpha \sin B(x)\, dx$$

$$= \sin\alpha \left[\int_0^1 \sin B(x)\, dx - \frac{\alpha^2}{2!}\int_0^1 (1-x)^2 \sin B(x)\, dx + \cdots\right]$$

$$-\cos\alpha \left[\alpha \int_0^1 (1-x)\sin B(x)\, dx\right.$$

$$\left. -\frac{\alpha^3}{3!}\int_0^1 (1-x)^3 \sin B(x)\, dx + \cdots\right] \tag{75}$$

For convenient reference the numerical values of the various constants defined above are listed below:

Table I—Coefficients of series.

r	A_{2r}	a_{2r-1}
1	+ 0.2026 4237	+ 0.6366 1977
2	+ 0.0381 8764 9	+ 0.0277 3348 4
3	+ 0.0157 6383 3	+ 0.0120 0217 9
4	+ 0.0085 3135 24	+ 0.0067 1503 08
5	+ 0.0053 2421 80	+ 0.0042 9638 47
6	+ 0.0036 3048 72	+ 0.0029 8731 66
7	+ 0.0026 3007 68	+ 0.0021 9851 74
8	+ 0.0019 9111 69	+ 0.0016 8627 01
9	+ 0.0015 5870 85	+ 0.0013 3469 26
10	+ 0.0012 5273 99	+ 0.0010 8288 24
11	+ 0.0010 2843 08	+ 0.0008 9631 463
12	+ 0.0008 5917 525	+ 0.0007 5421 946
13	+ 0.0007 2836 649	+ 0.0006 4348 833
14	+ 0.0006 2520 910	+ 0.0005 5551 416
15	+ 0.0005 4244 140	+ 0.0004 8445 478
16	+ 0.0004 7503 452	+ 0.0004 2623 091
17	+ 0.0004 1941 739	+ 0.0003 7792 389
18	+ 0.0003 7299 795	+ 0.0003 3740 056
19	+ 0.0003 3385 832	+ 0.0003 0307 238
20	+ 0.0003 0055 446	+ 0.0002 7373 666

Table II—Coefficients of series.

r	C_{2r-2}	D_{2r-1}	b_{2r-2}	b_{2r-1}
1	+ 0.11613332	+ 0.10530825	+ 0.32939940	+ 0.10795789
2	+ 0.0017607048	+ 0.0016415830	+ 0.026808163	+ 0.0053434186
3	+ 0.0^{4}23395690	+ 0.0^{4}22359827	+ 0.0^{3}88881623	+ 0.0^{3}12681524
4	+ 0.0^{6}22150550	+ 0.0^{6}21473423	+ 0.0^{4}15838534	+ 0.0^{5}17587851
5	+ 0.0^{8}15169048	+ 0.0^{8}14831752	+ 0.0^{6}17580118	+ 0.0^{7}15976602
6	+ 0.0^{11}77731757	+ 0.0^{11}76421020	+ 0.0^{8}13310393	+ 0.0^{9}10236666
7	+ 0.0^{13}30772144	+ 0.0^{13}30365529	+ 0.0^{11}73106970	+ 0.0^{12}48731396
8	+ 0.0^{16}96692705	+ 0.0^{16}95664962	+ 0.0^{13}30453713	+ 0.0^{14}17912268
9	+ 0.0^{18}24666493	+ 0.0^{18}24451078	+ 0.0^{16}99504696	+ 0.0^{17}52367339
10	+ 0.0^{21}52058190	+ 0.0^{21}51678045	+ 0.0^{18}26182140	+ 0.0^{19}12467054
11	+ 0.0^{24}92351097	+ 0.0^{24}91778804	+ 0.0^{21}56665921	+ 0.0^{22}24636400
12	+ 0.0^{26}13958831	+ 0.0^{26}13884328	+ 0.0^{23}102648147	+ 0.0^{25}41058009
13			+ 0.0^{26}15791113	+ 0.0^{28}58484185
14			+ 0.0^{29}18060548	+ 0.0^{31}72021871

When the series are evaluated and the results combined, the result is a table of $h_1(\alpha)$.

Table III—Numerical values of $h_1(\alpha)$.

α	$h_1(\alpha)$	α	$h_1(\alpha)$
0	+ 1.000000	4.0	— .043022
.1	+ .937356	4.1	— .042494
.2	+ .876763	4.2	— .041498
.3	+ .818245	4.3	— .040091
.4	+ .761818	4.4	— .038326
.5	+ .707496	4.5	— .036256
.6	+ .655289	4.6	— .033932
.7	+ .605203	4.7	— .031400
.8	+ .557238	4.8	— .028706
.9	+ .511391	4.9	— .025892
1.0	+ .467655	5.0	— .022997
1.1	+ .426019	5.1	— .020060
1.2	+ .386467	5.2	— .017114
1.3	+ .348979	5.3	— .014191
1.4	+ .313530	5.4	— .011320
1.5	+ .280095	5.5	— .008526
1.6	+ .248640	5.6	— .005833
1.7	+ .219131	5.7	— .003261
1.8	+ .191530	5.8	— .000829
1.9	+ .165794	5.9	+ .001449
2.0	+ .141877	6.0	+ .003560
2.1	+ .119733	6.1	+ .005493
2.2	+ .099309	6.2	+ .007241
2.3	+ .080552	6.3	+ .008798
2.4	+ .063407	6.4	+ .010161
2.5	+ .047815	6.5	+ .011328
2.6	+ .033715	6.6	+ .012300
2.7	+ .021047	6.7	+ .013079
2.8	+ .009747	6.8	+ .013670
2.9	— .000249	6.9	+ .014077
3.0	— .009007	7.0	+ .014308
3.1	— .016592	7.5	+ .013136
3.2	— .023071	8.0	+ .009134
3.3	— .028511	8.5	+ .003880
3.4	— .032978	9.0	— .001159
3.5	— .036539	9.5	— .004895
3.6	— .039259	10.0	— .006750
3.7	— .041204		
3.8	— .042438		
3.9	— .043023		

Asymptotic Series Expansion of $h_1(\alpha)$

For values of α greater than seven, the power series expansion does not converge rapidly enough for numerical computations, so an asymptotic expansion for the second integral with the infinite upper limit was necessary. Because of the discontinuity in the derivatives of $B(x)$ when $\omega = \omega_0$, it is not possible to expand about the point $x = 1$, so the lower limit will be $\beta > 1$, and the value of the integral for $1 \leq x \leq \beta$ will be determined by numerical integration. Consider the integral

$$I = \int_{\beta}^{\infty} \frac{1}{x} \sin \alpha x \cos B(1/x)\, dx = \int_{\alpha\beta}^{\infty} \frac{1}{y} \sin y \cos B(\alpha/y)\, dy. \quad (76)$$

Integrate by parts successively.

$$I = -\left[\frac{\cos y}{y} \cos B(\alpha/y)\right]_{\alpha\beta}^{\infty} + \int_{\alpha\beta}^{\infty} \cos y \frac{d}{dy}\left\{\frac{1}{y} \cos B(\alpha/y)\right\} dy$$

$$= \frac{\cos \alpha\beta}{\alpha\beta} \cos B(1/\beta) + \left[\sin y \frac{d}{dy}\left\{\frac{1}{y} \cos B(\alpha/y)\right\}\right]_{\alpha\beta}^{\infty}$$

$$- \int_{\alpha\beta}^{\infty} \sin y \frac{d^2}{dy^2}\left\{\frac{1}{y} \cos B(\alpha/y)\right\} dy. \quad (77)$$

When this process is continued, the derivatives evaluated with the help of the integral representation for $B(x)$, and numerical results collected, the result for $\beta = 4$ becomes

$$\int_{4}^{\infty} \frac{1}{x} \sin \alpha x \cos B(1/x)\, dx$$

$$= \cos 4\alpha \left\{\frac{0.2467\,9542}{\alpha} - \frac{0.0288\,0179\,9}{\alpha^3} + \frac{0.0187\,1959}{\alpha^5} - \frac{0.02682}{\alpha^7} + \cdots\right\}$$

$$+ \sin 4\alpha \left\{\frac{0.0600\,7691}{\alpha^2} - \frac{0.0203\,3862\,2}{\alpha^4} + \frac{0.0208\,97}{\alpha^6} - \frac{0.03719}{\alpha^8} + \cdots\right\} \quad (78)$$

For large values of α the first integral of Equation (35) was evaluated by numerical integration.

AN IMPROVED METHOD OF TESTING FOR RESIDUAL GAS IN ELECTRON TUBES AND VACUUM SYSTEMS*†

By

E. W. Herold

Research Department, RCA Laboratories Division, Princeton, N. J.

Summary—The small amount of residual gas in electron tubes is sometimes of concern to the user and, more often, of interest in the laboratory and factory. Existing methods of test employ a negative electrode in the tube or in an ionization gauge to collect ion current, which is measured with a direct-current meter. Unfortunately, leakage and other stray direct currents are of the same nature so that ion currents below the stray current level cannot be determined. The improved method described in the present paper converts the desired ion current to an alternating current by modulation of the ionizing electron stream while leaving the original undesired stray currents relatively unmodulated. Modulation is accomplished by a magnetic or an electric field and it is found that the chief undesired current of an alternating nature is now in phase quadrature with the desired ion current. It can be reduced by choice of a low frequency and a phase-sensitive alternating-current meter or by neutralization. The chief component of undesired alternating current is due to induced current in the ion-collecting electrode caused by the alternating charge of the nearby electron stream. Although the conventional gas measurement with direct current is often limited in sensitivity to ion currents of 10^{-7} ampere, the improved method will allow 10^{-9} ampere to be measured without special precautions; neutralization of the quadrature undesired components improves the sensitivity to 10^{-11} ampere. Some applications of the method to conventional and special tubes are shown.

A proposal to use an analogous method for the detection of small leaks in sealed-off tubes or vacuum systems is discussed. The pressure of an external gas probe is alternated at a slow cyclic rate and the internal ion current measured by a selective alternating-current amplifier. Present indications are that, for high-vacuum systems, the alternations must be at a very low frequency.

Introduction

One problem in the manufacture and testing of high-vacuum electron tubes is the determination of the residual gas pressure. The determination is usually made by a so-called gas test, in which the normal electron current in a tube ionizes the residual gas, and a positive-ion current is then collected by some electrode at a

* Decimal Classification: R331.

† Some of the material in this paper was presented March 9, 1949, at the National Convention of the Institute of Radio Engineers, New York City.

negative potential. This ion current is measured by a sensitive direct-current microammeter, whose reading is then proportional (roughly) to the ionization. In ordinary receiving tubes, gas current is measured in the control-grid lead or, in some cases, in the suppressor-grid lead, and tubes which have currents in excess of 0.5 to 1.0 microampere are considered to have excessive gas.

The chief inaccuracy in testing for gas is due to the stray leakage across tube support micas and other insulation and, in some cases, due to grid emission. Currents from both causes affect the gas-current meter in the same direction as the gas current. With a tube using a negative control-grid bias of some tens of volts and a positive anode voltage of some hundreds of volts, a microampere of current is caused by leakages of the order of several hundred megohms. To distinguish true positive-ion current and leakage current, a second test is sometimes made with normal anode voltages applied, but with the electron current cut off, either by opening the cathode circuit, or by turning off the heater, or by a control-grid bias well beyond cut-off. The theory behind these procedures is that any one of them will leave leakage currents relatively unchanged but will eliminate ion current since no electrons are present to ionize the gas. Unfortunately, leakage and grid-emission currents are notoriously variable and sometimes change rapidly with tube temperature; furthermore, the procedure alters the applied voltages or possible leakage paths and so the leakage currents also change.

Because of this confusion between leakage and gas current, it is seldom advantageous to increase the meter sensitivity (e.g., by a direct-current amplifier) for accurate readings, or because one wishes to detect smaller amounts of gas. The signal-to-noise ratio, so to speak, (i.e., the gas-to-leakage ratio) is too poor in the tube, and amplification only increases the leakage and gas currents in proportion. As a result, a close study of tubes with very low residual gas is not possible and all tubes with less than approximately 10^{-7} ampere of ion current must be thrown into one group, although there may be differences of 100 to 1 between the residual gas content of individual tubes. In a study of the life of highly-evacuated tubes, it might be very valuable first, to differentiate between the actual initial gas pressure of different tubes, and second, to be able to detect early in life an increase in residual gas, though it may be well below the danger point. In this way, it may even be possible to predict a life failure due to gas thousands of hours before it actually occurs.

A second problem in electron-tube manufacture and in experimental laboratories is the determination of the residual gas pressure in a

vacuum system. In this case, the use of special ionization gauge tubes greatly reduces the leakage and other stray current troubles, although direct-current amplification is then required to detect the very minute ion currents which must be measured.

In the present paper a basic method will be discussed for separating the ion currents from the stray direct currents. The method consists of converting the ion currents to alternating current by means which leave the major leakage currents substantially unaltered as direct current. Thus there are two major advantages; first, the desired ion currents can be easily separated from the leakage currents and second, an increase in sensitivity may be obtained by use of a stable, low-cost alternating-current amplifier instead of the less stable direct-current amplifier. However, undesired stray alternating currents which may affect the readings will now be of concern. As will be shown, these are all substantially in phase quadrature with the desired ion current since they are due to capacitance and induced-charge effects. Fortunately, therefore, they can easily be reduced to any desired degree by use of a low frequency, by neutralization, by making the alternating-current amplifier responsive to phase, or by all three. As a result, the new method has a sensitivity to ion currents which is from 100 to 10,000 times as great as the one now in use for testing conventional tubes.

The Conventional Gas Test

Figure 1 shows the conventional gas test using direct current. In the circuit for the pentode shown in Figure 1(a), a microammeter is placed in the negative control grid lead and measures the ion current plus the undesired leakages. Since the direct-current voltages are high, the leakages may easily lead to currents of the order of 0.1 microampere,

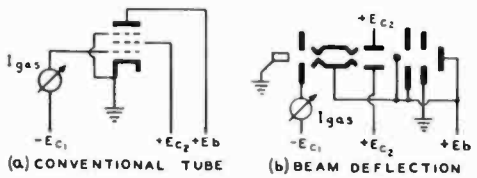

Fig. 1—Commonly used method of measurement of residual gas.

so that the sensitivity is limited to the order of 10^{-7} ampere. During the war, this laboratory did considerable work on an experimental beam-deflection mixer tube shown schematically in Figure 1(b). As sometimes happens with experimental tubes, considerable trouble was experienced with slow air leaks and it was found necessary to measure ion current and its variations with considerable accuracy. At first,

the conventional method was used with the microammeter connected to a negative electrode near the cathode since the electron current present to produce ionization was about 5 to 10 milliamperes, as with conventional tubes. In this way, an ion-current measurement of approximately one microampere corresponded with the same current in conventional tubes. Unfortunately, the leakage currents were so great and so variable that measurements were impossible. The alternating-current method to be described solved the problem and was used as indicated in Figure 2.

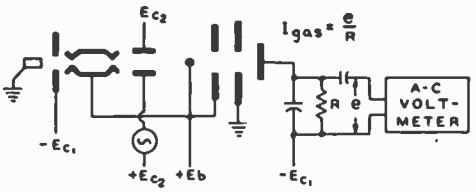

Fig. 2—Improved method applied to beam-deflection tube.

Application of the Improved Method

In the beam-deflection tube the cathode current of approximately 10 milliamperes is cut down by the two slits to a fine beam of only 200 microamperes. This passes through the small deflection plates and, when an input is applied to these plates, is deflected on and off the intercepting wire onto the anode. For the gas test, it was decided to put a 60-cycle alternating-current deflection voltage on the tube so that the beam would be alternately passed into and cut off from the anode region. By connecting the anode to a negative voltage, it was used to collect the ions, the current of which alternated at twice the frequency of the applied alternating current. A high resistance and an electronic alternating-current voltmeter completed the arrangement. Since the alternating-current input circuits were well shielded from the anode, capacitive currents were negligible; also alternating-current leakage currents were absent. The limiting sensitivity was not reached even with a pre-amplifier for the electronic voltmeter which permitted gas current readings down to 10^{-10} ampere. It can be shown that, in this case, the limiting sensitivity should be of this order or smaller and is imposed by noise and the induced current in the anode due to the electron beam. These limits to the sensitivity will be discussed in more detail in connection with conventional tubes. In the beam-deflection-tube test, the ionizing beam had only about 1/50 of the current of the cathode region but, since the ion-current sensitivity was about 1000 to 10,000 times higher, this was not a handicap. In summary, this application of the new method led to reliable ion-current determination down to currents of the order of 10^{-10} ampere. It was

quite simple and reliable to use, and the stray alternating currents were so small that no neutralization was needed at the low frequency used (60 cycles).

In applying this method to the simplest conventional tube, the triode, capacitive currents make modulation of the electron current by an alternating-current voltage less attractive. The use of an electrostatically shielded alternating magnetic field is therefore a possibility, as shown in Figure 3. Such a magnetic modulation method has been used in connection with photo-tubes[1, 2] but the problems in the present case are somewhat different. The figure shows ion current measured in the negative control grid, although with a triode ion gauge, a positive grid would be used and the ion current to a negative plate measured. With good electrostatic shielding, very small stray pick-up might be expected. Since the ion current is at twice the fundamental frequency of the modulating alternating current, the fundamental component of both inductive and stray capacitive pick-up can easily be eliminated. The magnetic modulation method is also applicable to more complex tube structures such as pentodes, etc.

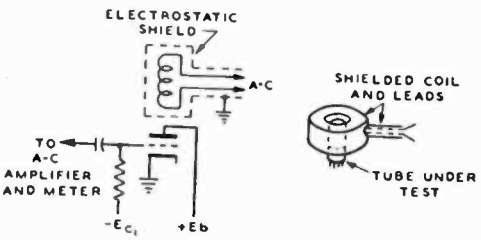

Fig. 3—Triode ion-current modulation by magnetic field.

Actually, the chief limitation[3] on sensitivity is due to a somewhat unusual effect which is not present in the phototube modulation problem, previously mentioned. The electron current in a tube induces a charge on the negative grid which varies when the current varies, and is in phase with it. Since the rate of change of charge is a current, there is an alternating current to the grid induced in it which is 90 degrees out of phase with the electron current. This induced current, which will be evaluated as to order of magnitude later in this paper, can easily be the chief limitation to the alternating-current gas measurement no matter how the modulation is applied. Fortunately, it is in phase quadrature with the alternating ion current and is eliminated by neutralization or by electronic wattmeter principles which allow the amplifier to respond only to in-phase currents. However, the presence of this current makes the magnetic field modulation not as advan-

---

[1] F. Gray, U. S. Patent Re. 18,400, filed Feb. 14, 1928.

[2] H. P. Kalmus and G. O. Striker, "New Radiation Meter", *Rev. Sci. Instr.*, Vol. 19, pp. 79-82, February, 1948.

[3] This limit to the sensitivity was called to the writer's attention by Howard J. Evans of the RCA Victor Division.

tageous as would otherwise be the case, and, even for the triode ion gauge, one might alternatively consider a voltage modulation on the cathode with a quadrature current neutralization for capacitive and induced currents. It will be found that unneutralized induced current limits the sensitivity at 60 cycles per second to ion currents of greater than 10^{-9} ampere; this, nevertheless, gives a factor of 100 improvement over conventional triode gas measurement.

In Figure 4 is shown the alternating ion-current modulation method applied to a pentode with separate suppressor grid connection. In this case, the electron current is modulated by a low-frequency voltage on the control grid and the ion current is measured in the suppressor-grid lead. The two-capacitor arrangement shown allows a $\pm$ 90 degree phase current to be fed into the alternating-current amplifier to neutralize capacitive and induced currents in the tube. To use this, the variable capacitor is adjusted until the output reading is a minimum; the remainder will be the in-phase current due to ions, which is desired,

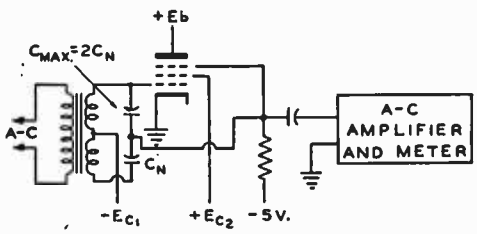

Fig. 4 — The alternating-current gas test applied to a pentode.

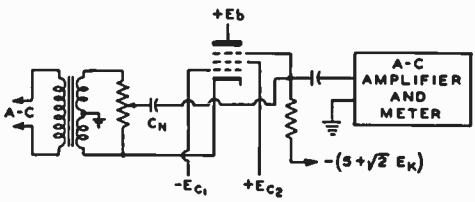

Fig. 5—Cathode modulation of a pentode.

together with possible in-phase currents due to partial leakage between control and suppressor grids. The latter will usually be negligible. The capacitor C_N should be of the order of 2 micromicrofarads.

A variation of the alternating-current gas measurement for pentodes is shown in Figure 5, in which cathode modulation is employed and the quadrature cancellation circuit uses a potentiometer. C_N should be about 2 micromicrofarads and the potentiometer should not be over 1000 ohms. As in previous circuits, adjustment is made to get a minimum and can presumably be left alone for different tubes of the same type. E_K is the r-m-s voltage on the cathode.

When the suppressor grid is not available with an external lead, magnetic field modulation must be resorted to or, alternatively, the tube can be operated with the plate as a negative ion-collector. Two circuits of this kind are given in Figure 6. In both of these circuits, the sensitivity without neutralization is several times better than the previous ones because the ion-collecting anode is shielded from the electron stream by the suppressor grid and both capacitance and

induced currents are reduced. However, two methods of neutralization are shown, Figure 6(a) using variable capacitance and Figure 6(b) the fixed suppressor-to-plate capacitance and a variable voltage. In all these cases, of course, it is also possible to substitute or supplement the action with a phase-sensitive amplifier.

Limits to Sensitivity

Among the undesired alternating currents, which limit the smallest detectable ion current by the above method, is the quadrature-phase induced current in the ion-collecting electrode due to the alternating electron flow in the tube. This has already been mentioned and is the chief cause of stray current when using the magnetic modulation method and an important cause in the grid-modulation method. The effect is the same as that found in pentagrid converter tubes called "space-charge coupling" in which current of oscillator frequency is induced in the signal grid.[4] The study of this effect in converters disclosed that it is equivalent to a negative capacitance of about one micromicrofarad between first (oscillator) grid and third (signal) grid. When the magnetic modulation method is employed, this concept is no longer applicable but still serves to indicate the order of magnitude of the effect and also indicates that the current is proportional to frequency. In converter tubes, the induced current could be neglected at frequencies below several megacycles; because the gas ion current here considered may be so small, the induced current is important even at frequencies as low as 60 cycles.

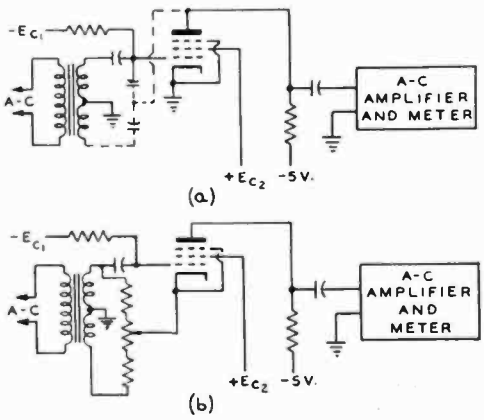

Fig. 6—Pentode with alternating ion current measured in anode.

The physical picture of the induced current is given by the change in charge on a negative electrode when the current of a nearby electron stream is alternately increased and decreased. The total charge of the electron stream is responsible for the induced charge and an approximation of the induced current is thereby readily determined. With a parallel-plane electrode system and a current flow normal to the electrode surface, the total charge between two electrodes is easily shown to be $i\tau$ where i is the current and τ is the transit time. Since this

[4] E. W. Herold, "The Operation of Frequency Converters and Mixers for Superheterodyne Reception", *Proc. I.R.E.*, Vol. 30, pp. 84-103, February, 1942.

charge is at least partially imaged in one electrode, presumed to be the negative ion-collecting electrode, the induced charge is of opposite sign and of the order

$$q_{\text{ind}} = k\, i\, \tau$$

where $0<k<1$, the value of k depending on how much of the total charge is imaged on the ion collector. If the entire electron stream passes through a grid-like ion collector, k is likely to be between ½ and 1. Thus the induced current (for one side of the electrode under consideration) is given by

$$i_{\text{ind}} = \frac{dq_{\text{ind}}}{dt} = k\tau \frac{di}{dt}.$$

If the electron stream has a sinusoidal modulation

$$i = i_0(1 + m \sin \omega t),$$

then

$$i_{\text{ind}} = km\, \omega\tau i_0 \cos \omega t.$$

This shows that the induced current is in phase quadrature with the electron and ion current, and has a maximum amplitude somewhat less than $i_0\omega\tau$. If the electron current passes *through* an electrode, there is a similar current induced on each side so that τ is the sum of the transit times on each side. In ordinary electron tubes, τ is of the order of $\frac{1}{4} \times 10^{-9}$ and, if we assume a 60 cycle-per-second frequency, $\omega \approx 400$, so that $\omega\tau \approx 10^{-7}$. Thus, an electron current of 10 milliamperes may induce a current of the order of 10^{-9} ampere. This may be considered as the order of sensitivity of a 60-cycle ion-measuring system in which no steps are taken to reduce quadrature current from this cause; the method is of the order of 100 times more sensitive than conventional direct-current gas measurement.

Capacitive currents may be of importance when using modulation on one of the tube electrodes, especially if screen grids and shielding are not used. At 60 cycles per second, with 3 volts on the modulation grid, a capacitance of 1 micromicrofarad between the modulation and the ion-collecting electrode will also give a current of 10^{-9} ampere. Since this current is in quadrature but opposite in phase to the induced current, the two would tend to cancel. This method of cancelling induced current (i.e., by connection of a capacitance between modulating grid and negative induction grid) is well known in superheterodyne converter practice.[4] In the circuits of Figures 4 - 6, provision is made for either polarity of quadrature current.

Alternating current through a partial leakage path is also a possibility when using voltage modulation on an electrode. This is less than

the direct-current leakage which gives trouble in the conventional gas test on two counts. First, the leakage is a partial one rather than a total leakage, so that it is reduced by phenomena analogous to those which keep the grid-plate capacitance of a screen-grid tube to values much less than the total capacitance of any one electrode. Second, the alternating-current modulating voltage is substantially less than the direct-current voltages which cause leakage in the conventional test. The combined effects probably reduce stray alternating-current leakage current to 10^{-3} of that of the direct-current leakage in the conventional test. Thus, a sensitivity of 10^{-10} ampere or less might be anticipated as far as trouble from this cause is concerned. With magnetic modulation, there is no trouble from this cause.

Fluctuation noise due to thermal agitation in the resistance or impedance coupling the ion-collector to an alternating-current amplifier would limit the sensitivity to

$$i = \sqrt{\frac{4kT}{R}\Delta f} = 1.3 \times 10^{-10}\sqrt{\frac{\Delta f}{R}} \text{ ampere}$$

where Δf is the noise bandwidth and R the coupling resistance. Since $\Delta f/R$ is easily made small, this limit to sensitivity is many times less than those above and may be disregarded.

There may be other causes of error in ion-current determination, such as grid emission, if they have alternating-current components not easily separated from the desired ion current. Grid emission will not be troublesome when voltage modulation is used but could be with the magnetic modulation method. It is not possible to generalize with respect to these other limits to sensitivity. In the ionization gauge, of course, the problems are somewhat different and, for the measurement of extremely low pressures, many additional phenomena must be considered.

In summary of this discussion of sensitivity, it would appear that the improved method allows an ion current of 10^{-9} ampere to be measured without special precautions, using 60-cycle modulation. By use of a lower frequency, or by neutralization, or by a phase-sensitive amplifier, or by all three, the lower limit of ion-current measurement can be reduced several orders of magnitude, leading to a current limit of 10^{-11} ampere. Thus, the improved method is from 100 to 10,000 times more sensitive than the conventional direct-current method and allows gas measurement in the conventional tube to the degree hitherto allowed only by a special ionization-gauge tube.

A Proposed Leak Detector

Detection of small vacuum leaks in a system or sealed-off tube by a method analogous to the above would be very desirable. One proposal to which some thought has been given is shown in Figure 7. If the leak is slowly scanned with a probe whose pressure is cyclically varied, and a selective alternating-current amplifier is employed to detect ions, it would appear possible to differentiate the steady direct ion current (due to residual gas, leakage, etc.) from the alternating-current component resulting when the probe is placed over the leak. A trial of this method at about 2 cycles per second by Howard J. Evans of the RCA Victor Division indicated that, for a high-vacuum system, a still lower frequency would be desirable to transmit the pressure changes uniformly inside the envelope, because of the low-pass filter action of the long mean-free path inside the tube and the attenuation of the leak itself which was through a ⅛″ thick envelope. Operation at a lower alternating frequency, of course, decreases the possible speed of leak detection.

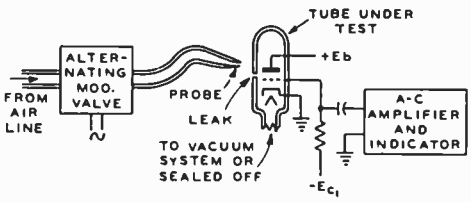

Fig. 7 — Possible leak testing by alternating-current method.

Conclusion

The improved alternating-current method of gas measurement appears to reduce most of the trouble with leakage found in conventional gas tests using direct-current with conventional tubes. When the undesired stray alternating currents are evaluated, it appears that the improved method allows ion-current determination down to values of 1/100 to 1/10,000 of those using the direct-current method with conventional tubes. With a conventional ionization gauge, no great improvement in sensitivity is to be expected, but the alternating-current method allows use of simpler amplifiers. By the use of specially-devised ion gauges, designed for the alternating-current method, many practical advantages should be attainable.

the white layer by washing and drying; while one appearing purple before washing will be straw color after.

A film which is purple when dry is usually desired, since this means low reflection for green light, which is the color for greatest eye sensitivity.

Since the uniformity of treatment of the glass depends on the slow diffusion of the vapor, best results are obtained with a single uniform piece of glass across the tray. If several pieces are used, separated by a small air gap, uniformity will be lacking near the edges. This makes the treatment of small discs, lenses, and prisms rather difficult, but care in reducing the size of the discontinuity will improve the result. Curved surfaces may also present difficulty due to the difference in acid to glass distances at various points.

In developing the present method, numerous experiments were performed in order to observe the effect of several variables on the quality of the films. Many of the variables also affect the time required to produce a film one quarter of a wavelength thick. These effects are described in the following paragraphs in order to give a better understanding of what is involved in low-reflection treatment by this method.

The Effect of Tray Height and Area

Early experiments with fluosilicic acid indicated that the distance between the acid solution and the glass had a definite effect on the production of the low reflecting layer. The rate at which acid vapor arrives at the glass is largely determined by diffusion through the space between the acid and the glass. As the distance is increased, the time of treatment to produce minimum reflection increases more or less proportionally. At the same time, the character of the film changes, becoming harder and of higher index at the greater acid-to-glass distances, the treatment eventually becoming rather irregular. Best all around results are usually obtained by the use of an acid-to-glass distance of about two inches.

In the original hydrofluoric acid vapor process, the ratio of tray area to height, had a pronounced effect on the treatment of the glass, but with the fluosilicic acid method no such effect exists. This is probably due to the fact that no temperature difference is needed between the acid and the glass, thus eliminating any extraneous convection effects in the vapor.

The Effect of Acid Composition

The composition of the fluosilicic acid has a very pronounced effect on the treating process. Some of the commercially available acids have

the correct composition and merely require dilution; others, however, require adjustment of the silica and hydrofluoric acid content. Acid obtained from one source may require the addition of a small amount of hydrofluoric acid while that obtained from another may require the addition of a small amount of silica.

These observations have led to some interesting facts concerning the chemistry of fluosilicic acid, and it is hoped that these may be presented in detail in a future publication.

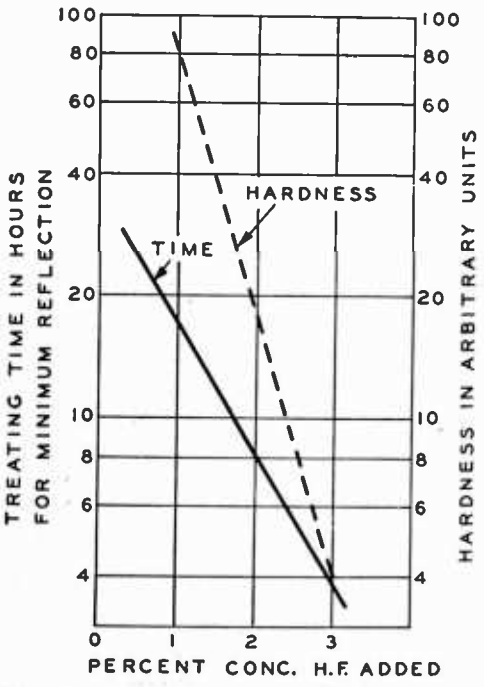

Fig. 2—The effect of adding hydrofluoric acid to the fluosilicic acid solution made with acid from source A.

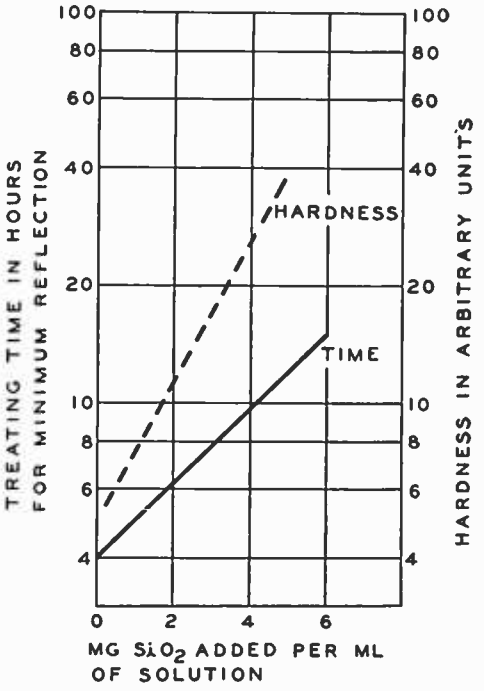

Fig. 3—The effect of adding silicon dioxide to the fluosilicic acid solution made with acid from source B.

Determination of the acid composition can be made chemically, and the required adjustment calculated from a knowledge of the desired composition. It has been found, however, that for experimental work particularly, it is very satisfactory to run actual tests on the glass using the original acid and samples modified by the addition of hydrofluoric acid and silica.

Figure 2 shows the variation of time of treatment for minimum reflection as a function of the quantity of hydrofluoric acid added to fluosilicic acid from source A. The dotted line on the same figure shows the results for film hardness. Figure 3 shows similar results as a function of the amount of hydrated silica added to acid from source B. It is apparent that acid from source A must have already contained

much more silica than that from B. In addition to the information about the acid, the curves indicate that long treatment times are usually associated with very hard films, whereas very short treatment times produce soft films. Hardness is also to some extent an indicator of refractive index of the film. A very soft film, for instance, usually has a very low index (less than 1.25) because of the high degree of skeletonization.

In view of the above results, it is often desirable and sometimes necessary to perform a series of experiments on small trays in order to obtain the correct adjustment of the acid for optimum film characteristics.

The Effect of Acid Concentration

It has been found that the time of treatment and the character of the film are altered considerably by the concentration of the acid. In general, as the acid concentration increases, the time of treatment for minimum reflection decreases, the rate of decrease being more rapid for low concentrations as shown in the curve of Figure 4. This change of treatment time is accompanied by a very considerable change in character of the film. As the concentration of the acid is increased, film hardness increases, but this is largely due to an increase in the refractive index of the film, caused by the skeleton structure of the film being less open. At high acid concentrations (23 per cent) further difficulties may be encountered, due to non-uniformity of treatment, which is perhaps caused by the rapid action of the vapor.

The Effect of Temperature on Treatment Time

Figure 5 shows the relation between the time of treatment for minimum reflection and the temperature of the glass and container. The process shows considerable sensitivity to temperature, giving about a 10 per cent variation in treating time for a 1-degree Centigrade variation in temperature. For this reason, it is usually preferable to check the time of treatment by test samples, or by inspection rather than by direct timing, although timing is practical if the temperatures are maintained sufficiently constant. The results of Figure 5 would seem to indicate the desirability of operating at higher than room temperature. The difficulties of operation, however, become much greater if this is done. It has been found desirable to start the treatment with the glass at the same temperature as the tray and acid. In addition, temperature uniformity throughout the treating space assists in obtaining uniform films. Since the vapor pressure of the acid is considerably greater at the higher temperature, difficulty may be

experienced with loss of vapor and consequent changing of the acid composition. Loss of vapor while placing the glass in position, also makes the determination of the starting time of treatment less accurate.

Reflection as a Function of Treating Time

As the acid vapor attacks the surface of the glass, a surface film is formed by skeletonizing the surface layer of the glass. In general, the acid attacks the silica slightly allowing the non-silica portion to form fluosilicates on the surface of the glass. The presence of these fluosilicates, as a white diffusing layer on the glass, alters the true reflection of the skeletonized layer beneath, as described earlier in this paper.

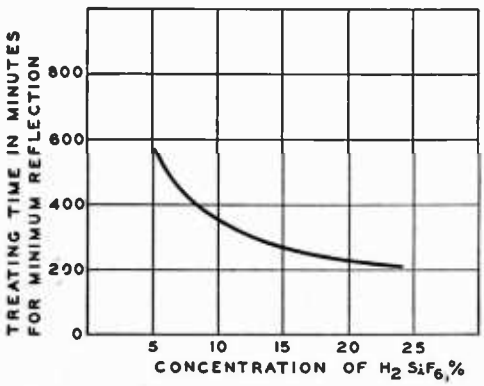

Fig. 4—The effect of acid concentration on the time of treatment.

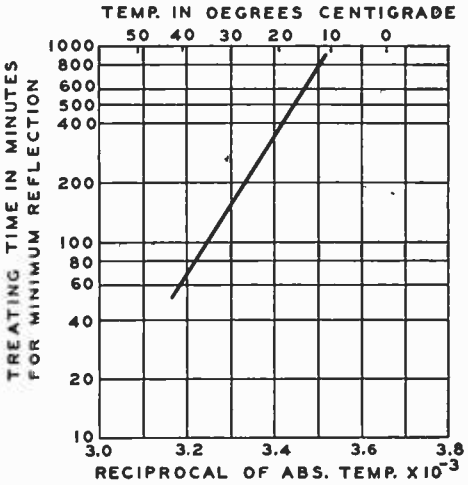

Fig. 5—The effect of temperature on the time of treatment.

Figure 6 shows reflection measurements on the skeletonized layer alone, as a function of the time of treatment. These were obtained by washing and drying samples after various times of treatment. The reflection was measured with a phototube arrangement having a spectral characteristic approximately that of the eye. The reflection obtained after a given time of treatment is determined by the film thickness and its index of refraction. These are both changing as the treatment progresses.

Reflection as a Function of Wavelength

Reflectivity was measured as a function of wavelength of the incident light for a piece of glass treated to give minimum reflection for green light. This was done on a recording spectroradiometer[4] using

[4] V. K. Zworykin, "An Automatic Recording Spectroradiometer for Cathodoluminescent Materials", *Jour. Opt. Soc. Amer.*, 29, 84-91, February, 1939.

an attachment which measured the reflected light for a beam incident at right angles to the surface. As shown in Figure 7, the reflected light increases considerably at the short and long wavelength ends of the curve, but this increase is much less than that occurring in many other types of low-reflecting film, particularly some of those made by vacuum evaporation of multi-layers of material on the glass surface.

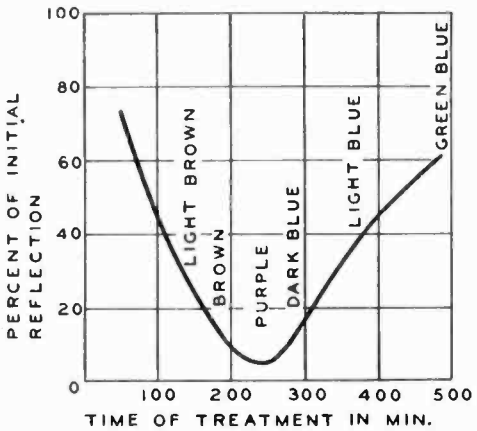

Fig. 6—Reflection as a function of treating time.

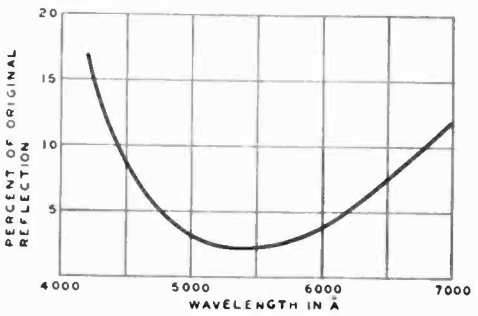

Fig. 7—Reflection as a function of wavelength.

Properties of the Low Reflecting Layer

It has previously been reported[2] that the film produced by the hydrofluoric acid vapor process was almost 100 per cent silica with a multitude of voids about 200 Å in size throughout the silica network. The new process may not only duplicate the results of the earlier process, but is capable of many variations in time of treatment, degree of hardness, and the refractive index of the film. Control of refractive index is obtained by varying the degree of skeletonization and if desired it can be made equal to $\sqrt{n}$ where n is the refractive index of the glass being treated. Such a film made experimentally one quarter wavelength thick will give almost zero reflection for monchromatic light at normal incidence. For practical use a somewhat higher index may be chosen in order to increase hardness and durability.

Treatment of Various Glasses

Because of the additional control obtained by varying the silica content of the acid, the fluosilicic acid-vapor process is applicable to a greater variety of glasses than the hydrofluoric acid vapor process. The acid composition should be determined independently for each glass, although several types can usually be treated over the same acid. Pyrex does not, in general, respond as satisfactorily to the vapor

treatment as the common window and polished plate glasses. A large number of optical glasses give satisfactory results, but used prisms and lenses may present considerable difficulty, due to surface weathering and slight deterioration which shows up only when an attempt is made to reduce reflection by exposure to the acid vapor.

Cleanliness of the glass is an important factor in obtaining uniform and reproducible results. Because of the nature of the vapor attack, a piece of glass which gives a uniform gray breath figure is usually sufficiently clean. This can usually be achieved by cleaning with powdered chalk and polishing dry with a clean cloth. It is sometimes necessary tc give in addition a 20 second dip in 0.5 per cent hydrofluoric acid solution to remove any etched surface film.

Conclusion

An improved chemical method for reducing reflections of flat glass surfaces has been described. Its application is an extremely simple process. Good results can be obtained on most of the common window glasses with available fluosilicic acid diluted to approximately 16 per cent and used at room temperature. In those cases where trouble is experienced, it can usually be traced to acid composition or the surface condition of the glass.

Acknowledgments

The author wishes to acknowledge the work contributed by F. E. Williams, now with the General Electric Co., in the development of this new method, and to thank R. E. Shrader for assistance in measuring the spectral reflectivity of the film.

A NETWORK BISECTION THEOREM*†

By

V. D. Landon

Research Department, RCA Laboratories Division,
Princeton, N. J.

Summary—It is shown how any given symmetrical ladder network A *may be split into two simpler networks* B *and* C *in such a manner that the transmission as a function of frequency* A *is equal to half the product of the transmission curves for* B *and* C.

Introduction

THE theorem about to be discussed has previously been used by the author[1] without being formally stated. It is believed to be a sufficiently useful theorem to warrant separate treatment in order to call attention to the way in which it simplifies certain problems.

Bisecting a Network

Consider any four terminal symmetrical ladder network as in Figure 1. If there is a shunt arm on the axis of symmetry it should be replaced by two shunt arms in parallel, each having twice the impedance of the original. If a series arm crosses the axis of symmetry it should be replaced by two series elements of half the impedance of the original arm. Now labelling the points on the axis of symmetry P_1 and P_2, the network may be bisected into two similar parts by breaking the connection at P_1 and P_2.

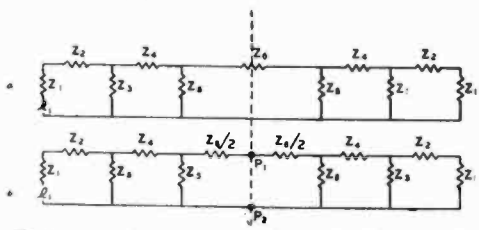

Fig. 1—A symmetrical ladder network.

Transfer Factor

The transfer factor $G_1(f)$ of the first network is here defined as the ratio of output current to input voltage, as a function of frequency.

The transfer factor $G_2(f)$ of the derived network fragment on the

---

* Decimal Classification: R143.

† This theorem should not be confused with Bartlett's Bisection Theorem. It involves a similar bisection of a network but is concerned with a different network characteristic.

[1] V. D. Landon, "Cascade Amplifiers with Maximal Flatness," *RCA Review*, Vol. V, No. 3-4, p. 496, January-April, 1941.

left is defined as the ratio of the output *voltage* to the input voltage.

The transfer factor $G_3(f)$ of the network fragment on the right is defined as the ratio of the output current to the input voltage (inserted from P_1 to P_2).

The transfer factors were defined narrowly only to simplify the proof. Thus, G_1 is a transfer conductance, G_2 is a voltage ratio, and G_3 is a transfer conductance. To change G_1 to a voltage ratio or a current ratio requires only an application of Ohm's law or Thevenin's theorem.

THEOREM

When the bisection of a network is carried out as stated above then,

$$G_1(f) = \tfrac{1}{2}\, G_2(f) \times G_3(f)$$

where the transfer factors are as defined above.

ILLUSTRATIONS

Various networks illustrating the theorem are shown in Figures 1, 2 and 3. It should be noted that where a shunt element is on the axis of symmetry in the original network, the element appears doubled in value in the network on the left, but is short circuited by the input voltage generator (having zero impedance) and may be omitted in the network on the right. Similarly where a series element is cut by the line of symmetry in the original network, the element appears with half value in the network on the right, but in the network on the left it feeds an open circuit and hence may be omitted.

From Figure 2 it can be seen that the equivalent of a pair of

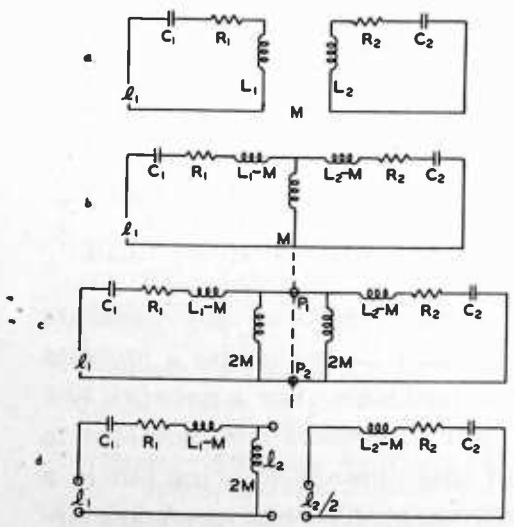

Fig. 2—Bisection applied to coupled circuits.

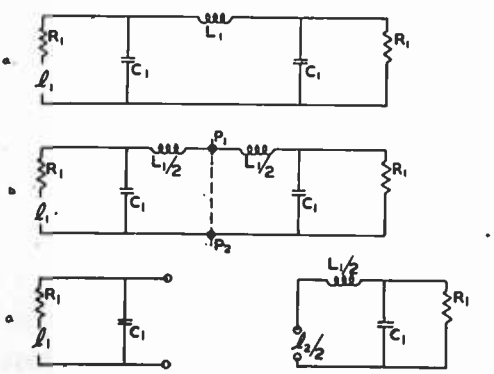

Fig. 3—Bisection applied to a low pass filter.

resonant circuits with inductive coupling is a pair of cascaded circuits detuned respectively by plus and minus M.

From Figure 3 it can be seen that a three-reactance low-pass filter is equivalent to a single-reactance filter cascaded with a two-reactance filter.

As used above, the word cascade means an arrangement whereby the output voltage of one network becomes the input voltage of the next. While there is no known method of accomplishing this for the exact circuits shown, with slight circuit modification to adapt them to tube use it can be accomplished, in effect, by the use of vacuum tubes.

Proof of Theorem

Consider a network which is suitable for bisection such as that of Figures 1b, 2c, or 3b. Let a voltage e_1 be applied at each end of the network. The voltage from P_1 to P_2 has twice the value it would have if e_1 were applied at only one end. The current to the right is balanced by the current to the left, hence the network may be open circuited at P_1 and P_2 without changing any voltages or currents.

The voltage from P_1 to P_2 is

$$e_2 = G_2(f)\ e_1$$

so that

$$e_1 = e_2/G_2(f).$$

However, in the original circuit with e_1 applied only at the left end, the output current is,

$$I_0 = \frac{e_2}{2} G_3(f).$$

Therefore

$$G_1(f) = \frac{I_0}{e_1} = \tfrac{1}{2}\, G_2(f)\ G_3(f).$$

Discussion

The theorem finds its chief use in solving circuits of only moderate difficulty such as those of Figure 2 and Figure 3. It changes a problem of moderate difficulty to two very simple problems. For a network like that of Figure 1 the theorem is valid but in general does not lead to a very useful result. Probably its chief usefulness is to bring out in a very graphic way the relationship between coupled and cascaded circuits of a rather simple type.

RCA TECHNICAL PAPERS†

Second Quarter, 1949

Any request for copies of papers listed herein should be addressed to the publication to which credited.

"Absorption Spectra of Some Double Salts Containing Bivalent Cobalt", M. L. Schultz, *Jour. Amer. Chem. Soc.* (April).. 1949

"Analysis by the Two-Frequency Intermodulation Method of Tracing Distortion Encountered in Phonograph Reproduction", H. E. Roys, *RCA Review* (June) 1949

"An Analysis of Absorption Traps", J. Avins, *RCA Licensee Bulletin LB-780* (July 10) 1949

"Automatic Antenna Tuning", Sidney Wald, *Radio News* (May) 1949

"Automatic Frequency Phase Control of Television Sweep Circuits", E. L. Clark, *Proc. I.R.E.* (May) 1949

"Beam-Deflection Mixer Tubes for UHF", E. W. Herold and C. W. Mueller, *Electronics* (May) 1949

"Calculation of Noise Factor of Conventional Amplifiers and Converters", R. F. Romero, *RCA Licensee Bulletin LB-778* (June 24) 1949

"Crossover Filter for Disc Recording Heads", H. E. Roys, *Audio Eng.* (June) 1949
Broadcast News (June) 1949

"DB Calculations Made Easy", Berthold Sheffield, *Radio Maintenance* (April) 1949

"Demonstration of Large-Screen Television at Philadelphia", Roy Wilcox (coauthor), *Jour. Soc. Mot. Pic. Eng.* (May) .. 1949

"Development and Performance of Television Camera Tubes", R. B. Janes, R. E. Johnson and R. S. Moore, *RCA Review* (June) 1949

"Disc Recorder for Motion Picture Production", J. L. Pettus, *Jour. Soc. Mot. Pic. Eng.* (April) 1949

"Drive-In Theater Service and Maintenance", E. Stanko, *The Box Office* (April) 1949

"The Electron Coupler—A Developmental Tube for Amplitude Modulation and Power Control at Ultra-High Frequencies", C. L. Cuccia, *RCA Review* (June) 1949

"Electron Microscopy of Colloidal Systems", J. Hillier and J. Turkevich, *Journal of Analytical Chemistry* (April)..... 1949

ELECTRON TUBES, Volume I (1935-1941), RCA Review, RCA Laboratories Division, Princeton, N. J., (March).... 1949

ELECTRON TUBES, Volume II (1942-1948) RCA Review, RCA Laboratories Division, Princeton, N. J., (March).... 1949

"Electronic Digital Counters", W. H. Bliss, *Elec. Eng.* (April) 1949

"Elimination of Reflections on Video Lines", C. A. Meyer and R. G. Middleton, *Radio News* (May) 1949

"Factors Affecting Spurious Printing in Magnetic Tapes", S. W. Johnson, *Jour. Soc. Mot. Pic. Eng.* (June) 1949

"FM Proof-of-Performance Measurement Techniques", F. E. Talmage, *Communications* (April)..... 1949

† Report all corrections or additions to RCA Review, Radio Corporation of America, RCA Laboratories Division, Princeton, N. J.

"High-Quality Recording Electronic Mixer", Kurt Singer, *Jour. Soc. Mot. Pic. Eng.* (June) 1949
"High-Speed Production of Metal Kinescopes", H. P. Steier and R. D. Faulkner, *Electronics* (May) 1949
"How to Get the Best Picture Out of Your Image Orthicon Camera", H. Kozanowski, *Broadcast News* (April) 1949
"Image Orthicon—Making Fine Mesh Screens", H. B. Law, *Broad. Eng. Jour.* (May) 1949
"Improvement of FM Receiver Tuning Characteristics with Automatic Frequency Control", Kerim Onder and Earl Schoenfeld, *RCA Licensee Bulletin LB-779* (June 24) 1949
"An Inexpensive Waveform Monitor for TV Broadcasters", J. R. De Baun, *Broad. Eng. Jour.* (May) 1949
"Large Screen Projection Television", R. V. Little, *Elec. Eng.* (April) 1949
"Letter Reading Machine", V. K. Zworykin, L. E. Flory and W. S. Pike, *Electronics* (June) 1949
"Mechanical Filters for Radio Frequencies", L. L. Burns, Jr. and W. Van B. Roberts, *RCA Licensee Bulletin LB-773* (May 16) 1949
"Method of Multiple Operation of Transmitter Tubes Particularly Adapted for Television Transmission in the Ultra-High-Frequency Band", G. H. Brown, W. C. Morrison, W. L. Behrend and J. G. Reddeck, *RCA Review* (June) 1949
"The New Portable Tape Recorder", W. E. Stewart *Broadcast News* (April) 1949
"New Portable Tape Recorder Performs with Studio Quality", W. E. Stewart, *Tele-Tech*, (April) 1949
"A New 150 KW AM Transmitter", T. J. Boerner, *Broadcast News* (June) 1949
"Noise Factor and Its Measurement", H. Johnson, *RCA Licensee Bulletin LB-775* (June 20) 1949
"Optimum High-Frequency Bias in Magnetic Recording", G. L. Dimmick and S. W. Johnson, *Broadcast News* (June) 1949
"Oscilloscopes and Vacuum Tube Voltmeters", G. E. Reiling and P. A. Greenmeyer, *Broadcast News* (June) 1949
"Phase Contrast in Electron Microscope Images", E. G. Ramberg, *Jour. Appl. Phys.* (May) 1949
"The Philosophy of Our TV System (Part II)", J. H. Roe, *Broadcast News* (April) 1949
"The Philosophy of Our TV System (Part III)", J. H. Roe, *Broadcast News* (June) 1949
PHOTOELECTRICITY AND ITS APPLICATIONS, V. K. Zworykin and E. G. Ramberg, John Wiley & Sons, Inc., New York, N. Y. (April) 1949
"The Pictorial Situation Display in Air Navigation and the Control of Aerial Traffic", by H. H. Spencer, *Aero Digest* (April) 1949
"Portable Magnetic-Recording System", O. B. Gunby, *Jour. Soc. Mot. Pic. Eng.* (June) 1949
"A Precision Radar Range Calibrator", R. L. Rod, *Electronics* (April) 1949
"Preselection of Variable-Gain Tubes for Compressors", Kurt Singer, *Jour. Soc. Mot. Pic. Eng.* (June) 1949
"Radiopath Dependability for Communication", H. H. Edwards, *Teleg. and Teleph Age* (May) 1949

"Recommendations for Support and Insulation of Kinescope RCA-16AP4", *RCA Application Note AN-140*, RCA Tube Department, Harrison, N. J. (May 2) 1949

"A Record Changer and Record of Complementary Design", B. R. Carson, A. D. Burt and H. I. Reiskind, *RCA Review* (June) 1949

"Research on Reading Aids for the Blind", V. K. Zworykin, L. E. Flory and W. S. Pike, *Jour. Frank. Inst.* (May) 1949

"Reversible-Beam Antenna for Twelve-Channel Television Reception", O. M. Woodward, Jr., *RCA Review* (June) 1949

"Some Observations on the Photoeffect in Cadmium Sulfide", A. Rose, P. K. Weimer and S. V. Forgue, *Amer. Phys. Soc. Bulletin* (April 28) 1949

"Sound Co-Channel Interference Measurements on Conventional and Intercarrier Television Receivers", George Hesse and Jack Avins, *RCA Licensee Bulletin LB-774* (May 20) 1949

"A Sprial-Beam Method for the Amplitude Modulation of Magnetrons", by J. S. Donal, Jr., and R. R. Bush, *Proc. I.R.E.* (April) 1949

"A Television and FM Noise Generator", I. J. Melman, *RCA Licensee Bulletin LB-776* (June 20) 1949

"Television Film Recording", R. V. Little, Jr., *Broadcast News* (April) 1949

"Television Receiving Systems", C. M. Sinnett, *Elec. Eng.* (June) 1949

"Tips on Use of Image Orthicons", booklet, Tube Department, RCA Victor Division, Harrison, N. J. (April) 1949

"Tracing Distortion in Phonograph Records", M. S. Corrington, *RCA Review* (June) 1949

"TV and FM Site Testing", E. S. Clammer and E. M. Brown, *Broadcast News* (June) 1949

"TV Film Projectors", G. W. Tunnell, *Inter. Project.* (May) .. 1949

"Video Announcer", E. P. Bertero, *RCA Review* (June) 1949

NOTE—Omissions or errors in these listings will be corrected in the yearly index.

AUTHORS

LESLIE L. BURNS, JR. received the B.S. degree in Electrical Engineering from the Agricultural and Mechanical College of Texas in 1944, having joined the U.S. Army Signal Corps the previous year. While with the army he was a student at the Harvard-M.I.T. Radar School. From there he went to the Army Communications Service and was sent to the India-Burma Theater where he served as a fixed station radio engineer until near the end of the war. Since 1946 he has been with RCA Laboratories Division at Princeton, N. J. Mr. Burns is a Member of the Institute of Radio Engineers and an Associate Member of the American Institute of Electrical Engineers.

MURLAN S. CORRINGTON received the B.S. degree in Electrical Engineering in 1934, from the South Dakota School of Mines and Technology, and the M. Sc. degree in 1936, from Ohio State University. From 1935 to 1937 he was a graduate assistant in the Physics Department of Ohio State University. In 1937 he joined the Rochester Institute of Technology, and taught mathematics, mechanics, and related subjects. Since 1942 Mr. Corrington has been engaged in mathematical engineering in the Advanced Development Section of the RCA Victor Division at Camden, N. J.

WILLIAM A. HARRIS received his B.S. degree in Electrical Engineering from Rose Polytechnical Institute, Terre Haute, Indiana in 1927. He was employed by the General Electric Co. from 1927 to 1929, and was transferred to the RCA Victor Division in Camden in 1930 where he worked in the Receiver Design Laboratories. He has been with the Application Engineering Laboratory of the RCA Tube Department at Harrison, N. J. since 1931. Mr. Harris has been connected with much of the tube development and application work on frequency converters and on high-frequency circuit problems.

E. W. HEROLD received the B.S. degree from the University of Virginia in 1930, and the M.S. degree from Polytechnic Institute of Brooklyn in 1942. From 1924 to 1926, he was associated with the Bell Telephone Laboratories, and from 1927 to 1929 with E. T. Cunningham, Inc. In 1930 he entered the Research and Engineering Department of the RCA Manufacturing Company at Harrison, New Jersey, and in 1942 transferred to RCA Laboratories Division. Mr. Herold is a member of Phi Beta Kappa and Sigma Xi, and a Fellow of the Institute of Radio Engineers.

VERNON D. LANDON attended Detroit Junior College. From 1922 to 1929, he was in charge of the Radio-Frequency Laboratory of the Westinghouse Electric and Manufacturing Company. In 1930 he was Assistant Chief Engineer of the Radio-Frequency Laboratories and in 1931 he became Assistant Chief Engineer of the Grigsby Grunow Company. In 1932, he joined RCA Manufacturing Company in Camden, N. J. Since 1942, he has been with RCA Laboratories Division at Princeton, N. J. engaged in research work on radio circuits. Mr. Landon is a Member of Sigma Xi, and a Senior Member of the Institute of Radio Engineers.

FREDERICK H. NICOLL received the B.Sc. degree in Physics from Saskatchewan University, Canada, in 1929 and the M.Sc. degree in 1931. He held an 1851 Exhibition Scholarship to Cambridge University, England for three years research and received the Ph.D. degree from that university in 1934. He was a research physicist with Electric and Musical Industries, Ltd. in London from 1934 to 1939. From 1939 to 1941 he was with the RCA Victor Division, Radio Corporation of America, at Camden, N. J. as a research engineer. Since 1941 he has been with the RCA Laboratories Division in Princeton, N. J. engaged in research on cathode-ray tubes and electron optics. Dr. Nicoll is a senior member of the Institute of Radio Engineers and a member of the American Physical Society and of Sigma Xi.

HARRY F. OLSON received the B.S. degree in 1924, the M.S. degree in 1925, the Ph.D. degree in 1928 and the E.E. degree in 1932 from the University of Iowa. From 1928 to 1930 he was in the Research Department of Radio Corporation of America; from 1930 to 1932, in the Engineering Department of RCA Photophone; from 1932 to 1941, in the Research Division of RCA Manufacturing Company; since 1941, with RCA Laboratories Division. Dr. Olson is a member of Tau Beta Pi, Sigma Xi and the American Physical Society, a Fellow of the Institute of Radio Engineers and of the Acoustical Society of America.

DONNELL W. POWER received the B.S. degree in Electrical Engineering from Purdue University in 1929. From 1929 to 1930 he was employed as a tube engineer for the General Electric Company at Nela Park in Cleveland, Ohio. In 1930 he joined the Tube Department of the RCA Manufacturing Company at Harrison, N. J. Since that time he has been engaged in the advanced development of receiving tubes. Mr. Power is a Senior Member of the Institute of Radio Engineers.

JOHN PRESTON received his education in England, attended Manchester Scientific Institute taking courses in Mechanical Engineering. He then joined the engineering staff of the Bolton Power and Electrical Company. He became a member of Radio Corporation of America in 1929 and was associated with the Research Department of RCA Victor from 1930 to 1935; the Research Department of RCA Manufacturing Company from 1935 to 1941, and RCA Laboratories Division from 1941 to date. His work has been in the field of Acoustics since joining Radio Corporation of America. Mr. Preston is a member of the Acoustical Society of America and of Sigma Xi.

WALTER VAN B. ROBERTS received the B.S. degree from Princeton University in 1915, the E.E. degree in 1917, the M.A. in 1923, and the Ph.D. in Physics in 1924. He served as the technical officer of a sound ranging station during World War I. From 1919-1924 he was an Instructor in physics and electrical engineering at Princeton University. In 1924, he joined the Radio Corporation of America in the Technical and Test Department, and from 1927 to 1943 served in the Patent Department. From 1943-1946 he was on leave of absence from RCA performing development work at Johns Hopkins and Princeton on proximity fuses, guided missiles and telemetering. He returned to RCA Laboratories Division, Princeton, N. J., as a research engineer in 1946. Dr. Roberts is a Member of Sigma Xi and Phi Beta Kappa and a Fellow of the Institute of Radio Engineers.

GEORGE M. ROSE received the B.S. degree in Electrical Engineering from the University of North Carolina in 1928, and remained there as a Teaching Fellow until 1929. From 1929 until 1931 he was an engineer in the Vacuum Tube Engineering Department of the General Electric Company at Schenectady. In 1931 he joined the Tube Department of the RCA Manufacturing Company at Harrison, N. J. as a member of the Tube Research Group. He later transferred to the Advanced Development Group and has been Manager of this Group since 1941. Mr. Rose is a Member of Tau Beta Pi and a Senior Member of the Institute of Radio Engineers.

PAUL K. WEIMER received the B.A. degree from Manchester College in 1936, the M.A. degree in Physics from the University of Kansas in 1938, and the Ph.D. degree in Physics from Ohio State University in 1942. While at Ohio State University, he was a graduate assistant in physics. During 1936 and 1937, he was a graduate assistant in physics at the University of Kansas. From 1937 to 1939, he taught physics and mathematics at Tabor College, Hillsboro, Kansas. Since 1942, he has been engaged in television research at RCA Laboratories Division at Princeton, N. J. Dr. Weimer is an Associate Member of the Institute of Radio Engineers, a Member of the American Physical Society, and a Member of Sigma Xi.